SAIC-91/1061

SIMULATION OF THE DETECTION AND LOCATION CAPABILITY OF REGIONAL SEISMIC NETWORKS IN THE SOVIET UNION

Thomas J. Sereno, Jr.

Science Applications International Corporation
10260 Campus Point Drive
San Diego, California 92121

March 1, 1991

Final Report
1 January 1989 – 31 December 1990

Sponsored By:

Defense Advanced Research Projects Agency (DARPA)
Nuclear Monitoring Research Office (NMRO)
Seismic Detection Capability Modeling

ARPA Order No. 4511 (Amendment 19)

Issued by AFTAC under Contract F08606-88-C-0033.

Principal Investigator:

Dr. Thomas J. Sereno, Jr.
(619) 458-2593

Effective Date of Contract: 1 January 1989

Contract Expiration Date: 31 December 1990

SAIC-91/1061

SIMULATION OF THE DETECTION AND LOCATION CAPABILITY OF REGIONAL SEISMIC NETWORKS IN THE SOVIET UNION

Thomas J. Sereno, Jr.

Science Applications International Corporation
10260 Campus Point Drive
San Diego, California 92121

March 1, 1991

Final Report
1 January 1989 – 31 December 1990

Sponsored By:

Defense Advanced Research Projects Agency (DARPA)
Nuclear Monitoring Research Office (NMRO)
Seismic Detection Capability Modeling

ARPA Order No. 4511 (Amendment 19)

Issued by AFTAC under Contract F08606-88-C-0033.

Principal Investigator:

Dr. Thomas J. Sereno, Jr.
(619) 458-2593

Effective Date of Contract: 1 January 1989

Contract Expiration Date: 31 December 1990

REPORT DOCUMENTATION PAGE

1a. REPORT SECURITY CLASSIFICATION Unclassified	1b RESTRICTIVE MARKINGS
2a. SECURITY CLASSIFICATION AUTHORITY	3 DISTRIBUTION/AVAILABILITY OF REPORT Approved for public release with distribution unlimited.
2b. DECLASSIFICATION/DOWNGRADING SCHEDULE	
4. PERFORMING ORGANIZATION REPORT NUMBER(S) SAIC–91/1061	5 MONITORING ORGANIZATION REPORT NUMBER(S)
6a. NAME OF PERFORMING ORGANIZATION Science Applications International Corporation 6b OFFICE SYMBOL (*If applicable*)	7a. NAME OF MONITORING ORGANIZATION Air Force Technical Applications Center/TTR
6c. ADDRESS (*City, State, and ZIP Code*) 10260 Campus Point Drive San Diego, CA 92121	7b. ADDRESS (*City, State, and ZIP Code*) HQ/AFTAC/TTR Patrick Air Force Base, FL 32925–6001
8a. NAME OF FUNDING/SPONSORING ORGANIZATION Defense Advanced Research Projects Agency 8b. OFFICE SYMBOL (*If applicable*) DARPA	9. PROCUREMENT INSTRUMENT IDENTIFICATION NUMBER F08606–88–C–0033
8c. ADDRESS (*City, State, and ZIP Code*) 1400 Wilson Blvd. Arlington, VA 22209	10 SOURCE OF FUNDING NUMBERS PROGRAM ELEMENT NO. 62714E; PROJECT NO. 8A10; TASK NO. SOW 3.3; WORK UNIT ACCESSION NO.
11 TITLE (*Include Security Classification*) Simulation of the Detection and Location Capability of Regional Seismic Networks in the Soviet Union	
12. PERSONAL AUTHOR(S) Thomas J. Sereno, Jr.	
13a. TYPE OF REPORT Final Report 13b. TIME COVERED FROM 1/1/89 TO 12/31/90	14. DATE OF REPORT (*Year, Month, Day*) 1991 March 1 15. PAGE COUNT 115
16. SUPPLEMENTARY NOTATION	

17 COSATI CODES		
FIELD	GROUP	SUB-GROUP
8	11	

18. SUBJECT TERMS (*Continue on reverse if necessary and identify by block number*)
Detection Capability, Location Capability, Regional Seismic Networks, Treaty Monitoring, Cavity Decoupling

19 ABSTRACT (*Continue on reverse if necessary and identify by block number*)

The main objective of this two-year project is to assess the treaty monitoring capability of existing and proposed seismic networks in the Soviet Union. We estimate the number of in-country single stations or arrays that are required to monitor nuclear explosion testing to a threshold of 1 kt. This corresponds to an approximate magnitude of 2.5 if the explosion is fully-decoupled. We estimate that 10 internal NORESS-type arrays or 30 internal IRIS-type single stations are required to achieve a 90% detection threshold of M_L 2.5 throughout the Soviet Union. However, only 15 in-country single stations are needed to reach this threshold in regions of bedded or domed salt (e.g., regions for which full-decoupling is feasible). These estimates are based on detection of 3 phases involving at least 2 stations, which gives location uncertainties ≤ 20 km at the 90% confidence level. If secondary phases are not

20 DISTRIBUTION/AVAILABILITY OF ABSTRACT ☐ UNCLASSIFIED/UNLIMITED ☒ SAME AS RPT. ☐ DTIC USERS	21. ABSTRACT SECURITY CLASSIFICATION Unclassified
22a. NAME OF RESPONSIBLE INDIVIDUAL Dr. Dean Clauter	22b TELEPHONE (*Include Area Code*) (407) 494–2251 22c. OFFICE SYMBOL AFTAC/TTR

DD FORM 1473, 84 MAR 83 APR edition may be used until exhausted. All other editions are obsolete.

included in the detection criteria, then $\geq$ 20 internal NORESS-type arrays or $\geq$ 50 single stations are required to reach the M_L 2.5 threshold throughout the Soviet Union. These estimates are based on the frequency-dependent signal and noise conditions in Fennoscandia. Of course, these conditions may not accurately represent conditions within the Soviet Union, so we also determine the sensitivity of our simulations to signal and noise characteristics.

Table of Contents

LIST OF FIGURES

(THIS PAGE INTENTIONALLY LEFT BLANK)

LIST OF TABLES

(THIS PAGE INTENTIONALLY LEFT BLANK)

1. SUMMARY

1.1 Objectives

The objective of this two-year study is to simulate detection and location capability of seismic networks that include regional stations and arrays in and around the Soviet Union. Three specific tasks are:

(1) Enhance and validate the extended version of the Seismic Network Assessment Program for Detection [*SNAP/D, Ciervo et al.*, 1985] called *SNAP/DX* [*Bratt et al.*, 1987] to accurately represent the treaty monitoring capability of seismic networks that include regional stations and arrays.

(2) Normalize *SNAP/DX* to the observed performance of existing stations and expected conditions in and around the Soviet Union.

(3) Apply the normalized simulation methods to assess the treaty monitoring capability of existing and proposed seismic networks.

The first two tasks were addressed in semi-annual and annual reports of this contract (reports 1, 4, and 5 in the following section). This final report summarizes these previous results, and presents the new results from the third project task.

1.2 Reports and Publications

The following reports and papers were completed under support by this contract:

1. *Sereno, T.*, "Numerical Modeling of *Pn* Geometric Spreading and Empirically Determined Attenuation of *Pn* and *Lg* Phases Recorded in Eastern Kazakhstan," *Semi-Annu. Tech. Rep. SAIC 89/1555*, Sci. Appl. Int. Corp., San Diego, Calif., 1989.

This is the first semi-annual report of this contract. It includes (1) a theoretical study of the sensitivity of *Pn* geometric spreading to the velocity gradient in the upper mantle, and (2) an empirical study of signal and noise characteristics of regional phases recorded by the NRDC stations in the Soviet Union.

2. *Sereno, T.*, "*Pn* Geometrical Spreading and Empirically-Determined *Pn* and *Lg* Attenuation in Eastern Kazakhstan," Proceedings of the DARPA/AFTAC Annual Seismic Research Review (28–29 November), Patrick Air Force Base, Florida, 195–216, 1989.

This short paper summarizes the results presented in the first semi-annual report of this contract (see report #1 above).

3. *Sereno, T., and J. Given,* "*Pn* Attenuation for a Spherically Symmetric Earth Model," *Geophys. Res. Lett., 17,* 1141–1144, 1990.

This paper presents a theoretical study of the effect of earth sphericity on the frequency-dependent attenuation of regional *Pn* phases. Complete synthetic seismograms are computed using wavenumber integration for elastic and anelastic models of a spherical earth. The results indicate that both elastic and anelastic earth structure effect the frequency dependence of *Pn* attenuation.

4. *Sereno, T., S. Bratt, and G. Yee,* "NETSIM: A Computer Program for Simulating the Detection and Location Capability of Regional Seismic Networks," *Annual Tech. Rep. SAIC 90/1163,* Sci. Appl. Int. Corp., San Diego, Calif., 1990.

This is the first annual report of this contract. It describes our enhancements to the *SNAP/DX* computer program. The most important is the introduction of frequency dependence into the estimates for the source, station noise (for primary and secondary phases), attenuation, and array gain. This report includes functional descriptions of the detection and location modules and detailed descriptions of each input and output parameter.

5. *Sereno, T.,* "Attenuation of Regional Phases in Fennoscandia and Estimates of Arrival Time and Azimuth Uncertainty Using Data Recorded by Regional Arrays," *Semi-Annu. Tech. Rep. SAIC 90/1472,* Sci. Appl. Int. Corp., San Diego, Calif., 1990.

This is the third semi-annual report of this contract. It describes our normalization of the simulations using NORESS and ARCESS data. Estimates of the uncertainty of arrival time and azimuth measurements are included to normalize simulations of the location capability of regional networks. Frequency-dependent attenuation of regional phases, source scaling relations, and noise spectra for primary and secondary phases are estimated to normalize simulations of detection capability. We validate our normalization by comparing the detection and location capabilities predicted by *NetSim* to those actually achieved by NORESS and ARCESS. We also use tectonic and geological maps of Eurasia to develop propagation and source media grids on a 5°×5° scale.

6. *Sereno, T.,* "Attenuation of Regional Phases Recorded at NORESS and ARCESS," Proceedings of the 12th Annual DARPA/GL Seismic Research Symposium (18–20 September), Key West, Florida, 360–366, 1990.

This short paper summarizes the results presented in the third semi-annual report of this contract (see report #5 above).

7. *Sereno, T.*, "Frequency-Dependent Attenuation in Eastern Kazakhstan and Implications for Seismic Detection Thresholds in the Soviet Union," *Bull. Seismol. Soc. Am., 80*, 2089–2105, 1990.

This paper presents the attenuation results described in the first semi-annual report (report #1 above) for paths to the NRDC stations in the Soviet Union. The results are compared to those of similar studies that use data recorded in eastern North America and Scandinavia, and the implications for the accuracy of simulations that are based on attenuation in these regions are discussed.

8. *Sereno, T.*, "Frequency-Dependent Attenuation of Regional Phases Recorded at NORESS and ARCESS," *Bull. Seismol. Soc. Am.*, [in preparation], 1991.

This paper summarizes the attenuation results described in the third semi-annual report (report #5 above). We describe our inversion method that simultaneously estimates source scaling parameters, frequency-dependent attenuation of up to four seismic phases, and station corrections. This method is applied to data from nearly 100 regional events recorded at NORESS and ARCESS.

9. *Sereno, T.*, "Simulation of Detection and Location Capability of Existing and Hypothetical Seismic Networks in Eurasia," *Bull. Seismol. Soc. Am.*, [in preparation], 1991.

This paper presents the results and conclusions of this final report. It includes simulations of detection and location capability of regional seismic networks in the Soviet Union, and estimates of the number of in-country arrays and 3-component stations that are required to achieve a detection threshold of $\leq M_L$ 2.5 (e.g., the approximate magnitude of a fully-decoupled, 1-kt nuclear explosion).

1.3 Summary of "Simulation of the Detection and Location Capability of Regional Seismic Networks in the Soviet Union"

1.3.1 Introduction

In this report we estimate the detection and location capability of existing and hypothetical regional seismic networks in and around the Soviet Union. Our goal is to estimate the number of internal single stations or arrays that are required to monitor nuclear explosion testing to a threshold of 1 kt. This corresponds to an approximate magnitude of 2.5 if the explosion is fully-decoupled. Therefore, we estimate the number of internal stations that are required to achieve a detection threshold of $\leq M_L$ 2.5 for (1) any epicenter in the Soviet Union, and (2) epicenters in regions of bedded or domed salt (e.g., regions for which full-decoupling is feasible). We use estimates of the frequency-dependent attenuation and noise derived from data recorded at the NORESS and ARCESS arrays in Norway to normalize these simulations. NORESS and ARCESS were designed as prototype arrays for regional monitoring, and are located within regional distances to parts of western USSR. Therefore, the capability of these arrays provides a reasonable basis for normalizing the simulations of hypothetical networks in the Soviet Union. However, the actual attenuation and noise for the stations in our hypothetical network may be different from those in Fennoscandia, so we also determine the sensitivity of the simulations to changes in the signal and noise characteristics.

1.3.2 Approach

Our approach involves four main steps:

1. Extend *SNAP/D* to accurately represent the treaty monitoring capability of networks that include *regional* stations and arrays.
2. Normalize *SNAP/D* to the observed performance of the NORESS and ARCESS arrays.
3. Validate the normalization by comparing simulations of detection and location capability of NORESS and ARCESS to the observed performance of these arrays.
4. Extrapolate the NORESS/ARCESS results to predict the capability of hypothetical networks in the Soviet Union.

Step 1: Extend SNAP/D

SNAP/D [*Ciervo et al.*, 1985] and its predecessor, *NETWORTH* [*Wirth*, 1977], are computer programs that were designed to assess the capability of seismic networks to detect and locate seismic events. A major limitation of these programs for regional networks is that they do not include frequency-dependent signal and noise characteristics. Since the frequency of the maximum signal-to-noise ratio (*snr*) for regional signals depends on distance and wave type, these programs cannot give accurate estimates

of the detection threshold for networks that include broadband stations. In addition, these programs do not account for the fact that the noise for secondary phases (which includes the coda of earlier arrivals) depends on event size. In our third semi-annual report, we demonstrate the importance of both of these effects for regional signals recorded at NORESS and ARCESS [*Sereno*, 1990*a*]. Therefore, our extensions to *SNAP/D* include: (1) frequency dependence into the estimates for the source, attenuation, noise, and array gain, (2) a new parameterization of the signal-generated component of the noise for secondary phases in terms of the amplitude spectra and coda decay rate of earlier arrivals. This new network simulation computer program, *NetSim*, is introduced in our first annual report [*Sereno et al.*, 1990].

Step 2: Normalize SNAP/D

Most of the effort on this two-year project was spent normalizing the simulation method to the observed performance of the NORESS and ARCESS arrays. This includes estimating the frequency-dependent attenuation of regional phases, source spectra and scaling relations, noise spectra for primary and secondary phases, local site response and array gain, and azimuth and arrival time uncertainties. We developed an inversion method that simultaneously estimates source scaling parameters, frequency-dependent attenuation of up to four seismic phases, and station corrections [*Sereno*, 1990*a*]. This method was applied to data from nearly 100 events with magnitudes between 2.0 and 3.6, and epicentral distances between 200 and 1600 km. Our results for the frequency-dependent attenuation of *Pn*, *Pg*, *Sn*, and *Lg* are plotted in Figure 1.1. The signal and noise characteristics at NORESS and ARCESS were compared to those derived from a smaller data set recorded by the three NRDC stations in the Soviet Union. We find that conditions at the NRDC sites are similar to conditions in Fennoscandia, which gives confidence in extrapolating our NORESS/ARCESS results to the Soviet Union. A complete description of all of our normalization results is given in our third semi-annual report [*Sereno*, 1990*a*].

Step 3: Validate Normalization

We validate our normalization by comparing the detection and location capabilities predicted by *NetSim* to those actually achieved by NORESS and ARCESS. For example, Figure 1.2 plots a simulation of the 90% M_L threshold for NORESS and ARCESS (these are duration-based magnitudes determined by the University of Helsinki). Two phases are required for detection of events within 200 km of either array, but three phases (with at least on at each array) are required for detection of more distant events. These criteria are based on the minimum number of phases required for accurate location. The M_L threshold is 2.4–2.6 for events in mining regions near Estonia and Leningrad. These results are consistent with the results of an empirical study that compared the event bulletins produced by the University of Helsinki to detections at the NORESS and ARCESS arrays [*Bratt et al.*, 1990]. Similarly, our simulations for NORESS detection capability are in close agreement with the results of empirical studies [e.g., *Ringdal*, 1986; *Gibowicz*, 1987; *Mykkeltveit*, 1986]. Thus, we have confidence that we have accurately parameterized the attenuation and noise in this

$Pn : n(f) = 0.072 f + 1.40$

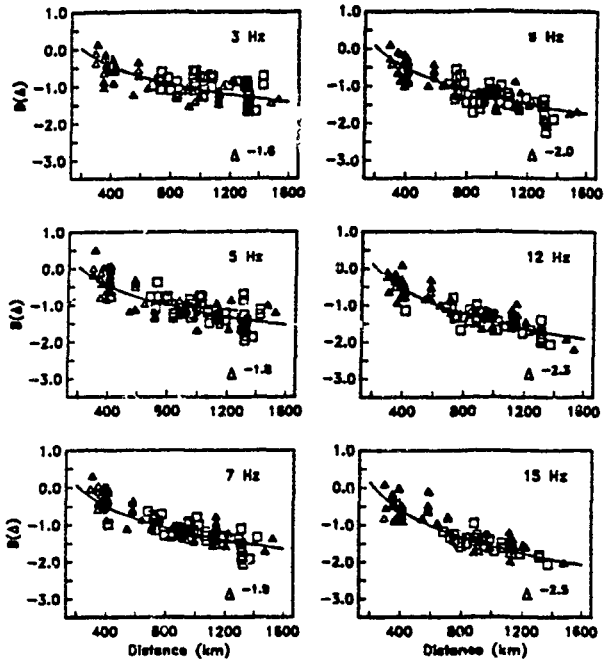

$Pg : n(f) = 0.122 f + 2.33$

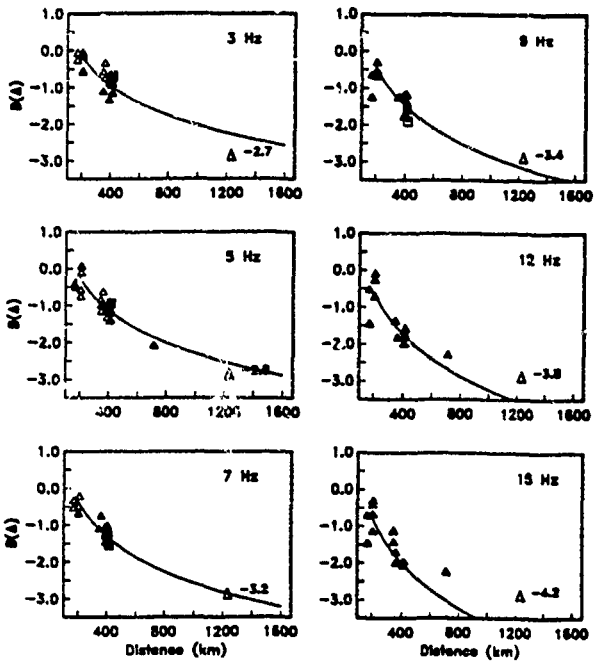

$Sn : n(f) = 0.125 f + 1.62$

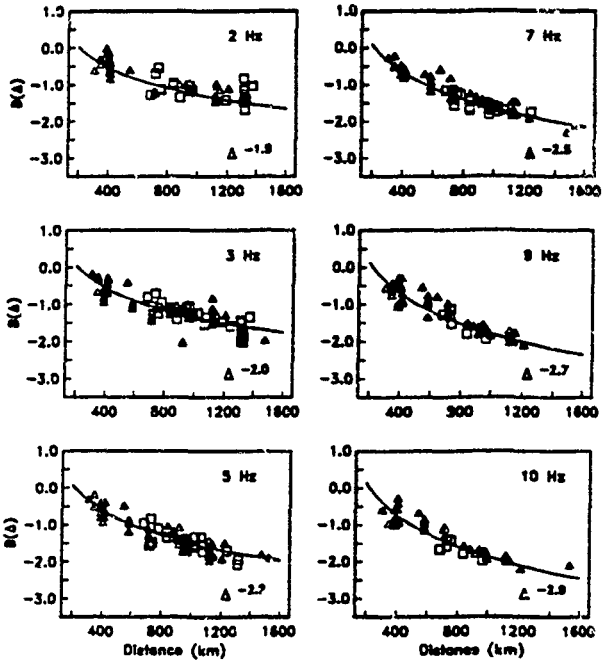

$Lg : n(f) = 0.630 f + 0.29$

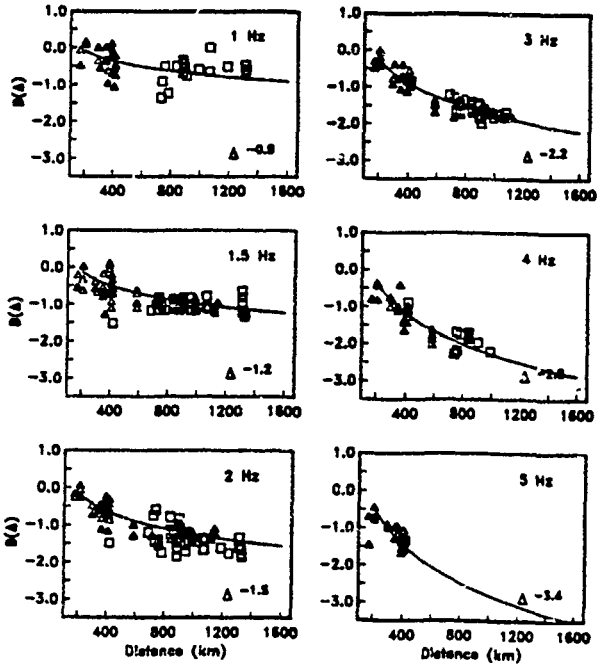

Figure 1.1. Attenuation is plotted at six frequencies for *Pn*, *Pg*, *Sn*, and *Lg*. The attenuation (geometrical spreading and anelasticity) is parameterized as $\Delta^{-n(f)}$, where $n(f)$ has a linear frequency dependence. The solid curves plot the attenuation estimated using generalized inverse techniques. Symbols are used to plot source-corrected log amplitudes (squares for NORESS data, triangles for ARCESS data).

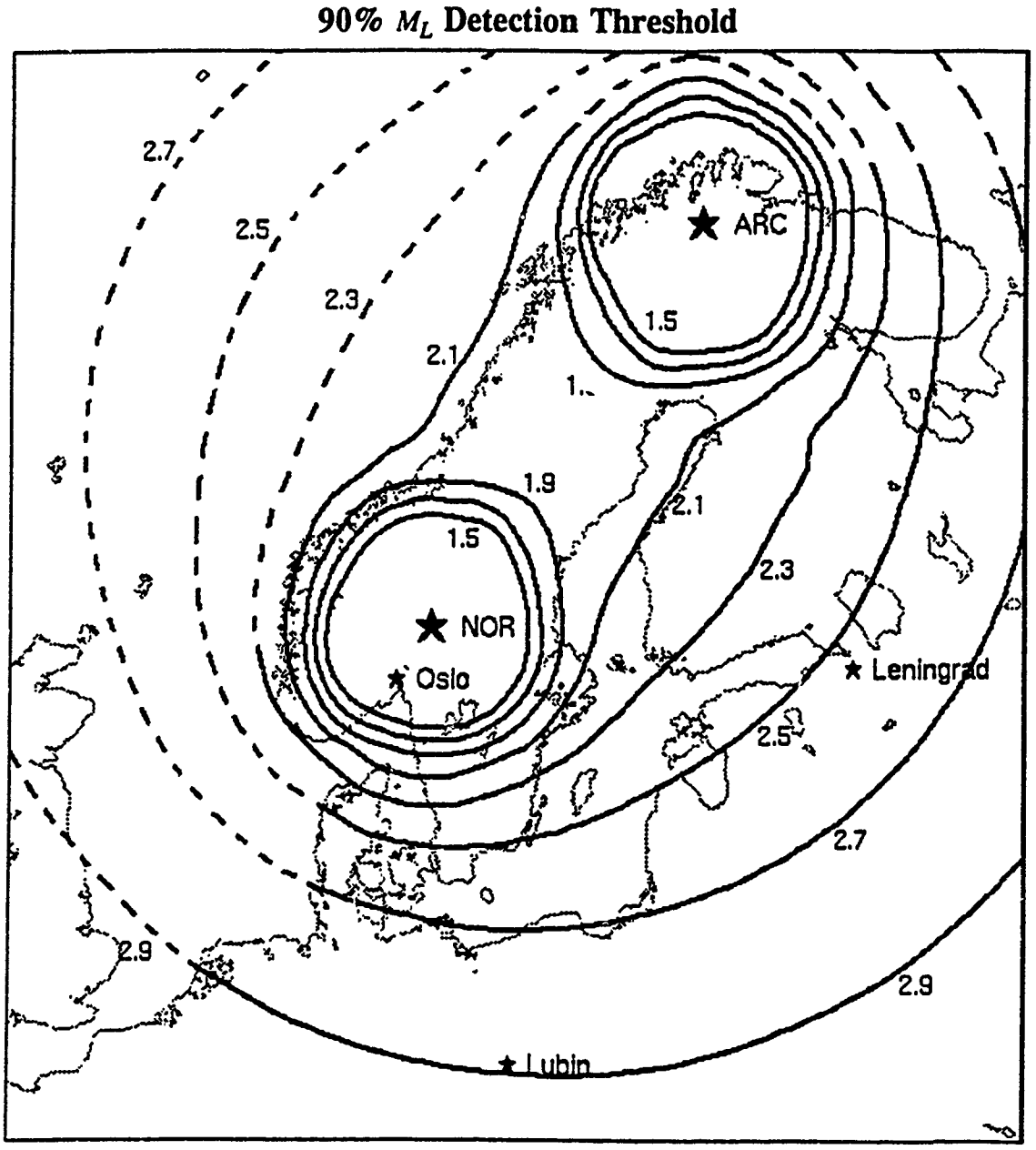

Figure 1.2. The 90% M_L detection threshold is plotted for the NORESS and ARCESS arrays. Dashed lines are used for off-shore epicenters since our normalization did not include events from these locations.

region, and that we can use the normalized simulation method to (1) determine the sensitivity of the detection thresholds to various network parameters (e.g., number of stations/arrays, noise levels, station location, etc), and (2) estimate the detection threshold for other regions with similar propagation and noise characteristics.

Step 4: Extrapolate

The main objective of this study is to assess the detection and location capability of seismic networks that include regional stations and arrays in the Soviet Union. However there are too few data recorded in the Soviet Union to form an accurate normalization. Therefore, we extrapolate the NORESS/ARCESS results to predict the capability of hypothetical networks in the Soviet Union. First, we define network performance criteria (e.g., define the goals of the monitoring network). Next, we determine the number of in-country arrays or single stations that are required to satisfy these performance criteria. Of course, conditions at NORESS and ARCESS may not accurately represent conditions within the Soviet Union, so we also determine the sensitivity of our simulations to signal and noise characteristics. These results are summarized in the next section.

1.3.3 Results

Performance Criteria

The goal of the internal network is to detect and accurately locate all nuclear explosions in the Soviet Union with yields greater than or equal to 1 kt. This corresponds to about m_b 4.0 for tamped explosions and this threshold can already be achieved with existing external networks [e.g., *OTA report*, 1988]. However, signals from these small explosions could be reduced by cavity decoupling. Experience with the testing program in the United States suggests that the approximate magnitude of a fully-decoupled 1-kt nuclear explosion is 2.5. Therefore, in this report we estimate the number of internal single stations and arrays that are required to achieve a magnitude threshold of 2.5 at the 90% confidence level for all epicenters in the Soviet Union. However, these are conservative estimates of the number of stations that are required reach the 1-kt threshold since decoupling opportunities in the Soviet Union are primarily limited to regions of bedded or domed salt [for review, see *OTA report*, 1988]. Therefore, we also estimate the number of internal stations that are required to achieve a threshold of M_L 2.5 in salt regions, while higher thresholds are accepted elsewhere.

Detection criteria are based on the minimum number of phases required to accurately locate events. We find that for the networks of arrays or 3-component stations considered here, the location uncertainty for an M_L 2.5 event is $\leq$ 20 km if we require detection of at least 3 phases involving at least 2 stations in the network. Therefore, we use this detection criterion for most of our simulations. However, since detection of secondary phases is often less reliable than detection of primary phases (e.g., due to lateral variations in the crustal wave guide), we also simulate the capability of proposed networks to detect 3 *P* phases involving 3 stations.

Seismic Networks

All of the simulations in this report use an external network of 49 existing digital stations. We use regional arrays in Europe (NORESS, ARCESS, FINESA, GERESS), and single stations from CDSN, DWWSSN, SRO, and IRIS. The objective of this study is to determine the parameters of internal networks (e.g., number stations/arrays, station locations, frequency bandwidth, etc) that satisfy the performance criteria listed above.

We consider internal networks that consist of either single stations or arrays. Of course, there are combinations of these station types that could satisfy the performance criteria, but by using one type or the other we can bound the number of stations that are required. We assume that the arrays are identical to the NORESS array (25 elements, aperture of 3 km, digitization rate of 40 samples/s), and that the single stations are identical to the 3-component IRIS stations already installed in the Soviet Union (digitization rate is 20 samples/s). We begin with an internal network that consists of 6 existing and 7 proposed IRIS 3-component stations. Next, we consider internal networks that consist of 5, 10, 20, 30, 40, and 50 approximately equally-spaced stations. Finally, we estimate the locations and number of stations required to achieve a detection threshold of M_L 2.5 in regions with bedded or domed salt.

Capability Estimates Based on Conditions in Fennoscandia

Most of the simulations in this report are normalized to the observed performance of the NORESS and ARCESS arrays in Norway. That is, we assume that the signal and noise characteristics in the Soviet Union are identical to those observed in Fennoscandia. Under this assumption, we simulated the detection capability of a network that consists of the 49 external stations and 13 internal IRIS stations. The 90% M_L threshold for detecting 3 phases involving at least 2 stations for this network is 2.0–3.5 for epicenters in the Soviet Union. This broad magnitude range is caused by the unequal geographic distribution of the IRIS stations (note that these sites were not selected to optimize monitoring performance). If we require detection of 3 P phases at 3 stations, then the 90% M_L threshold is 2.4–4.3. Thus, the proposed IRIS internal network does not satisfy the performance criteria for monitoring tests of decoupled nuclear explosions with yields as low as 1 kt.

The median value of the 90% M_L threshold for detecting 3 phases involving at least 2 stations for epicenters in the Soviet Union is plotted as a function of the number of internal single stations or arrays in Figure 1.3*a*. The median threshold for each internal network is calculated from the thresholds at 21 epicenters throughout the Soviet Union. Approximately 8 internal arrays or 20 internal single stations are required to achieve a *median* threshold of M_L 2.5. However, to achieve this threshold for all epicenters in the Soviet Union requires 10 internal arrays or 30 internal single stations. The 90% M_L detection thresholds for these networks are plotted in Figure 1.4. The threshold for the network with 10 internal arrays is 2.1–2.5 for epicenters in the Soviet Union, and it is 1.9–2.5 for the network with 30 internal single stations.

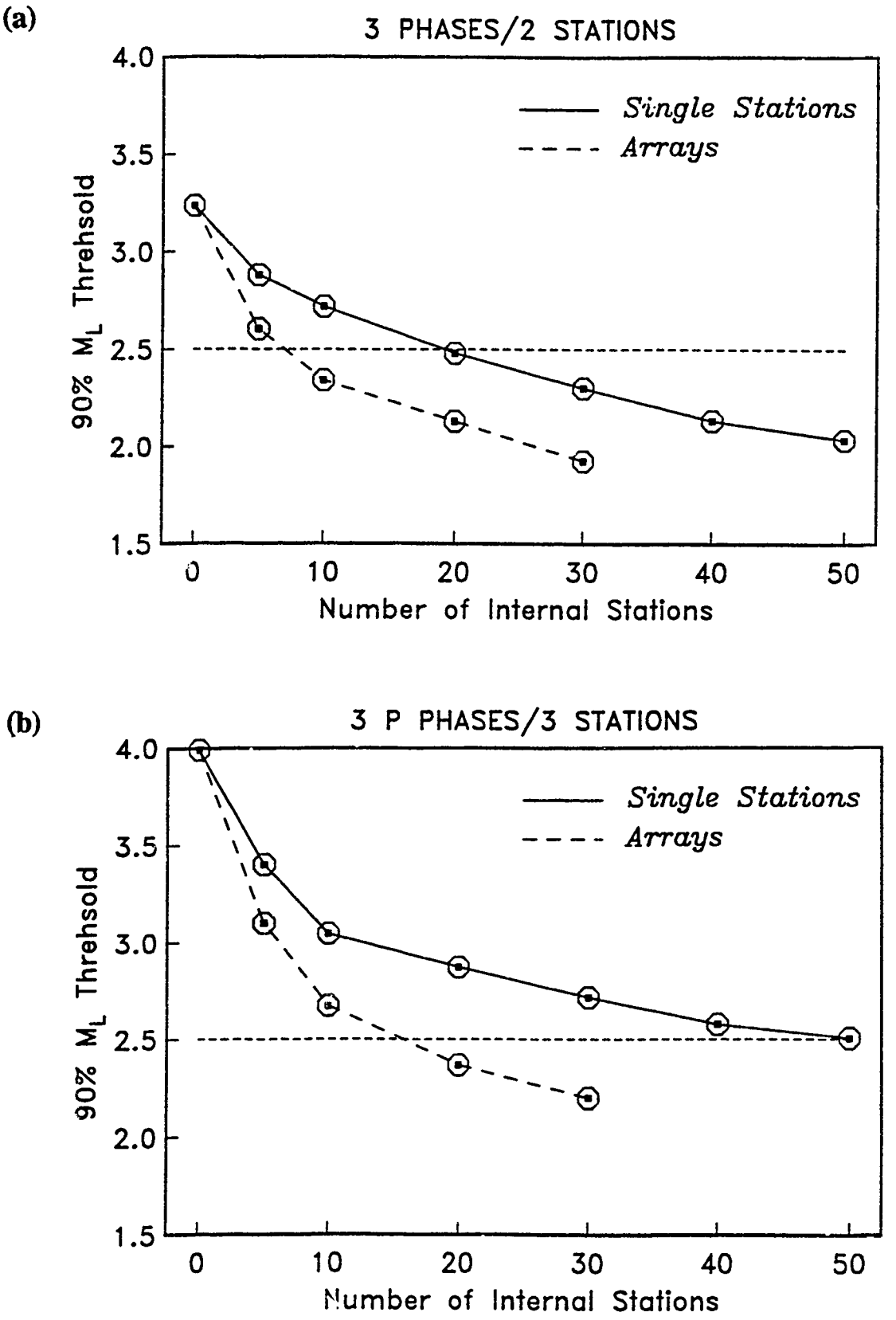

Figure 1.3. The median value of the 90% M_L detection threshold for epicenters in the Soviet Union is plotted as a function of the number of internal arrays or single stations. For detection, we require a minimum of (*a*) 3 phases and 2 stations, or (*b*) 3 *P*-type phases and 3 stations. The dashed line at M_L 2.5 indicates the goal of the monitoring network.

(a)

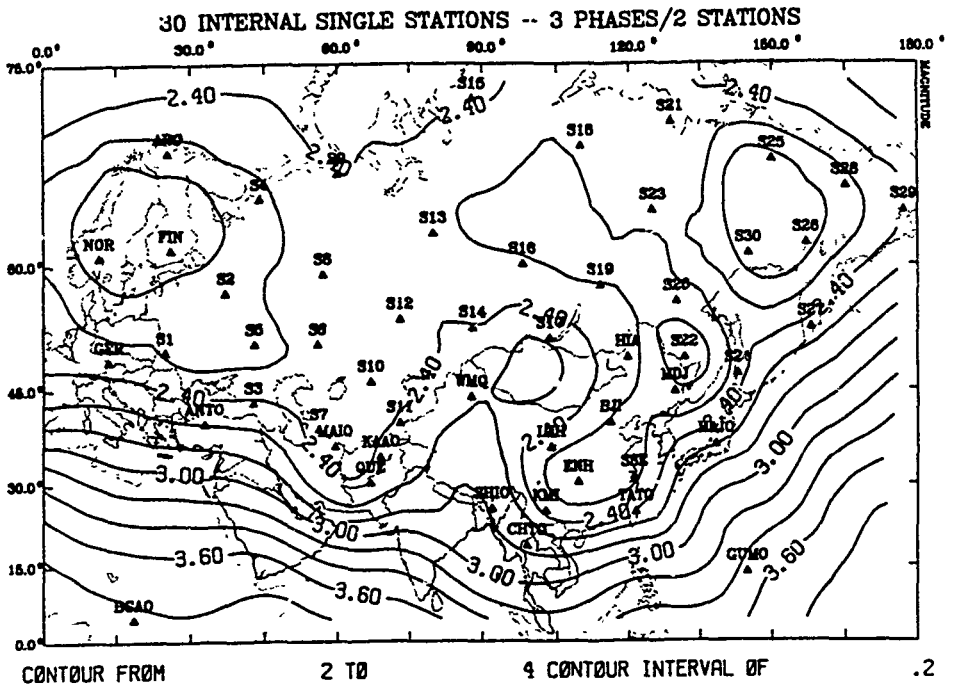

(b)

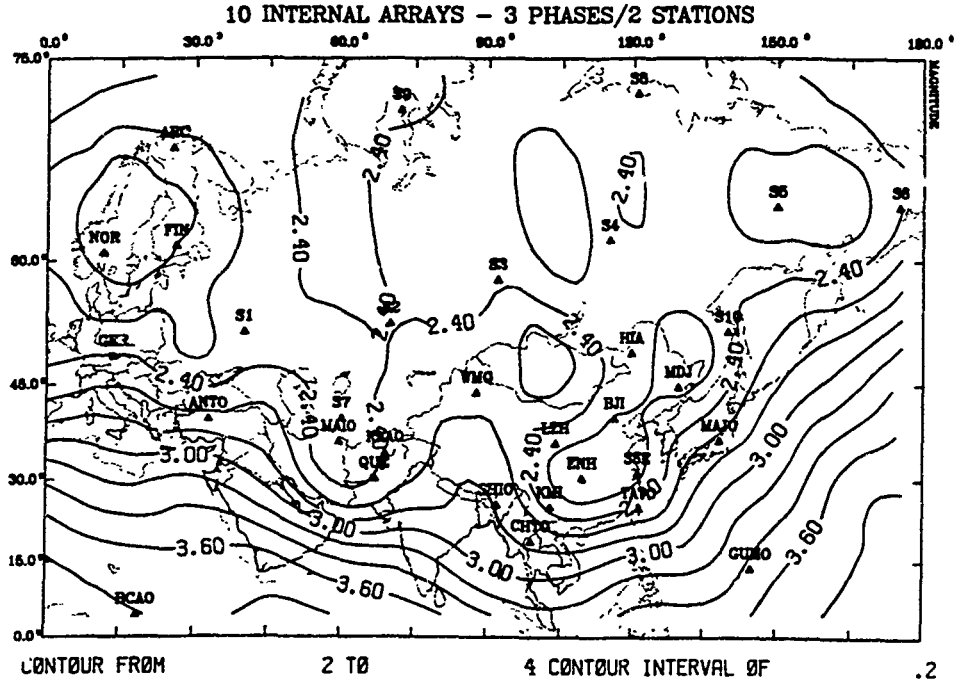

Figure 1.4. Estimates of the 90% M_L detection threshold are plotted for networks that include (*a*) 30 internal three-component stations, and (*b*) 10 internal NORESS-type regional arrays. The external network consists of 49 existing stations/arrays.

The location uncertainty for an M_L 2.5 event in the Soviet Union for either of these networks is ≤ 20 km.

Figure 1.3*b* shows the median value of 90% M_L threshold for detecting 3 *P* phases involving a minimum of 3 stations. In this case, a *median* threshold of M_L 2.5 can be achieved with 16 internal arrays or 50 internal single stations. To achieve this threshold for all epicenters requires ≥ 20 arrays, or ≥ 50 single stations (the detection threshold for 30 internal stations is 2.3–2.7). The location uncertainty for an M_L 2.5 event in the Soviet Union is ≤ 15 km for networks with either 20 internal arrays or 50 internal single stations.

The digitization rate of the internal IRIS-type single stations is 20 samples/s, which is only half of the digitization rate used for the NORESS and ARCESS arrays. However, we find no reduction in the detection threshold for the network with 30 internal single stations if we increase the digitization rate to 40 samples/s. The reason is that the threshold is controlled by the capability to detect phases at distances greater than 500 km, and the frequency of the maximum *snr* in our parameterization for all regional phases is less than 10 Hz at these distances (the spacing of the internal stations is about 800 km). Of course, there may be other advantages of higher sampling rates for nuclear explosion monitoring. For example, these higher frequencies could be useful for identifying regional events.

Opportunities for cavity decoupling in the Soviet Union are primarily limited to regions with bedded or domed salt. Therefore, the number of stations needed to achieve a detection threshold of M_L 2.5 throughout the Soviet Union is a conservative estimate of the number of stations that are required to detect a 1 kt nuclear explosion. For example, Figure 1.5 plots the 90% M_L threshold for detecting 3 phases involving at least 2 stations for a network consisting of 15 internal IRIS-type single stations. The detection threshold for this network is ≤ M_L 2.5 for epicenters in known salt regions, and it is ≤ M_L 4.0 for all other epicenters in the Soviet Union. Thus, approximately half as many single stations are required to achieve a threshold of M_L 2.5 in regions of salt than are required to achieve this threshold throughout the Soviet Union.

Noise Conditions

A key assumption used in the simulations is that the noise at each station in the network is the same as the average noise at NORESS. However, *Given* [1990] found that the ambient noise levels at the four IRIS stations in the Soviet Union (ARU, GAR, KIV, and OBN) are much higher than the ambient noise levels at NORESS. For example, she found that the noise at Obninsk (OBN) is 10–16 dB higher than the noise at NORESS between 2 and 10 Hz. Similarly, she found that the noise at Garm (GAR) is 3-4 dB higher, and that the noise at Arti (ARU) and Kislovodsk (KIV) are 5-10 dB higher than at NORESS in this frequency band. Of course, if the noise for the stations in our hypothetical network is similar to the IRIS station noise, then our estimates of the number of stations that are required to satisfy the performance criteria are too low. For example, if we use the KIV noise spectrum from *Given* [1990] in our simulations (instead of the NORESS noise spectrum), then three times as many internal single stations are required to achieve detection threshold of M_L 2.5. However, the

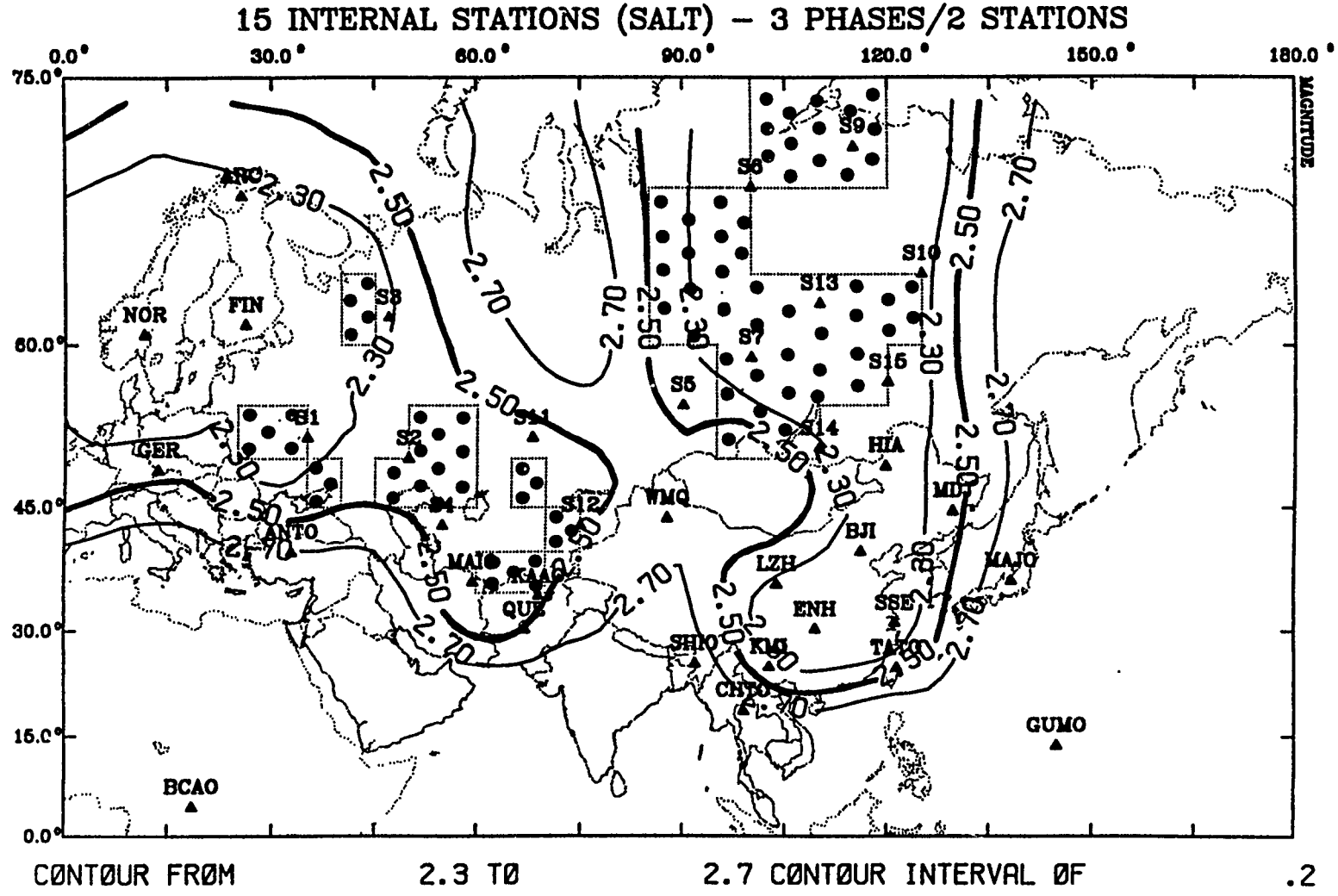

Figure 1.5. Estimate of the 90% M_L threshold for detecting 3 phases involving at least 2 stations is plotted for a network that includes 15 internal IRIS-type single stations. Only contours corresponding to M_L 2.3, 2.5, and 2.7 are shown. The dotted areas indicate regions with near-surface bedded or domed salt (this 5°×5° grid is based on a regionalization provided by W. Leith at the USGS).

noise at KIV may not represent the station noise for the internal network better than the noise at NORESS. For example, the NRDC station noise levels between 1 and 20 Hz in eastern Kazakhstan are within 2–3 dB of the noise levels at NORESS [*Sereno*, 1990*b*], and are much lower than the noise levels at the IRIS sites. The IRIS sites are in more populated regions than the NRDC stations or NORESS because they had to be close to existing communication lines for data telemetry [*Given*, 1990]. Therefore, it is likely that sites with lower noise levels could be found in more remote areas for a seismic monitoring network.

Lateral Variations in Wave Propagation

The simulations discussed so far are based on homogeneous wave propagation characteristics. However, this cannot be a good model for the propagation of regional phases in an area as large as the Soviet Union. Therefore, we developed a 5°×5° propagation grid from tectonic maps of Eurasia to approximate the effect of lateral variations. The grid includes "stable" regions (low attenuation) and "tectonic" regions (high attenuation). We use the NORESS attenuation for the "stable" regions, and we use two times the NORESS attenuation for the tectonic regions. We find that the 90% M_L threshold for detecting 3 phases involving 2 stations is 2.0–2.7 for the network with 30 internal single stations. The median value for this network is 2.4, which is only 0.1 higher than if homogeneous stable conditions are assumed (but the variation is larger).

It is well-known that *Lg* propagation can be disrupted by lateral variations in crustal structure [e.g., *Kennett*, 1986; *Baumgardt*, 1990]. Therefore, we repeated the simulation described above, but we assumed that *Lg* cannot propagate through tectonic regions. The 90% M_L threshold (including *Lg* blockage) is 2.0–2.9 for the network with 30 internal single stations. The median value of the detection threshold for epicenters in the Soviet Union is 2.5. If we use the network with 40 internal single stations, the median threshold is M_L 2.3 and the range is 2.1–2.8. It is likely that this large variation can be reduced by changing the locations of the internal stations.

Summary

The main results of this study are summarized in Table 1.1. If the signal and noise conditions in the Soviet Union are the same as those at NORESS, then 10 internal NORESS-type arrays or 30 internal IRIS-type single stations are required to achieve a detection threshold of $\leq M_L$ 2.5 for all epicenters in the Soviet Union (this is the approximate magnitude of fully-decoupled 1-kt nuclear explosion). Only half as many internal single stations are needed to reach this threshold for regions of bedded or domed salt (where opportunities for cavity decoupling are most feasible), if higher thresholds are accepted elsewhere. If secondary phases are not included in the detection criteria, then $\geq$ 20 internal NORESS-type arrays or $\geq$ 50 single stations are required to reach the M_L 2.5 threshold throughout the Soviet Union.

Table 1.1 Hypothetical monitoring networks.

Internal Network	Noise	Propagation	3 Phases/2 Stations M_L^{50}	3 Phases/2 Stations M_L^{min}–M_L^{max}	3 *P* Phases/3 Stations M_L^{50}	3 *P* Phases/3 Stations M_L^{min}–M_L^{max}
10 Arrays	NORESS	Stable	2.3	2.1–2.5	2.7	2.4–3.0
20 Arrays	NORESS	Stable	2.1	1.9–2.4	2.4	2.2–2.6
30 Arrays	NORESS	Stable	1.9	1.5–2.2	2.2	2.1–2.4
30 Single Stations	NORESS	Stable	2.3	1.9–2.5	2.7	2.4–2.8
50 Single Stations	NORESS	Stable	2.0	1.6–2.4	2.5	2.3–2.7
15 Single Stations	NORESS	Stable		2.1–2.5*		
30 Arrays	KIV	Stable	2.4	1.9–2.7		
50 Single Stations	KIV	Stable	2.5	1.9–2.9		
30 Single Stations	NORESS	Mixed	2.4	2.0–2.7		
30 Single Stations	NORESS	Mixed†	2.5	2.0–2.9		

* Thresholds given for regions of bedded or domed salt.
† Includes *Lg* blockage for tectonic regions.

More stations are required to achieve the M_L 2.5 threshold if the noise at the internal stations is assumed to be like that observed at the IRIS stations. For example, Table 1.1 shows that > 30 internal NORESS-type arrays or > 50 internal IRIS-type single stations are required to reach the M_L 2.5 threshold if the noise for the internal stations is the same as the noise at the IRIS station in Kislovodsk, USSR. However, the IRIS stations are closer to populated areas than is NORESS, and it is likely that quieter sites could be found for stations in the monitoring network. For example, the NRDC stations in eastern Kazakhstan have similar noise levels to those at NORESS, and much lower noise levels than the IRIS stations. More stations are also required to reach the M_L 2.5 threshold if we assume that regional wave attenuation is greater for tectonic regions than it is for stable regions. For example, the 90% M_L detection threshold for the network with 30 internal single stations is 2.0–2.7 if the attenuation in tectonic regions is two times higher than the attenuation in stable regions, and it is 2.0–2.9 if *Lg* is blocked by tectonic regions. However, it is likely that lower thresholds could be achieved with this same number of stations if the station locations were selected on the basis of known (or expected) lateral variations in attenuation.

The accuracy of the simulations depends on the accuracy of the normalization. We are confident that we have accurately parameterized the performance of the NORESS and ARCESS arrays in Norway, but there is still much uncertainty in extrapolating these capabilities to networks in the Soviet Union. The accuracy of the normalization can be improved as experience is gained from new stations installed in the Soviet Union. Once enough new data has been collected and analyzed, the capability of the hypothetical networks should be re-evaluated.

1.4 Outline of the Report

This report is divided into nine sections including this summary and the conclusions. Sections 2 and 5–9 present the new results from the third project task, and sections 3

and 4 review our earlier results. The seven main technical sections address the following issues:

- **Section 2.** Performance criteria are defined for seismic networks to monitor underground nuclear explosion testing in the Soviet Union.

- **Section 3.** Our method for simulating the performance of regional seismic networks is reviewed (for a detailed description, see report #4 above).

- **Section 4.** The normalization based on data recorded at NORESS and ARCESS is reviewed. This includes our estimates for source scaling, and frequency-dependent attenuation and noise (for a detailed description, see report #5 above).

- **Section 5.** The parameters of the external and internal seismic networks are described (e.g., number of stations, arrays vs. single stations, sample rate, etc).

- **Section 6.** Simulations of the detection and location capability of existing and proposed seismic networks are presented. These simulations are based on signal and noise characteristics in Fennoscandia. Trade-offs among the number of arrays versus single stations required to satisfy the performance criteria in Section 2 are discussed.

- **Section 7.** The sensitivity of our simulations to our assumptions regarding the ambient noise in the Soviet Union is discussed. We repeat some of the simulations in Section 6 after replacing the noise for Fennoscandia with an estimate of the average noise recorded at one of the IRIS stations in the Soviet Union.

- **Section 8.** The effects of lateral variations in wave propagation are investigated. We use a 5°×5° grid that is based on a tectonic map of Eurasia to define areas of low attenuation (stable) and high attenuation (tectonic).

2. PERFORMANCE CRITERIA

The main purpose of establishing a network of seismic stations inside the Soviet Union is to improve the capability to monitor underground nuclear explosion testing. Existing external networks can reliably detect and locate events with $m_b \geq 4.0$ [e.g., *OTA report*, 1988]. This is the approximate magnitude of a tamped nuclear explosion with a yield of 1 kt. However, signals from these small explosions could be reduced by cavity decoupling. Experience with the testing program in the United States suggests that the approximate magnitude of a fully-decoupled 1-kt nuclear explosion is 2.5. This is below the threshold of external networks, and in-country stations are required to monitor testing at this level. The goal of this study is to estimate the parameters of internal networks (e.g., number of stations/arrays, frequency bandwidth, station locations, etc) that can detect and accurately locate all nuclear explosions in the Soviet Union with yields greater than or equal to 1 kt. Of course, it is possible to achieve lower detection thresholds with more extensive internal networks, but there is little evidence to suggest that smaller nuclear explosions could be differentiated from the large number of earthquakes and mining explosions of comparable magnitude. Data recorded by a less extensive internal network could be used to determine the feasibility of monitoring at thresholds less than 1 kt.

We define the following performance criteria for internal networks based upon a 1-kt threshold:

1. Probability of detection (for the network) $\geq 90\%$.
2. Detection threshold for the network is $\leq M_L$ 2.5 for all epicenters in the Soviet Union.
3. Location uncertainty for an M_L 2.5 event is ≤ 20 km at the 90% confidence level for all epicenters in the Soviet Union.

The detection criteria are based on the minimum number of phases required to accurately locate events. We find that for the networks of arrays or 3-component stations considered here, the location uncertainty for an M_L 2.5 event is ≤ 20 km if we require detection of at least 3 phases involving at least 2 stations in the network (see Section 6.2). Therefore, we use this detection criterion for most of our simulations. However, since detection of secondary phases is often less reliable than detection of primary phases (e.g., due to lateral variations in the crustal wave guide), we also simulate the capability of proposed networks to detect 3 *P* phases involving 3 stations.

Decoupling opportunities in the Soviet Union are primarily limited to regions of bedded or domed salt [for review, see *OTA report*, 1988]. Therefore, the number of in-country stations or arrays that are required to satisfy the criteria listed above is a conservative estimate of the number of stations that are required reach the 1-kt threshold. Therefore, we also estimate the number of internal stations that are required to achieve a threshold of M_L 2.5 in salt regions, while higher thresholds are accepted elsewhere (Section 6.4).

(THIS PAGE INTENTIONALLY LEFT BLANK)

3. NETWORK CAPABILITY ASSESSMENT

The simulations of detection and location capability presented in this report were computed using a program called *NetSim* that we developed under support from this contract [*Sereno et al.*, 1990]. *NetSim* is based on the Seismic Network Assessment Program for Detection [*SNAP/D*; *Ciervo et al.*, 1985], and it reuses much of the original software. The main purpose for developing *NetSim* was to include frequency dependence into the estimates for the source, attenuation, noise, and array gain. A major limitation of *SNAP/D* [*Ciervo et al.*, 1985] and its predecessor, *NETWORTH* [*Wirth*, 1977], for regional networks is that they do not include frequency-dependent signal and noise characteristics. Since the frequency of the maximum signal-to-noise ratio (*snr*) for regional signals depends on distance and wave type, these programs cannot give accurate estimates of the detection threshold for regional networks that include broadband stations.

Another limitation of previous simulation methods is that they do not account for the fact that the noise for secondary phases (which includes the coda of earlier arrivals) depends on event size. We show that this is very important for *Lg* phases recorded at NORESS and ARCESS in Section 4.5. Therefore, *NetSim* uses a new parameterization of the noise for secondary phases that accounts for the distance and magnitude dependence of the signal-generated component of the noise. We define the "noise" for secondary phases as the sum of ambient noise and signal-generated noise. The signal-generated noise is approximated as the signal spectrum of an earlier arrival multiplied by a scaling factor that depends on distance (e.g., coda decay rate). The details of this parameterization are described in our annual report [*Sereno et al.*, 1990].

Figure 3.1 is a top-level data flow diagram for *NetSim*. There are five categories of input data: control, source, propagation, noise and site/station. In general, each category includes several input data types (indicated by the smallest boxes in Figure 2.1). The control data determine what type of calculations are to be performed (e.g., detection thresholds, probability of detection for fixed event size, location uncertainties). Other data in this category include the detection criteria (e.g., waves and number of stations required for detection) and the frequencies at which to perform the calculations. The source data are used to calculate the excitation of each wave as a function of frequency and source medium. These data include an epicenter grid, source scaling relations, excitation factors for each wave, and source spectra as a function of event size. The propagation data include frequency-dependent attenuation, amplitude variance, and travel time tables for each wave and path medium (e.g., stable or tectonic). The noise data include the ambient noise power spectral density for each station in the network, and estimates of the coda decay rates that are used to calculate noise spectra for secondary phases. The site/station data include the local site response, frequency-dependent array gain, *snr* thresholds required for detecting each wave, station coordinates, and station reliability. Determination of the input parameters for *NetSim* constitutes the normalization. We discuss this normalization based on data recorded at NORESS and ARCESS in Section 4.

The output of *NetSim* includes detection thresholds and probabilities, and/or location uncertainties. The detection module has two options. It can be used to calculate the detection threshold of the network at a fixed confidence level (these thresholds are

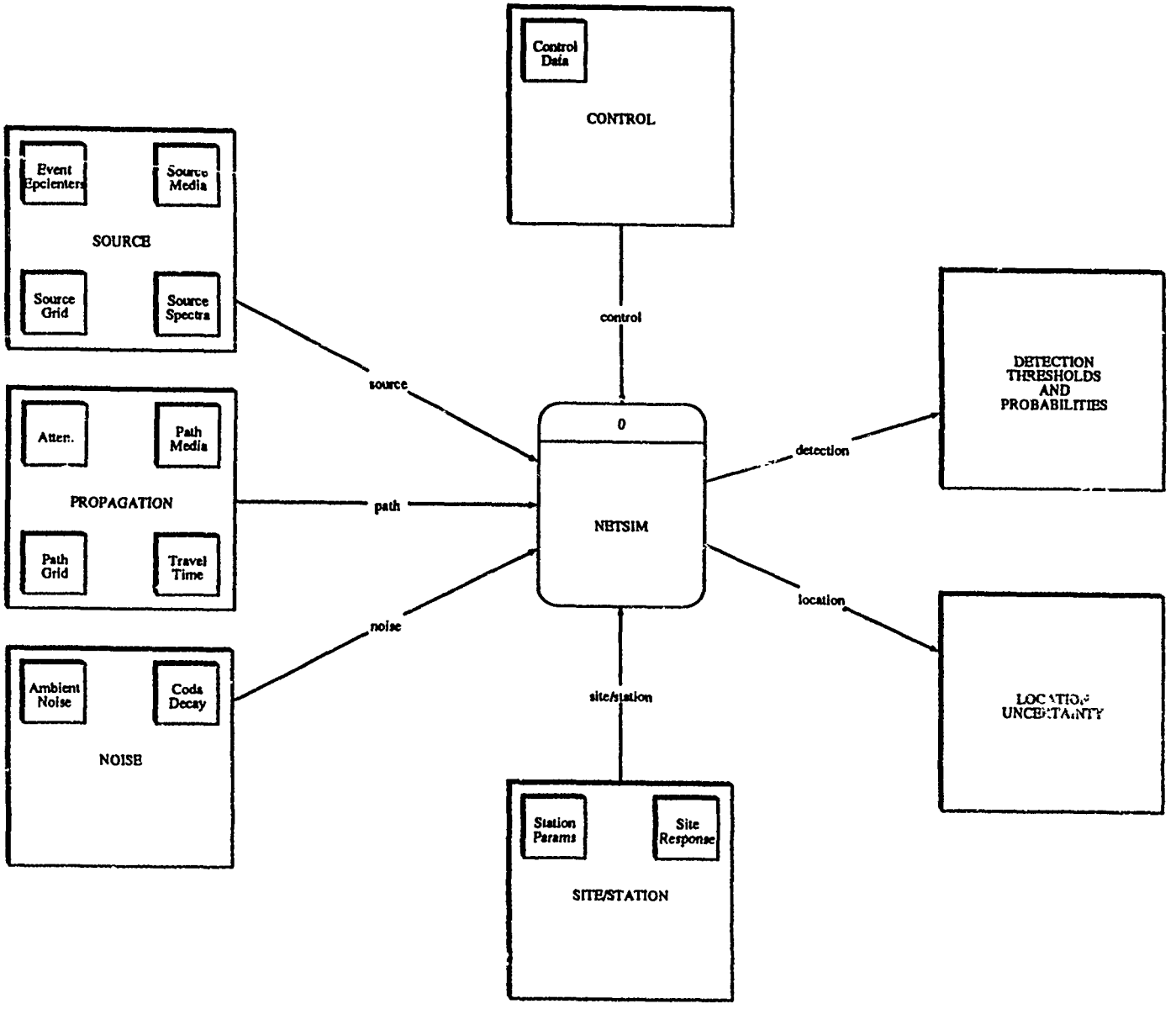

Figure 3.1 Top-level data flow diagram for *NetSim*.

determined by varying the event size until the detection probability of the network equals the desired confidence level), or it can calculate the probability that the network will detect an event of fixed size. First, the signal and noise amplitudes for each wave, station, epicenter, and frequency are calculated. The frequency of the maximum *snr* is determined, and the *snr* at this frequency is used to calculate the probability of detection at individual stations. The individual station probabilities are combined to determine the probability of detection for the network [*Ciervo et al.*, 1985].

The location module also has two options. It can be used to calculate location uncertainties for a fixed event size (the option used in this report), or it can be used to calculate location uncertainties at the detection threshold of the network. This module calculates the length of the semi-major and semi-minor axes of the epicenter location error ellipse, and the depth uncertainty. It is based on the *TTAZLOC* location program of *Bratt and Bache* [1988], and uses estimates of both arrival time and azimuth standard deviation to estimate the location uncertainty. We use the *probability-weighted* approach of *Ciervo et al.* [1985], whereby the standard deviation for each datum, σ, is is increased by a factor that depends on the probability of detection, P_{ijk}. The effective standard deviations ($\sigma/\sqrt{Pijk}$) are increased for phases with low probability of detection, and therefore these phases do not contribute much to constraining the event hypocenter. Detailed descriptions of the location algorithm are given by *Bratt et al.* [1987], *Bratt and Bache* [1988], and *Sereno et al.* [1990].

(THIS PAGE INTENTIONALLY LEFT BLANK)

4. NORMALIZATION

Estimates of the frequency-dependent attenuation and noise derived from data recorded by the NORESS and ARCESS arrays in Norway are used to normalize the simulations. NORESS and ARCESS are prototype arrays for regional monitoring, and are within regional distances to parts of western USSR. Therefore, the capability of these arrays provides a reasonable basis for normalizing the simulations of hypothetical networks in the Soviet Union. However, these simulations have large uncertainty since it is not known how well conditions in Fennoscandia represent stations in our hypothetical network. Therefore, we used data recently recorded by stations in the Soviet Union to test the validity of extrapolating our results for Fennoscandia. These data were recorded by three stations that were deployed in eastern Kazakhstan as part of a joint experiment involving the National Resources Defense Council (NRDC) in the United States and the Academy of Sciences in the Soviet Union [e.g., *Berger et al.*, 1988]. We found that conditions at the NRDC sites are similar to conditions in Fennoscandia, which gives confidence in extrapolating our NORESS/ARCESS results to the Soviet Union [*Sereno*, 1990*b*].

The normalization includes estimates of source, propagation, noise, and site parameters. We estimate source and attenuation parameters by inverting spectra from up to four regional phases recorded by NORESS and ARCESS. This method is briefly described in Section 4.1. Spectra from 97 regional events with M_L between 2.0 and 3.6, and epicentral distances between 200 and 1600 km are used in the inversion. These data are described in Section 4.2. The results of the inversion for source scaling are described in Section 4.3, and the attenuation results are described in Section 4.4.1. The normalization parameters required for location capability are arrival time and azimuth uncertainty. We use data from over 400 regional events that are stored in an on-line relational database produced by the *Intelligent Monitoring System* (*IMS*) at the Center for Seismic Studies. Our estimates of these parameters are given in Section 4.4.2. Section 4.5 gives estimates of the ambient noise spectrum at NORESS, and the coda decay rates used to calculate the signal-generated noise for secondary phases. The local site and station parameters are given in Section 4.6 (e.g., beam gain, *snr* thresholds required for detection of each wave). We validate the normalization by comparing simulations for NORESS and ARCESS to the observed performance of these arrays. These comparisons are discussed in Section 4.7.

4.1 Method

Frequency-dependent attenuation and source parameters are estimated from regional wave spectra recorded at NORESS and ARCESS using generalized inverse techniques. In a previous project we used a similar method to estimate *Pn* and *Lg* attenuation for paths to NORESS [*Sereno et al.*, 1988]. However, it was not possible to resolve trade-offs among source and attenuation parameters using data recorded by only one station. In this study, parameter trade-off resolution is improved by including spectra from up to four phases recorded by two arrays. This new method is described briefly here, a detailed description is given by *Sereno* [1990*a*].

The instrument-corrected amplitude spectrum $A_{ijk}(f)$ of the *kth* wave recorded at the *ith* station from the *jth* source is parameterized as

$$\log A_{ijk}(f) = \log A^0_{jk}(f) + B_k(\Delta_{ij}, \Delta^0, f) + \delta_{ik} \tag{4.1}$$

where $A^0_{jk}(f)$ is the amplitude spectrum at a reference distance Δ^0, $B_k(\Delta_{ij}, \Delta^0, f)$ is the frequency-dependent attenuation from the reference distance to the epicentral distance Δ_{ij}, and δ_{ik} is a station correction. The amplitude A^0_{jk} is expressed in terms of source parameters as

$$\log A^0_{jk}(f) = \log S_{0j} + \log s_j(f) + \log \kappa_k + \gamma_k \log f \tag{4.2}$$

where S_{0j} is the long-period level (proportional to seismic moment), $s_j(f)$ is the shape of the source spectrum, κ_k is a wave-dependent excitation factor, and γ_k accounts for different pulse shapes of crustal and mantle phases at the reference distance. For example, if the reference distance is close to the critical distance, then *Pn* and *Sn* can be approximated as head waves at Δ^0 and their pulse shapes are integrals of the direct or turning rays [e.g., *Aki and Richards*, 1980]. Therefore, γ_k is set to -1 for *Pn* and *Sn*, and it is set to zero for *Pg* and *Lg*.

The source spectrum is assumed to decay as f^{-2} beyond a corner frequency that scales inversely with the cube root of the long-period level [*Mueller and Murphy*, 1971]. Seismic moment M_0 can be estimated from the long-period level using

$$M_0 = \frac{S_0 \, 4\pi \, (\rho_s \, \rho_r \, v_s^5 \, v_r)^{1/2} \, G(\Delta^0)}{F \, R \, V} \tag{4.3}$$

where F is the free-surface amplification, R is the radiation pattern, V is the vector wavefield decomposition, ρ_r and ρ_s are the densities at the receiver and source, respectively, v_r and v_s are the compressional wave velocities at the receiver and source, respectively, and $G(\Delta^0)$ is the geometrical spreading at the reference distance.

The attenuation is parameterized in terms of a power law distance dependence with a frequency-dependent exponent. Our previous parameterization included separate terms for geometrical spreading and anelasticity [*Sereno et al.*, 1988]. That is, we assumed that the geometrical spreading was independent of frequency and that it could described by a power law distance dependence. However, the geometrical spreading of *Pn* and *Sn* are known to be frequency dependent even for very simple models of the upper mantle [e.g., *Sereno and Given*, 1990]. Since this complicated geometrical spreading is not accurately known for regional phases and separating it from anelasticity is not necessary to simulate detection capability, we parameterize the total attenuation (both geometrical spreading and anelasticity) as

$$B_k(\Delta_{ij}, \Delta^0, f) = -\log e \; \alpha^0_k f + n_k(f) \log(\Delta^0_k / \Delta_{ij}) \tag{4.4}$$

$$n_k(f) = a_k f + b_k \tag{4.5}$$

where the first term in (4.4) accounts for anelastic attenuation from the source to the reference distance, and the second term describes the total attenuation from the

reference distance to Δ_{ij}. *Chun et al.* [1989] used a similar parameterization to describe *Pn* attenuation in the Canadian Shield.

The source parameters estimated by the inversion are the long-period level for each event, S_{0j}, a corner frequency scaling parameter (which relates corner frequency and long-period level for all events in the data set), and the excitation factor for each wave, κ_k. The attenuation parameters for each wave are α_k^0, a_k and b_k from (4.4) and (4.5). The station corrections are determined relative to a reference station. The absolute corrections are obtained by applying the constraint that the sum of the station corrections is zero for each wave.

4.2 Data

The data are array-averaged log amplitude spectra for regional phases recorded at NORESS and ARCESS from 97 events that occurred between November 1987 and April 1988. The magnitudes range from 2.0 to 3.6, and the epicentral distances are 200 to 1600 km. There are 82 mining explosions, 3 earthquakes, and 12 events with unknown origin (these are probably explosions).

In most cases, the *Pn*, *Pg*, and *Sn* spectra are computed for a 10-s window starting 0.3 s before the arrival time. For the close events where *Pn* and *Pg* or *Sn* and *Lg* arrive within the same 10-s window, the *Pn* and *Sn* spectra are computed for a shorter time window that depends on group velocity to exclude the later phase. The *Lg* spectra are computed for a fixed group velocity window 3.0–3.6 km/s. A 10% cosine taper is applied to each vertical component waveform prior to computing the spectra. The frequency bands considered are 1–15 Hz for *Pn* and *Pg*, 1–10 Hz for *Sn*, and 0.5–7 Hz for *Lg*. However, the *snr* is required to be above a pre-selected threshold for each phase. This threshold is 3.5 dB for *Pn* and *Sn* and 2.0 dB for *Pg* and *Lg*. The spectra are sampled every 0.25 Hz for each phase. The total number of data used in the inversion is 10,801, and the number of parameters is 114.

4.3 Source Scaling

Seismic moment is plotted versus M_L in Figure 4.1*a*. The solid line indicates the least-squares linear fit, assuming the slope is one. Seismic moment is estimated from the long-period level using (4.3) and assuming the near-surface density is 2500 kg/m^3, the compressional-wave velocity is 5000 m/s, $G(\Delta^0) = \Delta^0$, and $F\ R\ V = 1$. This gives $\log M_0 = M_L + 17.2$, which is generally consistent with results obtained from near-field studies [e.g., *Bungum et al.*, 1982; *Hasegawa*, 1983]. The corner frequency of an M_L 3.0 event is estimated to be 9 Hz (assuming cube root scaling). Figure 4.1*b* plots a family of source spectra for M_L between 2.0 and 4.0 based on this parameterization. These spectra are used to normalize the simulations in the following sections.

The wave-dependent excitation factors ($\log \kappa_k$) are 0.10 for *Pg*, 0.41 for *Sn*, and 0.82 for *Lg* (it is set to zero for *Pn*). If the source generates both compressional and shear waves, then the amplitude of the shear waves should be about a factor of five greater than the amplitude of the compressional waves (e.g., assuming that the compressional wave velocity at the source is a factor of $\sqrt{3}$ larger than the shear wave

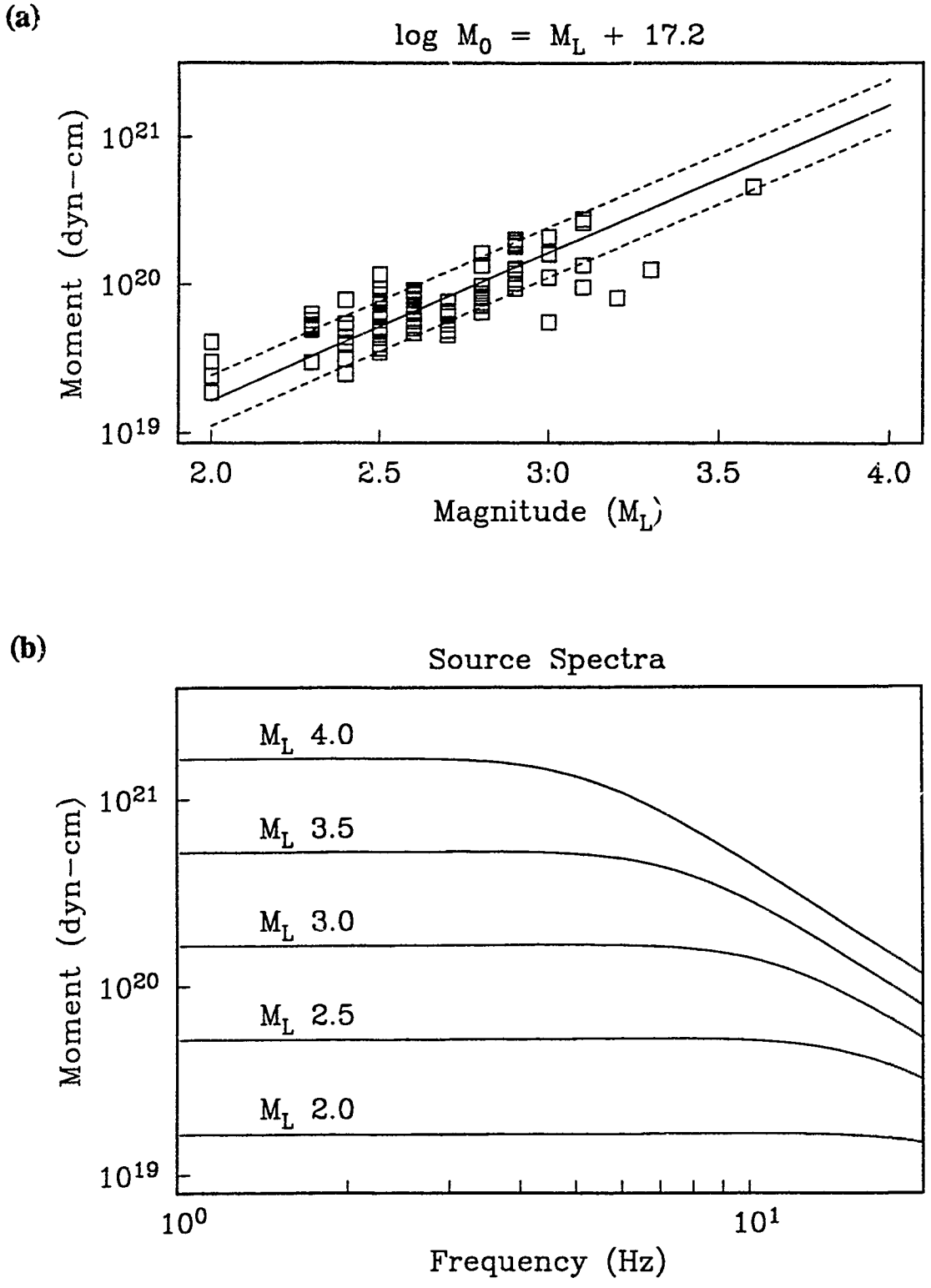

Figure 4.1. (*a*) Source moment is plotted versus the local magnitude determined by the University of Helsinki. The line indicates the least-squares fit for a slope of one, and the dashed lines indicate one standard deviation. (*b*) Source spectra based on the inversion results are plotted for five magnitudes between M_L 2.0 and M_L 4.0.

velocity). This gives log κ equal to 0.7 for shear phases. Our estimate for log κ_{Sn} is less than this, and our estimate for log κ_{Lg} is slightly greater than this. However, most of the events used in the inversion are mining explosions with unknown radiation patterns and surface velocity, so deviations in log κ of this order are not surprising.

4.4 Propagation Characteristics

The propagation characteristics needed to simulate detection capability include frequency-dependent attenuation of regional phases and amplitude variance, and those needed to simulate location capability include arrival time and azimuth uncertainty. Section 4.4.1 gives estimates of the frequency-dependent attenuation and amplitude variance of regional phases derived by inverting NORESS and ARCESS spectra. Section 4.4.2 gives estimates of the arrival time and azimuth uncertainty for array stations based on analysis of data produced by the *IMS*.

4.4.1 Attenuation

The attenuation and amplitude variance estimates obtained by inverting the NORESS and ARCESS spectra are summarized in Table 4.1. Figure 4.2 plots the attenuation $B(\Delta)$ for each each wave at several frequencies. *Lg* attenuation has the strongest frequency dependence, and *Pg* attenuates more rapidly with distance than the other phases. Note that meaningful estimates of *Pg* attenuation are obtained from relatively few data because the source parameters are constrained by spectra for other phases. Also, *Sn* attenuates more rapidly with distance than *Pn*, and it has a stronger frequency dependence. The attenuation estimates for *Pn* and *Lg* presented here are lower than the preferred model presented in an earlier paper where a similar method was used for data recorded at one array [*Sereno et al.*, 1988]. However, this preferred model was one of a suite of models that fit the data with nearly equal fidelity. Other models in this suite have lower attenuation and lower source amplitudes, and are more similar the model derived here using data from two arrays.

Table 4.1 Attenuation parameters and signal standard deviation.

Phase	# Data	σ^*	Δ^0† (km)	α^0 (s)	$n(f) = af + b$ a	b
Pn	5827	0.26	200	-0.02	0.072	1.40
Pg	954	0.25	200	0.11	0.122	2.33
Sn	2595	0.19	200	-0.03	0.125	1.62
Lg	1425	0.28	200	0.19	0.630	0.29

* Standard deviation of log amplitude.
† Fixed value.

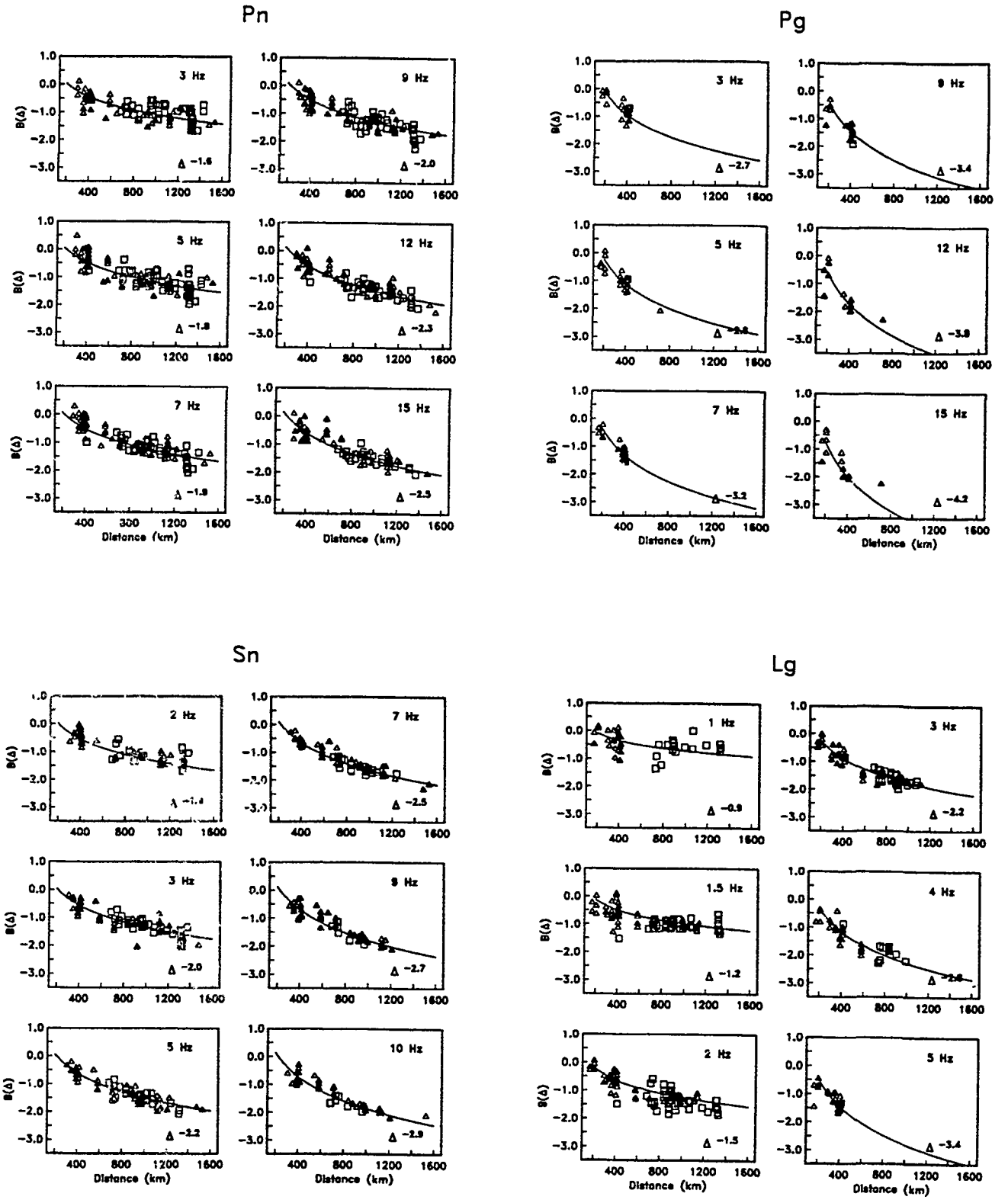

Figure 4.2. Attenuation is plotted at six frequencies for *Pn*, *Pg*, *Sn*, and *Lg*. The attenuation (geometrical spreading and anelasticity) is parameterized as $\Delta^{-n(f)}$, where $n(f)$ has a linear frequency dependence. The solid curves plot the attenuation estimated using generalized inverse techniques. Symbols are used to plot source-corrected log amplitudes (squares for NORESS data, triangles for ARCESS data).

The regional wave attenuation curves described above are used in our simulations to a distance of 20°. Beyond that, we use the 1-Hz amplitude versus distance curve for *P* phases derived by *Veith and Clawson* [1972]. We extend this curve to higher frequencies by assuming t^* ($=t/Q$) is equal to 1 s. We extrapolate our *Sn* results for NORESS and ARCESS to teleseismic distances, and we assume that *Pg* and *Lg* do not propagate to distances greater than 25°. These attenuation estimates for teleseismic distances are more uncertain than our estimates for regional distances. However, the detection thresholds for networks that satisfy the performance criteria in Section 2 are insensitive to the assumed attenuation at teleseismic distances.

4.4.2 Arrival Time and Azimuth Uncertainty

Azimuth and arrival time uncertainty are estimated for regional arrays using data from over 400 events recorded at NORESS and ARCESS between October 1989 and March 1990 [*Sereno*, 1990*a*]. Azimuth uncertainty is estimated by comparing the azimuth measured using a wide band $f-k$ method [*Kvaerna and Doornbos*, 1986] to the station-to-event azimuth determined from the *IMS* event location (after analyst review). We used a similar method to estimate arrival time uncertainty, but we found that these estimates were biased low (particularly for *P* phases) since these data are important for constraining the *IMS* event location. Therefore, we also used the arrival time difference between NORESS and ARCESS for mining explosions with accurate locations determined from satellite imagery to estimate the uncertainty. The use of arrival time difference between two stations eliminates the need for accurate estimates of event origin time, and it facilitates separation of measurement error (from the consistency of arrival time difference for repeated events in the same mine) from modeling error (by comparing the mean arrival time difference between NORESS and ARCESS for each mine to the theoretical arrival time difference based on travel time tables for Fennoscandia). These results are described in detail by *Sereno* [1990*a*].

Table 4.2 Arrival time and azimuth uncertainty.

Phase	σ_t (s)	Arrays σ_a (°)	3-C Stations σ_a (°)
Pn	0.7	7.0	14.0
Pg	0.7	5.9	12.0
Sn	2.1	7.0	–
Lg	2.4	7.1	–

Table 4.2 lists our results for the arrival time standard deviation, σ_t, and azimuth standard deviation, σ_a, for array stations. The azimuth standard deviation is close to 7° for all four regional phases. We do not include the modeling error in the arrival time standard deviations in Table 4.2 since these could be reduced (or eliminated) by path-specific corrections. Including the modeling errors increases the *Pn* arrival time

standard deviation to about 1.0 s, but it only increases the *Sn* and *Lg* arrival time standard deviations by 0.1 s.

We assume that the arrival time standard deviation is the same for three-component stations as it is for array stations. However, the *effective* standard deviation used in the simulations is equal to the standard deviation in Table 4.2 divided by the square root of the probability of detection (Section 3). Therefore, the *effective* standard deviation is larger for 3-component stations than it is for arrays since the probability of detection is lower for a 3-component station.

Several recent studies have investigated the performance of 3-component stations for estimating azimuth from regional data [e.g., *Jurkevics*, 1988; *Jarpe and Dowla*, 1989; *Harris*, 1990; *Suteau-Henson*, 1990]. *Jurkevics* [1988] used data from 93 regional events to estimate the *Pn* azimuth standard deviation. Using data from four 3-component stations in the NORESS array, he estimates the *Pn* azimuth standard deviation to be 10°–12°. *Suteau-Henson* [1990] used data from 68 regional events to estimate a *P*-wave azimuth standard deviation of 14° for the 3-component elements of the NORESS array (this data set included 48 events from the center array element, and 20 events from an element on the C-ring). Based on these results, we assume that the azimuth standard deviation for *P* phases is two times larger for a single 3-component station than it is for an array (Table 4.2). Azimuth estimates from 3-component data have much higher uncertainty for regional *S* phases than for *P* phases [e.g., *Jurkevicz*, 1988; *Jarpe and Dowla*, 1989; *Suteau-Henson*, 1990]. For this reason, we assume that azimuth cannot be estimated with confidence from secondary phases recorded by 3-component stations.

4.5 Noise

An estimate of the average ambient noise spectrum at NORESS is used in the normalization (except in Section 7 where we investigate the sensitivity of the results to our assumptions about station noise). Figure 4.3 plots the mean and average standard deviation of the ambient noise power spectrum at NORESS computed from 78 five-second time windows taken prior to *Pn*. The ambient noise at NORESS has been extensively studied by others, and the spectrum in Figure 4.3 is generally consistent with the results of these previous studies [e.g., *Bungum et al.*, 1985; *Fyen*, 1986, 1987; *Suteau-Henson and Rache*, 1988].

Detection of secondary phases depends on the ambient noise and the level of the coda of earlier arrivals. *Rivers et al.* [1985] compiled "noise" estimates to be used in simulations with the original *SNAP/D* program. The noise level for secondary phases was simply assumed to be 2.5 times the ambient noise level. However, this simple approximation does not properly account for the magnitude and frequency dependence of the signal-generated coda which contributes to the "noise." A simple approximation that does account for these dependencies is that the signal-generated noise for secondary phases is equal to the signal spectrum of an earlier arrival multiplied by a scaling factor that depends on distance. This is the approximation used by our network simulation program, *NetSim*, to determine the noise levels for secondary phases [*Sereno et al.*, 1990].

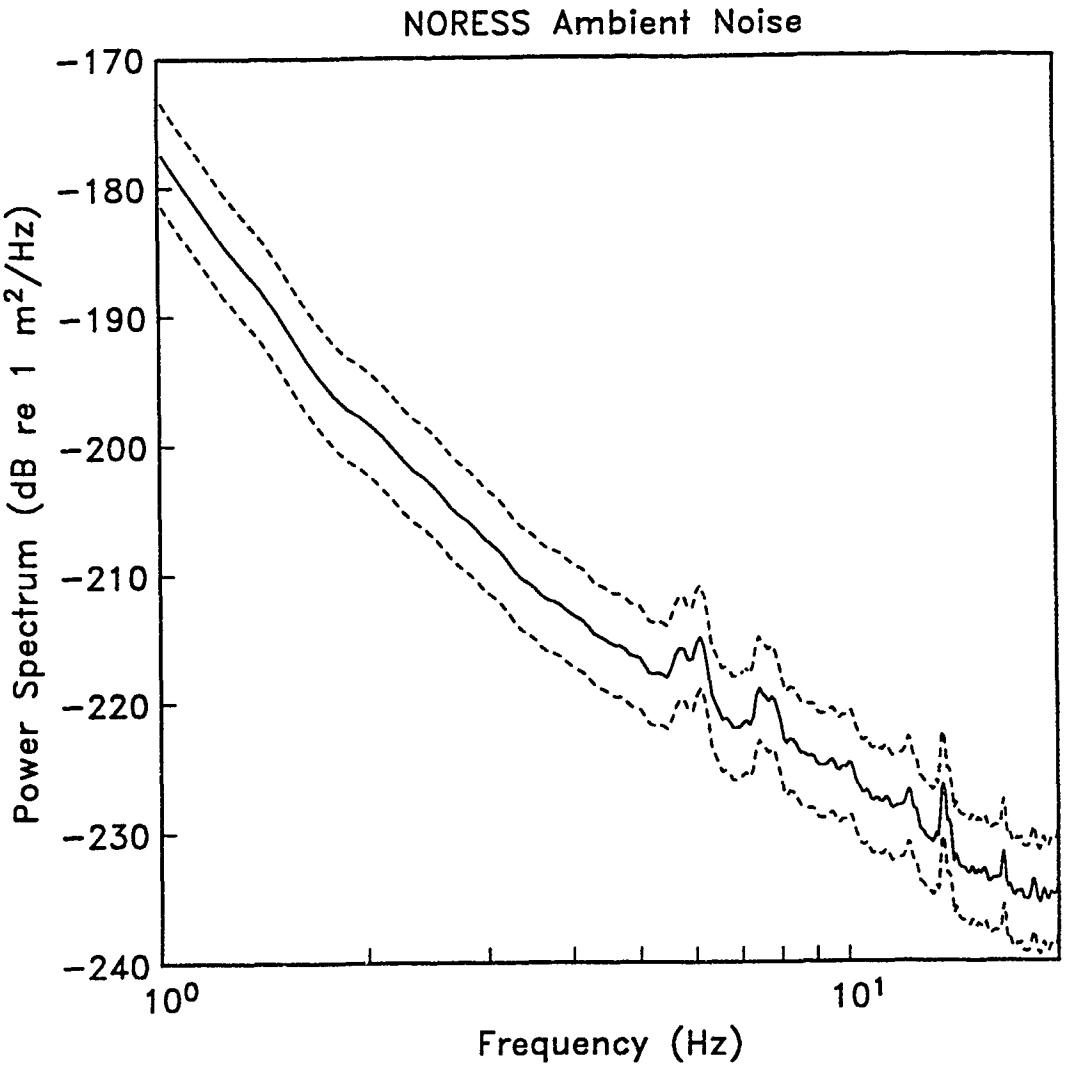

Figure 4.3. The ambient noise power spectral density at NORESS is plotted between 1 and 20 Hz. This spectrum was estimated from 78 five-second windows taken prior to *Pn*. The dashed curves indicate the average standard deviation (4 dB).

The importance of including magnitude dependence in the "noise" for secondary phases is demonstrated in Figure 4.4. The top panel plots *Lg snr* measured on a 2–4 Hz incoherent beam versus local magnitude for distances between 800 and 1000 km. *Lg snr* is nearly independent of magnitude in this distance range because the noise for *Lg* (which includes *Sn* coda) has nearly the same magnitude dependence as the *Lg* signal. The *snr* threshold used for detection on this beam is 7.6 dB, so there are no *Lg* phases with *snr* less than this. We parameterize the signal-generated component of the *Lg* noise as the *Sn* signal spectrum multiplied by a scalar that increases linearly with distance from 0.4 at 200 km to a maximum of 0.8 near 1200 km. The increase in the pre-*Lg* noise with distance is probably caused by surface multiples with one or more free-surface reflections. These phases can have amplitudes greater than *Sn* [e.g., *Kennett*, 1985], but they arrive after *Lg* for distances less than 400 km. For example, the bottom panel in Figure 4.4 plots travel time curves for *Sn*, *Lg*, and two surface multiples (*SSn* and *SSSn*). A schematic ray diagram for *SSn* is plotted as an inset to the bottom panel in Figure 4.4 (note that the surface reflection can occur near the source or near the receiver). *Kennett* [1985] explains that the larger amplitude of *SSn* over *Sn* is due to reduced geometrical spreading because the path length in the mantle is smaller, and because the reflection at the Moho is very efficient for near-critical incidence.

Fewer data were available to estimate the noise for *Pg* and *Sn*. The noise for *Pg* is equal to the ambient noise for distances less than the *Pn* critical distance, and it includes *Pn* coda at larger distances. We parameterize the signal-generated component of the noise for *Pg* as 0.3 times the *Pn* signal spectrum beyond the critical distance. This value was determined primarily from data recorded at ARCESS from events in the Kola Peninsula (distance is 300–400 km). Extrapolation to larger distances has much uncertainty. However, *Pg* attenuates much more rapidly than other phases in Fennoscandia, so the simulations are insensitive to the pre-*Pg* noise levels for distances greater than about 500 km. The noise for *Sn* includes energy that propagates in the upper mantle and in the crust. Since *Pg* attenuates much more rapidly than *Pn*, we relate the pre-*Sn* noise to the *Pn* signal spectrum. Specifically, we parameterize the signal-generated component of the *Sn* noise as the *Pn* signal spectrum multiplied by a scalar that decreases linearly with distance from 0.36 at 200 km to 0.26 at 1200 km [*Sereno*, 1990*a*].

4.6 Site/Station Parameters

The site or station parameters needed for the normalization include the *snr* thresholds required for detection of each wave, and the frequency-dependent beam gain for array stations. We use the beam gain (= noise suppression/signal loss) for *Pn* estimated by *Kvaerna* [1989] between 0.5 and 10 Hz, and we extrapolate to higher frequencies by assuming that the gain (in dB) decays linearly from the value at 10 Hz to zero at 20 Hz (Figure 4.5). The same frequency dependence is assumed for the *Pg* beam gain, but the level is about 3 dB lower [*Sereno*, 1990*a*]. This beam gain is applied to *Pg* and to the *Pn* coda. That is, we assume that coherent beamforming reduces the level of the ambient noise relative to *Pg*, but that it does not change the relative amplitude of *Pg* and *Pn* coda.

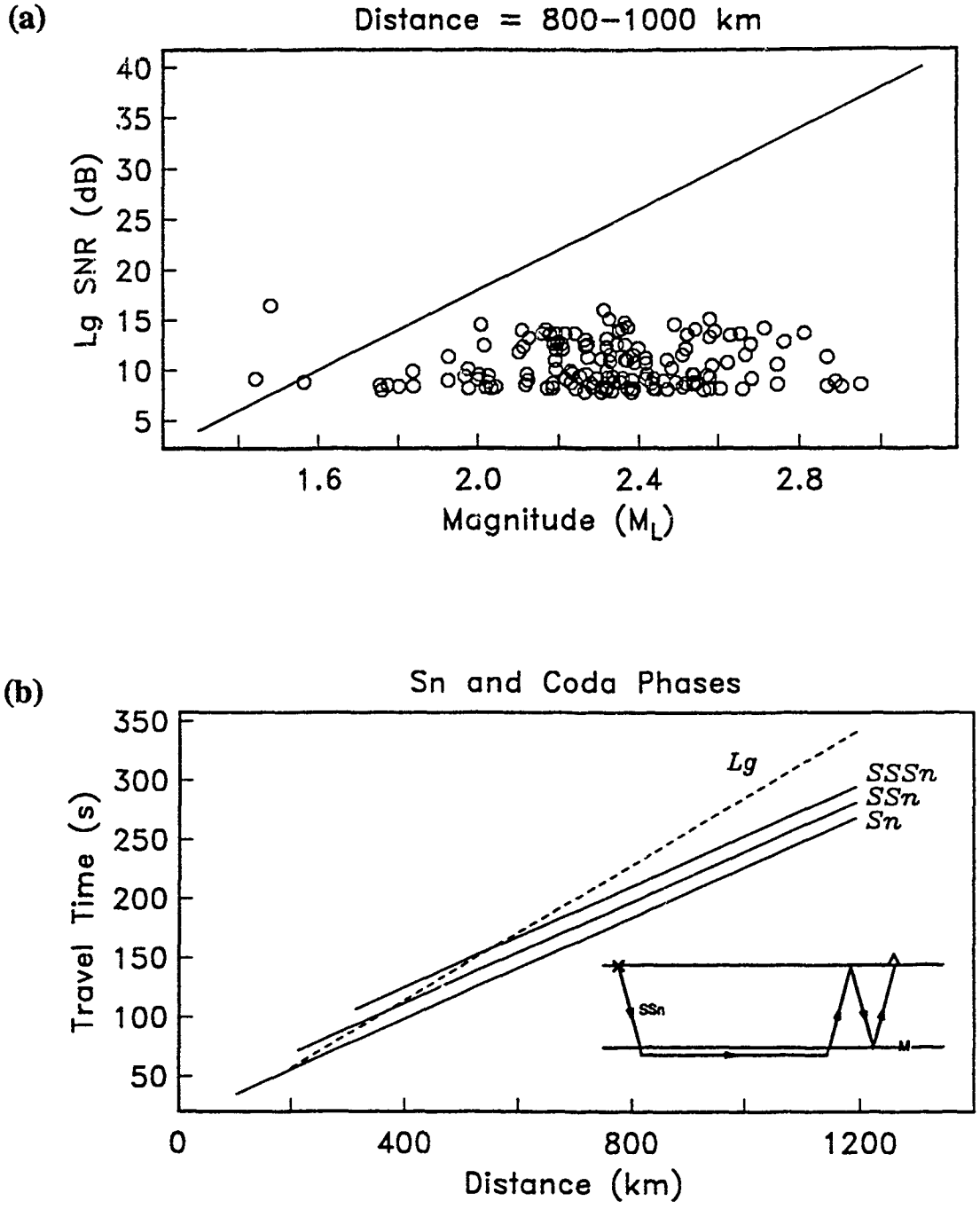

Figure 4.4. (*a*) *Lg snr* measured on a 2–4 Hz incoherent beam is plotted as a function of local magnitude for epicentral distances between 800 and 1000 km. The solid line indicates the expected dependence of the log *Lg* signal amplitude on M_L. (*b*) Travel time is plotted for *Sn*, *Lg*, and two surface multiples, *SSn* and *SSSn* (the inset is a schematic ray diagram for the surface multiple, *SSn*).

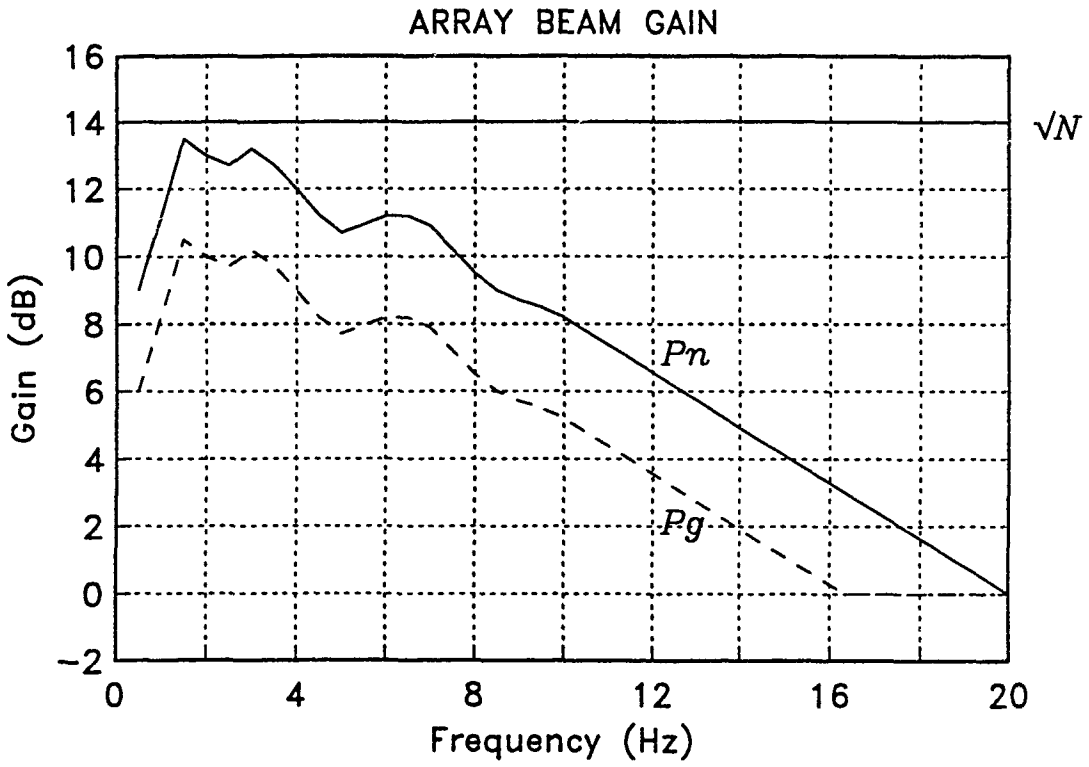

Figure 4.5. Estimates of the beam gain for array stations as a function of frequency are plotted for *Pn* and *Pg* [e.g., *Kvaerna*, 1989]. The beam gain approaches 14 dB between 1.5 and 3.5 Hz (which is equal to $\sqrt{N}$ for the full array, where N is the number of array elements).

Secondary phases are detected often on incoherent beams [e.g., *Ringdal*, 1985]. The *snr* measured on an incoherent beam is not much different from the *snr* measured on a single channel (e.g., the beam gain is close to 0 dB). The main advantage of forming incoherent beams is that the noise variance is lower. Thus, the *snr* threshold for an incoherent beam is lower than it is for single channel at a fixed rate of false alarms [T. Kvaerna, personal communication, 1990]. For the simulations, we assume that shear phases are detected on incoherent beams. Therefore, we assume the beam gain is 0 dB, and we use a lower *snr* threshold than we use for coherent beams (see below).

The *snr* thresholds for beams used in the *IMS* signal processing are based on a false alarm rate of 20–25% [*Kvaerna et al.*, 1987]. These thresholds (12 dB for coherent beams and 6–8 dB for incoherent beams) are based on time-domain amplitudes measured on filtered beams. However, our simulations are based on a parameterization of spectral amplitudes which require a different *snr* threshold to achieve the same rate of false alarms. The easiest way to determine the *snr* thresholds for our spectral parameterization is to compare the *snr* in the frequency domain to the *snr* in the time domain for a single channel. We find that the ratio of the frequency domain *snr* and time domain *snr* is approximately 0.8 for *Pn*, *Pg*, and *Sn*, and 0.6 for *Lg* (the *Lg* spectra are computed for a longer time window, so a lower ratio is expected). Therefore, the frequency-domain *snr* thresholds for a false alarm rate of 20–25% are about 10 dB for *Pn* and *Pg* (assuming detection on a coherent beam). If we assume that shear phases are detected on incoherent beams, then the frequency-domain *snr* thresholds are approximately 6 dB for *Sn*, and 3.5 dB for *Lg*. Table 4.3 summarizes the beam gain and *snr* thresholds used for the simulations.

Table 4.3 Beam gain and *snr* thresholds.

Phase	Beam Type	Arrays Gain (dB)	*snr* Threshold	3-C Stations *snr* Threshold
Pn	Coherent	Figure 4.5	10.0	10.0
Pg	Coherent	Figure 4.5	10.0	10.0
Sn	Incoherent	0.0	6.0	10.0
Lg	Incoherent	0.0	3.5	7.5

The *snr* threshold for *Pn* and *Pg* is the same for 3-component stations as it is for arrays, but the beam gain is 0 dB. However, the thresholds are raised by a factor of 1.6 (4 dB) for *Sn* and *Lg* to account for the lower noise variance on incoherent beams. This factor is equal to the *snr* threshold on the coherent beam divided by the *snr* threshold on the incoherent beam.

4.7 Validation

The detection thresholds at NORESS and ARCESS are estimated using *NetSim* with the normalization parameters described above. These simulations are compared to the observed capability of these arrays to validate the normalization. For example, Figure 4.6 plots the 90% M_L thresholds for detecting P at NORESS and ARCESS (top two panels), and for detecting P or a secondary phase (bottom two panels). For comparison, Table 4.4 lists previous empirical estimates of the detection thresholds for these arrays. The NORESS detection threshold for P phases is M_L 2.6–2.7 for epicenters in the mining regions in western USSR (Leningrad), and it is about M_L 2.4 if secondary phases are included in the detection criteria. This is consistent with results obtained by *Ringdal* [1986] who estimated the NORESS detection threshold by comparing detection lists to an independent bulletin produced by the University of Helsinki (Table 4.4). In a similar study, *Gibowicz* [1987] estimated the detection threshold to be about M_L 2.7 for mining events in Lubin, Poland. This is also consistent with our simulation in Figure 4.6. Our estimates of the detection thresholds at ARCESS are about 0.2–0.3 M_L lower than they are at NORESS because the ambient noise at ARCESS is lower than it is at NORESS for frequencies greater than 2 Hz [*Mykkeltveit et al.*, 1987; *Sereno*, 1990*a*]. This agrees with the empirical results of *Mykkeltveit and Ringdal* [1988] who estimated the detection capability at ARCESS using the same method that *Ringdal* [1986] used for NORESS. Comparing Table 4.4 and Figure 4.6 shows that our estimates of the detection thresholds are in close agreement with the results of empirical studies.

Table 4.4 Empirical estimates of detection capability at NORESS and ARCESS.

Reference	Station	Detection Criterion	Epicentral Region	Distance (km)	Confidence Level	M_L Threshold
Ringdal [1986]	NORESS	*P*	W. USSR	700–1400	90%	2.7
Ringdal [1986]	NORESS	any phase	W. USSR	700–1400	90%	2.5
Gibowicz [1987]	NORESS	*P*	Lubin, Poland	1000	90%	2.7
Mykkeltveit [1986]	NORESS	*P*	W. Norway	400	50%	1.8
Mykkeltveit [1986]	NORESS	any phase	W. Norway	400	70%	1.8
Mykkeltveit and Ringdal [1988]	ARCESS	*P*	W. USSR	800–1200	90%	2.5

To test our simualtion method for multiple stations, we compare simulations of the detection threshold for NORESS and ARCESS to the results of *Bratt et al.* [1990] who estimated the M_L threshold for events in Finland and western USSR by comparing detection lists to the bulletin produced by the University of Helsinki. Our estimate of the 90% M_L threshold is plotted in Figure 4.7. Two phases are required for detection of events within 200 km of either array, but three phases (with at least on at each array) are required for detection of more distant events. These criteria are based on the minimum number of phases required for accurate location. The M_L threshold is 2.4–2.6 for events in mining regions near Estonia and Leningrad. This is generally consistent with the empirical results of *Bratt et al.* [1990]. They estimate the 3-phase M_L threshold for events in this region to be 2.5 at the 83% confidence level. Thus, we

NORESS

90% M_L Threshold for Detecting P

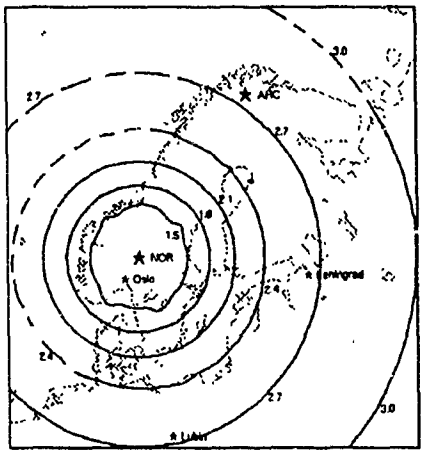

90% M_L threshold for Detecting Any Phase

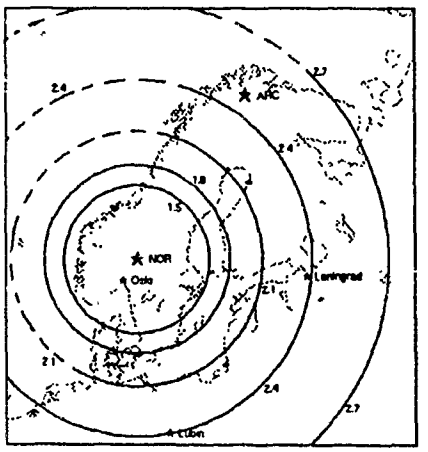

ARCESS

90% M_L Threshold for Detecting P

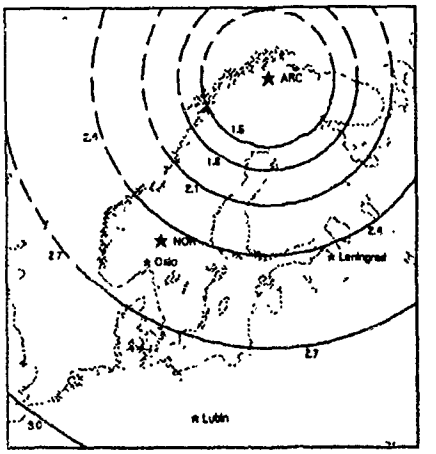

90% M_L threshold for Detecting Any Phase

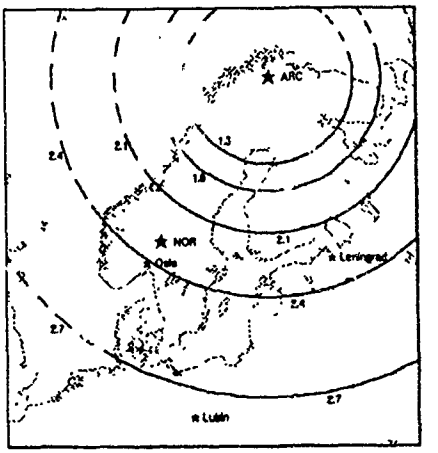

Figure 4.6. Estimates of the 90% M_L threshold at NORESS and ARCESS for detecting P (top two panels), and for detecting P or secondary phases (bottom two panels). Dashed lines are used for off-shore epicenters since our normalization did not include events from these locations. The irregular shape of the contour closest to NORESS is caused by insufficient epicenter grid sampling and has no physical significance.

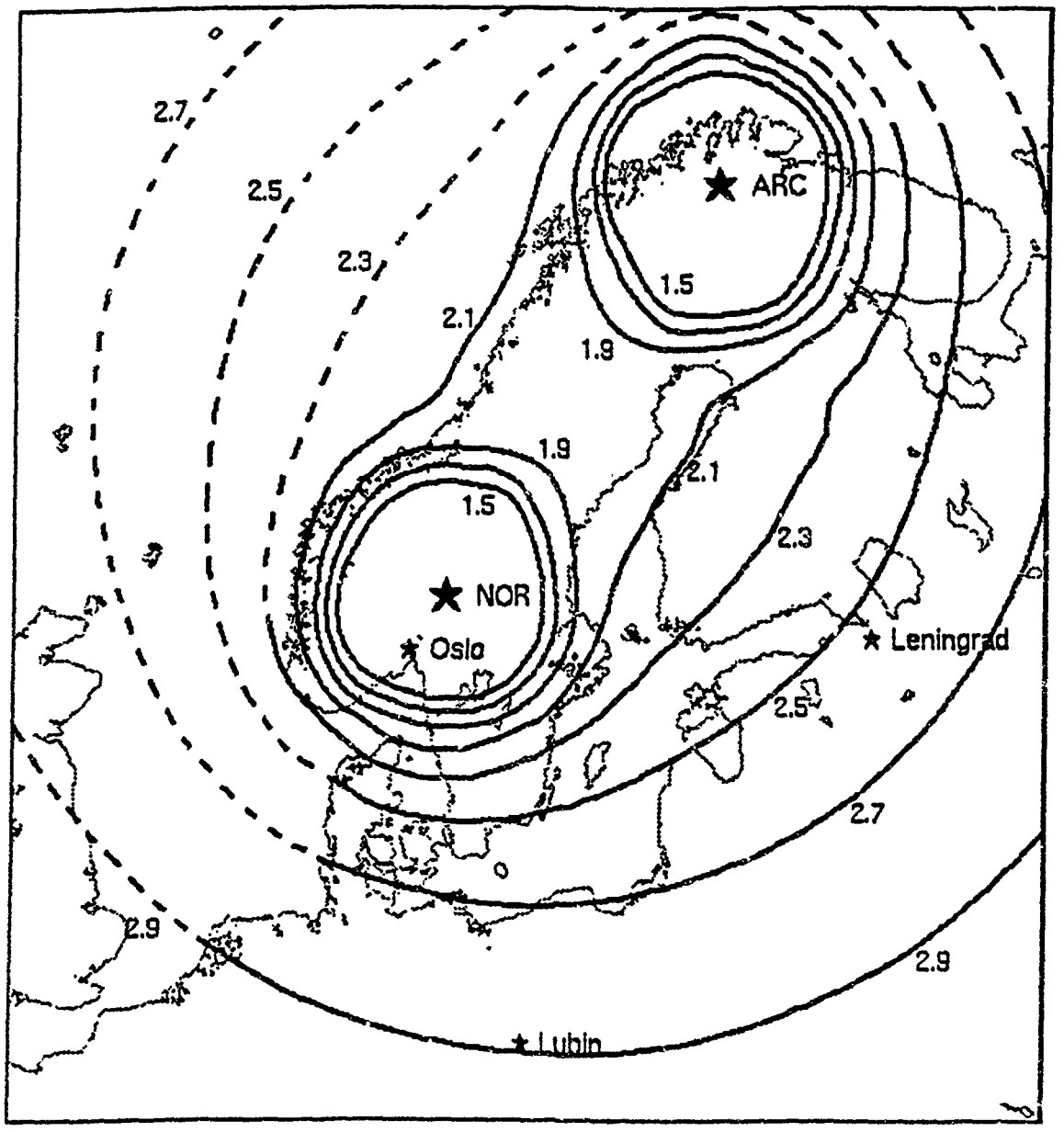

Figure 4.7. The 90% M_L detection threshold is plotted for the NORESS and ARCESS arrays. Either *Pg* and *Lg* must be detected at one array, or three phases must be detected by two arrays (with at least one at each array). Dashed lines are used for off-shore epicenters since our normalization did not include events from these locations.

have confidence that we have accurately parameterized the attenuation and noise in this region, and that we can use the normalized simulation method to (1) determine the sensitivity of the detection thresholds to various network parameters (e.g., number of stations/arrays, noise levels, station location, etc), and (2) estimate the detection threshold for other regions with similar propagation and noise characteristics.

(THIS PAGE INTENTIONALLY LEFT BLANK)

5. SEISMIC NETWORKS

The objective of this study is to determine the parameters of internal networks (e.g., number stations/arrays, station locations, frequency bandwidth, etc) that satisfy the performance criteria defined in Section 2. All of our simulations use a fixed external network that consists of existing digital stations and arrays. This external network is described in Section 5.1.

Section 5.2 describes the internal networks. The first network considered consists of existing and planned IRIS stations in the Soviet Union (Section 5.2.1). It is shown in Section 6.1 that this network does not satisfy the performance criteria in Section 2. Other internal networks considered consist of 5–50 approximately equally-spaced stations or arrays. These networks are described in Section 5.2.2.

5.1 External Network

All of the simulations in this report use an external network of 49 existing digital stations. This network consists of four regional arrays in Europe (ARCESS, FINESA, GERESS, NORESS), and 45 single stations from CDSN (Chinese Digital Seismic Network), DWWSSN (Digital World-Wide Standardized Seismograph Network), SRO (Seismic Research Observatories), and IRIS (Incorporated Research Institutions for Seismology). Table 5.1 lists the names, locations, and digitization rates for each station in the external network, and Figure 5.1 plots their locations on a world map. The probability of detection for any phase is set to zero for frequencies beyond the Nyquist frequency (= digitization rate/2) for each station.

5.2 Internal Networks

We consider internal networks that consist of either single stations or arrays. Of course, there are combinations of these station types that could satisfy the performance criteria in Section 2, but by using one type or the other we can bound the number of stations that are required. We assume that the arrays are identical to the NORESS array (25 elements, aperture of 3 km, digitization rate of 40 samples/s), and that the single stations are identical to the 3-component IRIS stations already installed in the Soviet Union (digitization rate is 20 samples/s). We begin with an internal network that consists of 6 existing and 7 planned IRIS 3-component stations (Section 5.2.1). Next, we consider internal networks that consist of 5, 10, 20, 30, 40, and 50 approximately equally-spaced stations (Section 5.2.2).

5.2.1 IRIS Stations

The IRIS internal network includes 6 existing and 7 planned 3-component stations [*Simarski*, 1991]. Table 5.2 lists the names and locations of these stations, and Figure 5.2 plots their locations on a map of the Soviet Union. These stations are equipped with Streckeisen STS-1 VBB seismometers that record continuous data at a rate of 20 samples/s. Eventually, the IRIS network will include 20–25 stations [*Simarski*, 1991].

Table 5.1 External seismic network.

Station Code	Description	Latitude	Longitude	Digitization Rate (sa/s)	Network†
AFI	Afiamalu, Samoa Islands	-13.906	-171.773	20	DWWSSN
ALE	Alert, Canada	82.483	-62.400	20	IRIS/IDA
ANMO	Albuquerque, New Mexico	34.941	-106.454	20	SRO/ASRO
ANTO	Ankara, Turkey	39.900	32.783	20	SRO/ASRO
ARC	ARCESS Array, Norway	69.535	25.506	40	ARRAY
BCAO	Bangui, C. African Republic	4.367	18.567	20	SRO/ASRO
BDF	Brasilia, Brazil	-15.658	-47.902	20	DWWSSN
BJI	Beijing (Peking), China	40.038	116.172	40	CDSN
BOCO	Bogota, Columbia	4.585	-74.039	20	SRO/ASRO
CCM	Cath. Caves, Missouri	38.056	-91.245	20	IRIS/IDA
CHTO	Chiengmai, Thailand	18.787	98.973	20	SRO/ASRO
COL	College Outpost, Alaska	64.900	-147.789	20	DWWSSN
COR	Corvalis, Oregon	44.586	-123.303	20	IRIS/Univ.
CTAO	Charters Towers, Austrailia	-20.086	146.252	20	SRO/ASRO
ENH	China	30.270	109.485	40	CDSN
ESK	Eskdalemuir, Scotland	55.317	-3.205	20	IRIS/IDA
FIN	FINESA Array, Finland	61.444	26.079	40	ARRAY
GDH	Godhavn, Greenland	69.250	-53.533	20	DWWSSN
GER	GERESS Array, Germany	48.820	13.570	40	ARRAY
GUMO	Marianas Islands, Guam	13.586	144.860	20	SRO/ASRO
HIA	Neimenggu Prov., China	49.267	119.738	40	CDSN
HRV	Harvard, Massachusetts	42.507	-71.563	20	IRIS/Univ.
JAS	Jamestown, California	37.947	-120.438	20	DWWSSN
KAAO	Kabul, Afganistan	34.538	69.039	20	SRO/ASRO
KIP	Kipapa, Hawaii	21.421	-158.009	20	DWWSSN
KMI	Kunming, China	25.121	102.737	40	CDSN
LEM	Lembang, Java	-6.833	107.617	20	DWWSSN
LON	Longmire, Washington	46.750	-121.806	20	DWWSSN
LZH	Lanchow, China	36.085	103.840	40	CDSN
MAIO	Mashhad, Iran	36.300	59.490	20	SRO/ASRO
MAJO	Matsushiro, Japan	36.538	138.205	20	SRO/ASRO
MDJ	Mudanjiang, China	44.610	129.589	40	CDSN
NNA	Nana, Peru	-11.988	-76.842	20	IRIS/IDA
NOR	NORESS Array, Norway	60.735	11.541	40	ARRAY
NWAO	Narrogin, W. Australia	-32.923	117.236	20	SRO/ASRO
PAS	Pasadena, California	34.148	-118.172	20	IRIS/Univ.
QUE	Quetta, Pakistan	30.186	66.950	20	DWWSSN
RPN	Rapa Nui, Easter Island	-27.158	-109.434	20	IRIS/IDA
SBA	Scott base, Antarctica	-77.850	166.754	20	DWWSSN
SCP	State College, Pennsylvania	40.790	-77.859	20	DWWSSN
SHIO	Shillong, India	25.567	91.883	20	SRO/ASRO
SLR	Silverton, S. Africa	-25.735	28.282	20	DWWSSN
SNZO	South Karori, New Zealand	-41.306	174.703	20	SRO/ASRO
SSE	China	31.091	121.185	40	CDSN
TATO	Taipei, China	24.972	121.486	20	SRO/ASRO
TAU	Tasmania Univ., Tasmania	-42.906	147.319	20	DWWSSN
TOL	Toledo, Spain	39.876	-4.043	20	DWWSSN
WMQ	Wulumuchi (Urumchi), China	43.819	87.690	40	CDSN
ZOBO	Zongo Valley (La Paz), Bolivia	-16.269	-68.122	20	SRO/ASRO

† Arrays have 25 elements, all others are single 3-component stations.

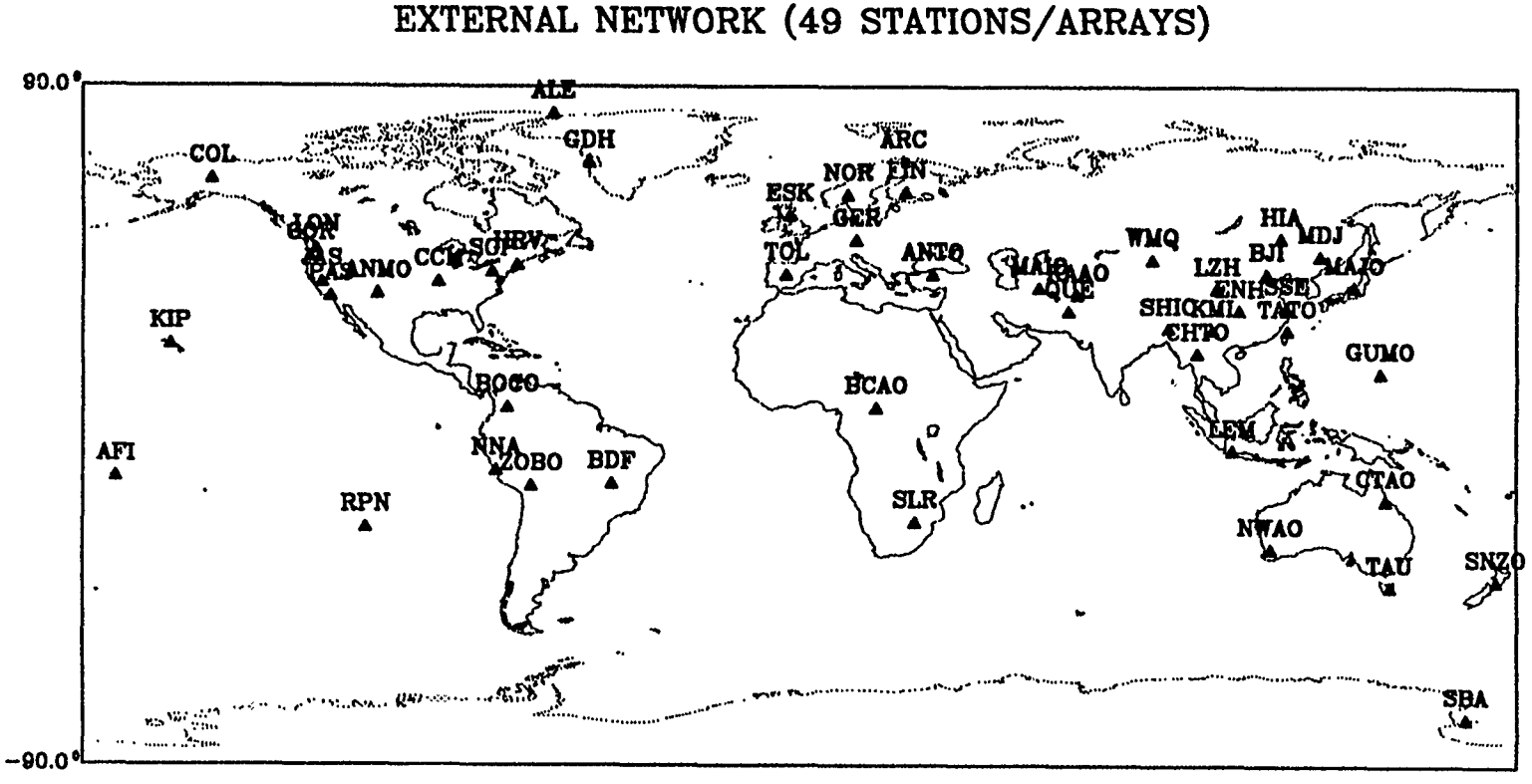

Figure 5.1. The external network consists of 49 digital stations/arrays (45 single stations from CDSN, DWWSSN, IRIS, and SRO, and 4 regional arrays in Europe). This external network is used for all of the simulations in this report.

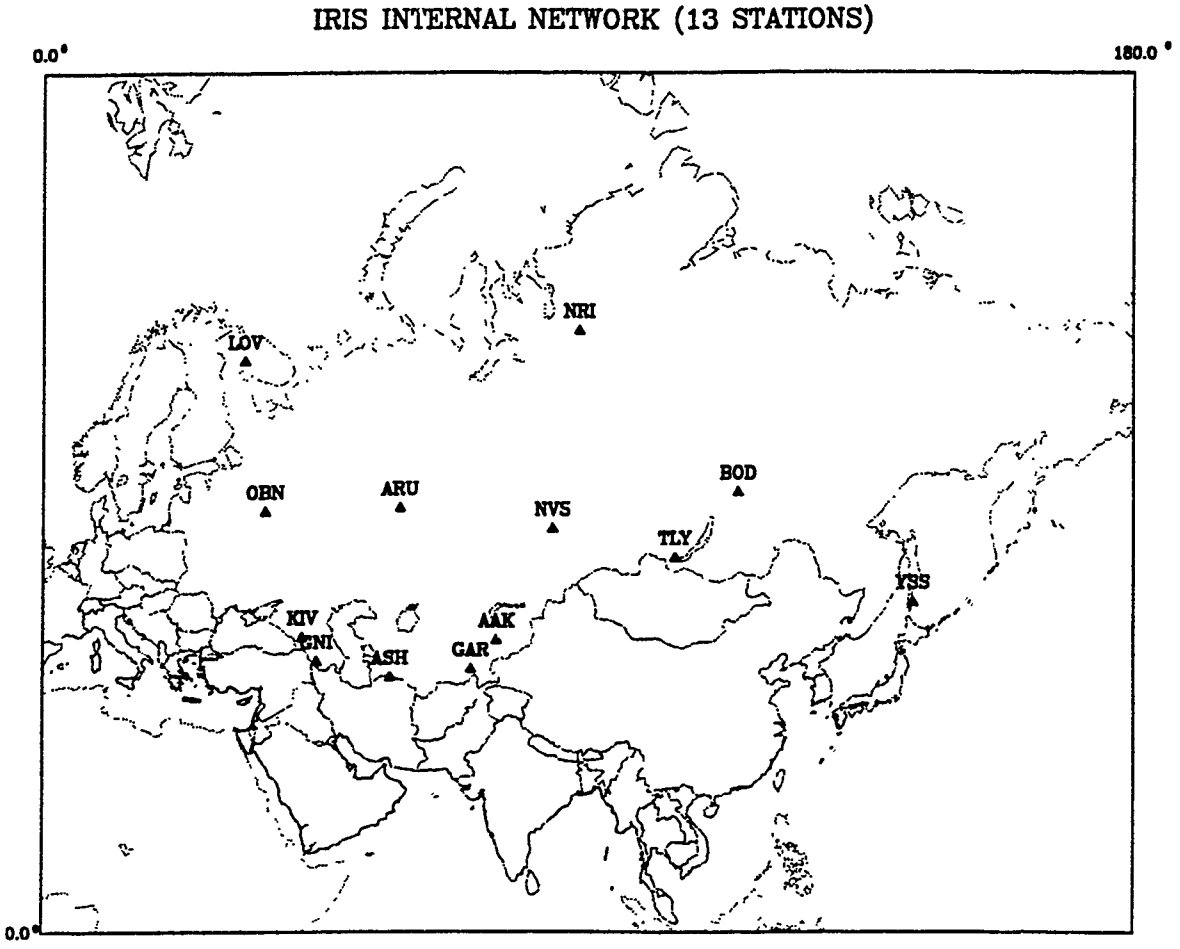

Figure 5.2. This map shows the locations of existing and planned IRIS 3-component stations in the Soviet Union [*Simarski*, 1991].

Table 5.2 IRIS internal seismic network.

Station Code	Location	Latitude	Longitude	Network
AAK	Ala-Archa	42.600	74.500	IRIS/IDA†
ARU	Arti	56.400	58.600	IRIS/IDA†
ASH	Ashkhabad	38.000	57.000	IRIS/IDA
BOD	Bodaibo	57.800	114.000	IRIS/IDA
GAR	Garm	39.000	70.320	IRIS/IDA†
GNI	Garni	40.000	45.000	IRIS/USGS
KIV	Kislovodsk	42.950	42.680	IRIS/IDA†
LOV	Lovozero	67.600	33.300	IRIS/IDA
NRI	Norilsk	69.400	88.000	IRIS/IDA
NVS	Novosibirsk	54.500	83.700	IRIS/IDA
OBN	Obninsk	56.100	36.600	IRIS/IDA†
TLY	Talaya	51.700	103.600	IRIS/IDA†
YSS	Yuzhno-Sakhalinsk	47.000	142.800	IRIS/IDA

† Station is in operation; others are being installed.

The existing and proposed IRIS sites will not provide uniform detection capability throughout the Soviet Union (e.g., there are no stations in the northeast region). This is because other factors were considered in the final site selection for the IRIS stations. For example, in addition to investigating problems related to monitoring underground nuclear explosion testing, data from the IRIS network are used to study earthquake hazard reduction, Earth structure, and the nature of earthquake sources [*The Monitor*, 1990]. Since we want to determine the parameters of internal networks that are required to achieve a fixed detection threshold for all epicenters in the Soviet Union, we consider other internal networks (with more evenly-distributed stations) for purpose of monitoring nuclear explosion testing. These networks are described in the next section.

5.2.2 Hypothetical Networks

The hypothetical internal networks considered in this report consist of approximately equally-spaced stations or arrays. Actually, the sites were selected to provide nearly uniform detection thresholds throughout the Soviet Union (including the stations in the external network). We consider networks with 5, 10, 20, 30, 40 and 50 stations. All stations are either NORESS-type arrays or IRIS-type single (3-component) stations. Figure 5.3 plots the mean station separation versus the number of stations in the internal network, and Figure 5.4 plots the station locations for each network on a map of the Soviet Union. About 18 internal stations are needed to duplicate the spacing of the regional arrays in Fennoscandia.

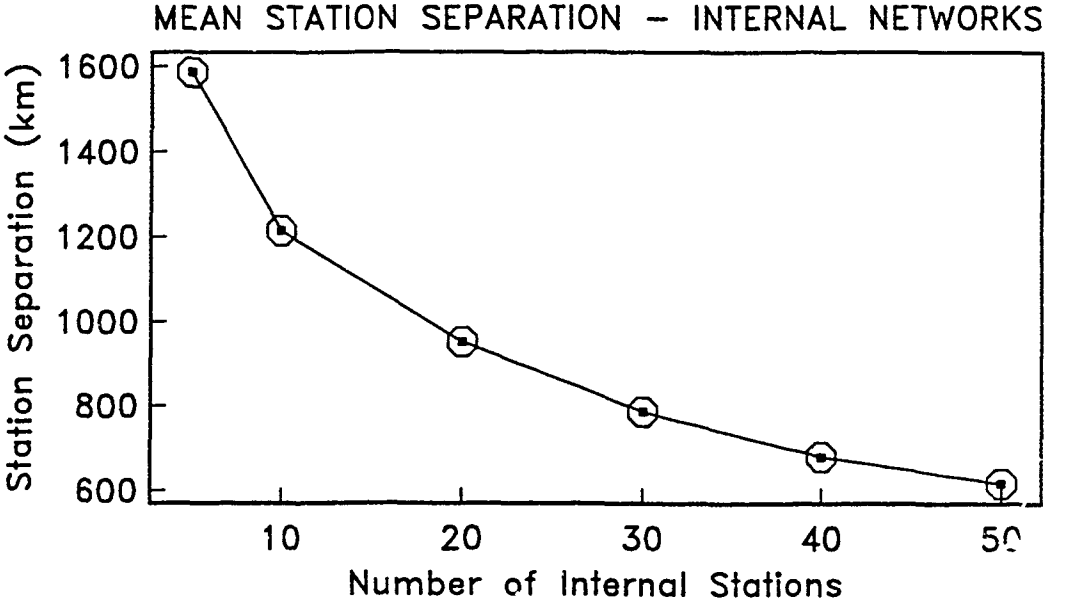

Figure 5.3. The mean station separation is plotted versus the number of internal stations. The distance between any station and its closest neighbor is used to estimate the mean separation.

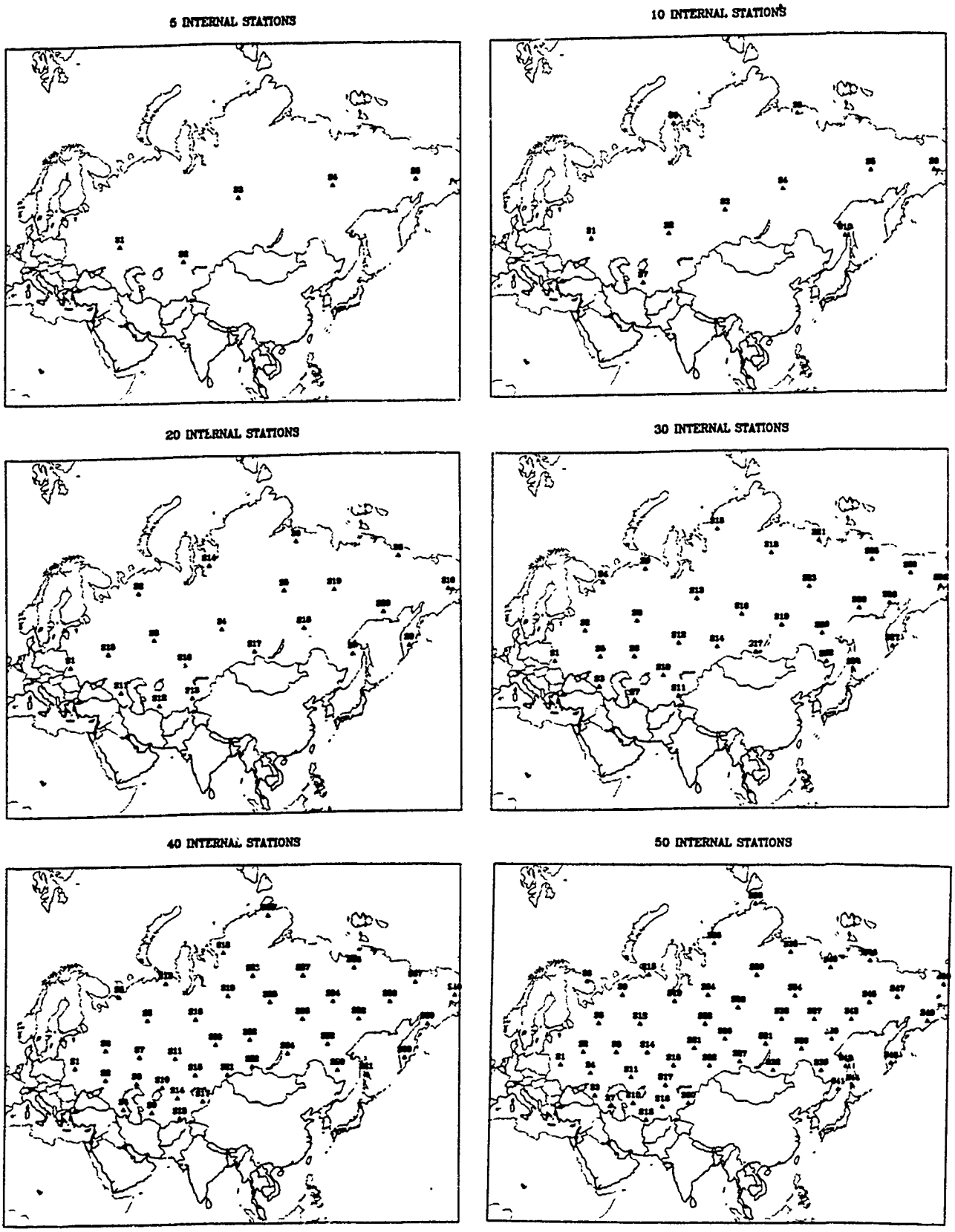

Figure 5.4. Hypothetical internal networks are plotted that consist of 5, 10, 20, 30, 40, and 50 stations. These sites were selected to give nearly uniform detection thresholds throughout the Soviet Union.

(THIS PAGE INTENTIONALLY LEFT BLANK)

6. DETECTION AND LOCATION CAPABILITY BASED ON CONDITIONS IN FENNOSCANDIA

In this section, we estimate the detection and location capability of existing and hypothetical regional seismic networks in and around the Soviet Union. Our goal is to estimate the number of internal single stations or arrays that are required to monitor nuclear explosion testing to a threshold of 1 kt (Section 2). The simulations in this section are normalized to the observed performance of the NORESS and ARCESS arrays in Norway. That is, we assume that the signal and noise characteristics in the Soviet Union are identical to those observed in Fennoscandia. However, the actual attenuation and noise for the stations in our hypothetical network may be different from those in Fennoscandia. Therefore, in later sections we determine the sensitivity of the simulations to changes in the signal and noise characteristics.

Estimates of the detection capability of the seismic networks described in the previous section are given in Section 6.1. We estimate the number of internal stations or arrays that are required to achieve a detection threshold of M_L 2.5 for any epicenter in the Soviet Union (e.g., the approximate magnitude of a fully-decoupled 1 kt nuclear explosion). Section 6.2 gives estimates of the location uncertainty for these networks. In Section 6.3, we investigate the dependence of the detection thresholds on the digitization rate of the internal single stations. Since decoupling opportunities in the Soviet Union are primarily limited to regions of bedded or domed salt, we also estimate the number of internal stations that are required to achieve a threshold of M_L 2.5 in salt regions, while higher thresholds are accepted elsewhere. These results are are discussed in Section 6.4.

6.1 Detection Capability

Figure 6.1 plots estimates of the 90% M_L detection threshold for a network that includes the existing and planned IRIS internal 3-component stations (Figure 5.2). The 90% M_L threshold for detecting 3 phases involving at least 2 stations for this network is 2.0–3.5 for epicenters in the Soviet Union. This broad magnitude range is caused by the unequal geographic distribution of the IRIS stations (note that these sites were not selected to optimize monitoring performance). If we require detection of 3 *P* phases at 3 stations, then the 90% M_L threshold is 2.4–4.3. Thus, the proposed IRIS internal network does not satisfy the performance criteria for monitoring tests of decoupled nuclear explosions with yields as low as 1 kt.

Table 6.1 lists the median, M_L^{50}, and the minimum and maximum values of the 90% M_L threshold for epicenters in the Soviet Union as a function of the number of internal stations or arrays. The median threshold for each internal network is calculated from the thresholds at 21 epicenters throughout the Soviet Union. The median value of the 90% M_L threshold for detecting 3 phases involving at least 2 stations for epicenters in the Soviet Union is plotted as a function of the number of internal single stations or arrays in Figure 6.2*a*. Approximately 8 internal arrays or 20 internal single stations are required to achieve a *median* threshold of M_L 2.5. However, to achieve this threshold for all epicenters in the Soviet Union requires 10 internal arrays or 30

(a)

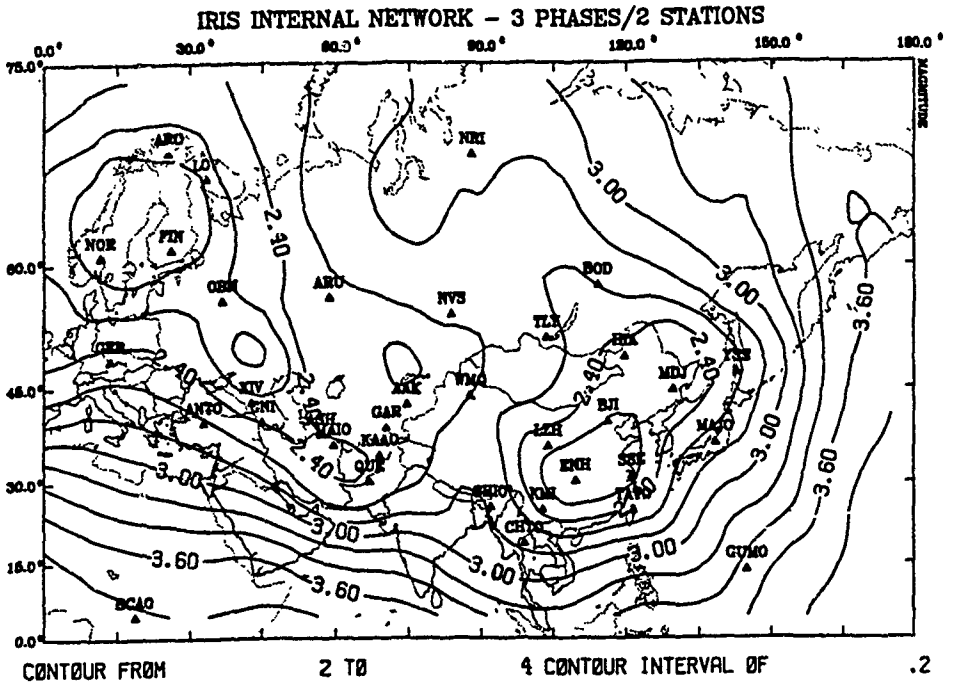

(b)

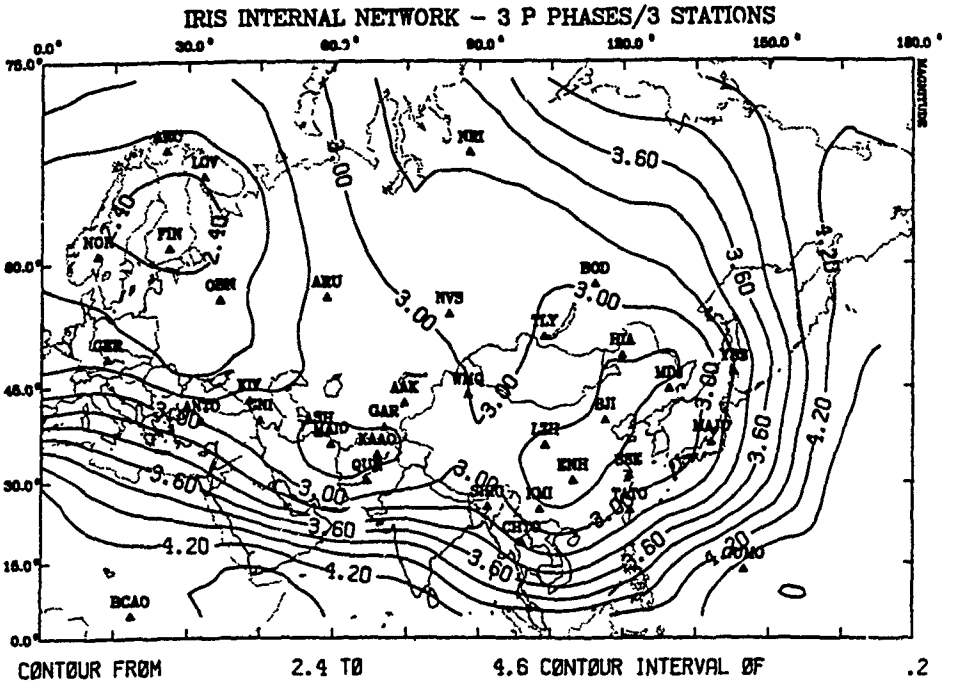

Figure 6.1. Estimates of the 90% M_L threshold for detecting (*a*) 3 phases involving at least two stations, and (*b*) 3 *P* phases involving at least three stations are plotted for the IRIS internal network. The external network consists of 49 existing stations/arrays.

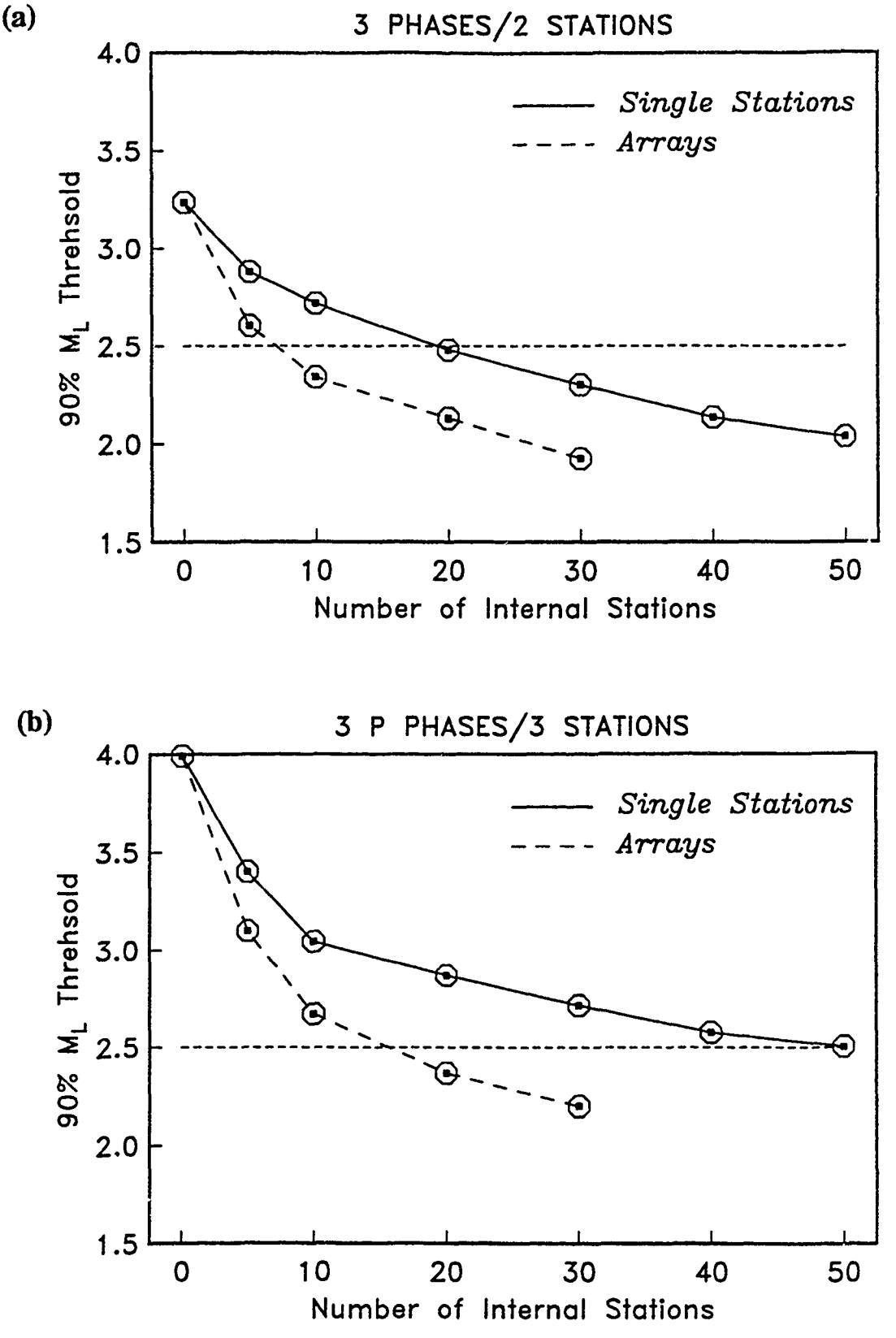

Figure 6.2. The median value of the 90% M_L detection threshold for epicenters in the Soviet Union is plotted as a function of the number of internal arrays or single stations. For detection, we require a minimum of (*a*) 3 phases and 2 stations, or (*b*) 3 *P*-type phases and 3 stations. The dashed line at M_L 2.5 indicates the goal of the monitoring network.

internal single stations. The 90% M_L detection thresholds for these networks are plotted in Figure 6.3. The threshold for the network with 10 internal arrays is 2.1–2.5 for epicenters in the Soviet Union, and it is 1.9–2.5 for the network with 30 internal single stations. The location uncertainty for an M_L 2.5 event in the Soviet Union for either of these networks is ≤ 20 km (Section 6.2).

Table 6.1 90% M_L detection thresholds in the Soviet Union.

Internal Network	3 Phases/2 Stations M_L^{50}	3 Phases/2 Stations M_L^{min}–M_L^{max}	3 *P* Phases/3 Stations M_L^{50}	3 *P* Phases/3 Stations M_L^{min}–M_L^{max}
None	3.2	2.2–3.8	4.0	2.6–4.4
5 Arrays	2.6	2.2–2.9	3.1	2.5–4.0
10 Arrays	2.3	2.1–2.5	2.7	2.4–3.0
20 Arrays	2.1	1.9–2.4	2.4	2.2–2.6
30 Arrays	1.9	1.5–2.2	2.2	2.1–2.4
5 Single Stations	2.9	2.2–3.2	3.4	2.6–4.1
10 Single Stations	2.7	2.2–2.8	3.0	2.5–3.6
13 Single Stations (IRIS)	2.7	2.0–3.5	3.0	2.4–4.3
20 Single Stations	2.5	2.2–2.7	2.9	2.5–3.0
30 Single Stations	2.3	1.9–2.5	2.7	2.4–2.8
40 Single Stations	2.1	1.9–2.5	2.6	2.4–2.8
50 Single Stations	2.0	1.6–2.4	2.5	2.3–2.7

Figure 6.2*b* shows the median value of 90% M_L threshold for detecting 3 *P* phases involving a minimum of 3 stations. In this case, a *median* threshold of M_L 2.5 can be achieved with 16 internal arrays or 50 internal single stations. To achieve this threshold for all epicenters requires ≥ 20 arrays, or ≥ 50 single stations. The 90% M_L detection thresholds for these networks are plotted in Figure 6.4. The threshold for the network with 20 internal arrays is 2.2–2.6 for epicenters in the Soviet Union, and it is 2.3–2.7 for the network with 50 internal single stations. The location uncertainty for an M_L 2.5 event in the Soviet Union is ≤ 15 km for networks with either 20 internal arrays or 50 internal single stations (Section 6.2). Simulations corresponding to each network in Table 6.1 are given in Appendix A.

6.2 Location Capability

We use *NetSim* to calculate the dimensions of the location error ellipse at the 90% confidence level using *a priori* estimates of the arrival time and azimuth standard deviations [e.g., *Bratt et al.*, 1987; *Bratt and Bache*, 1988]. The location uncertainty at the 90% confidence level, *D*, can be calculated from these dimensions using:

(a)

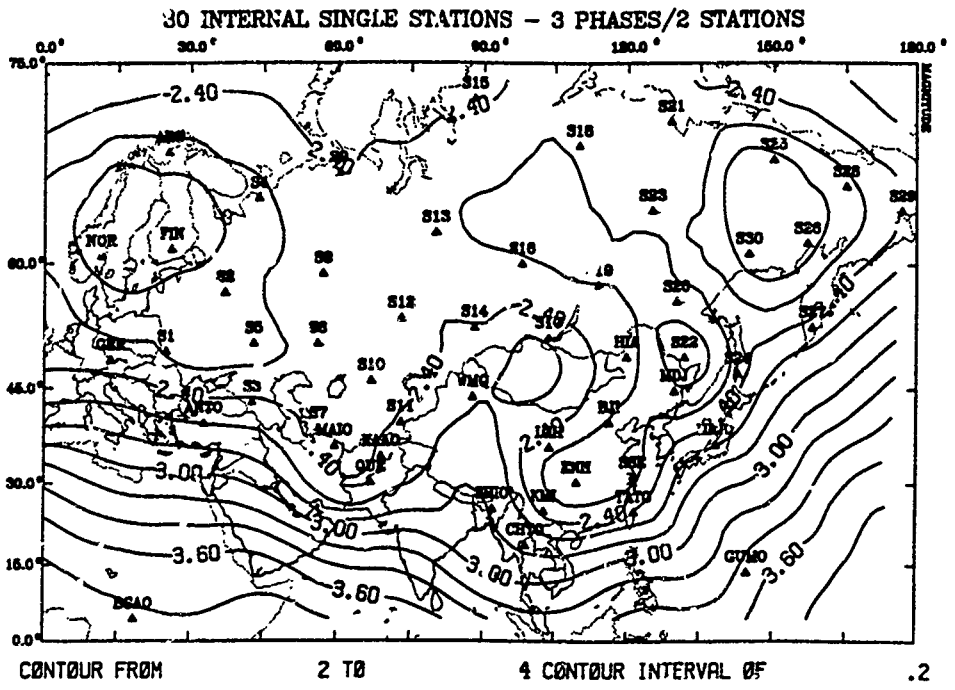

(b)

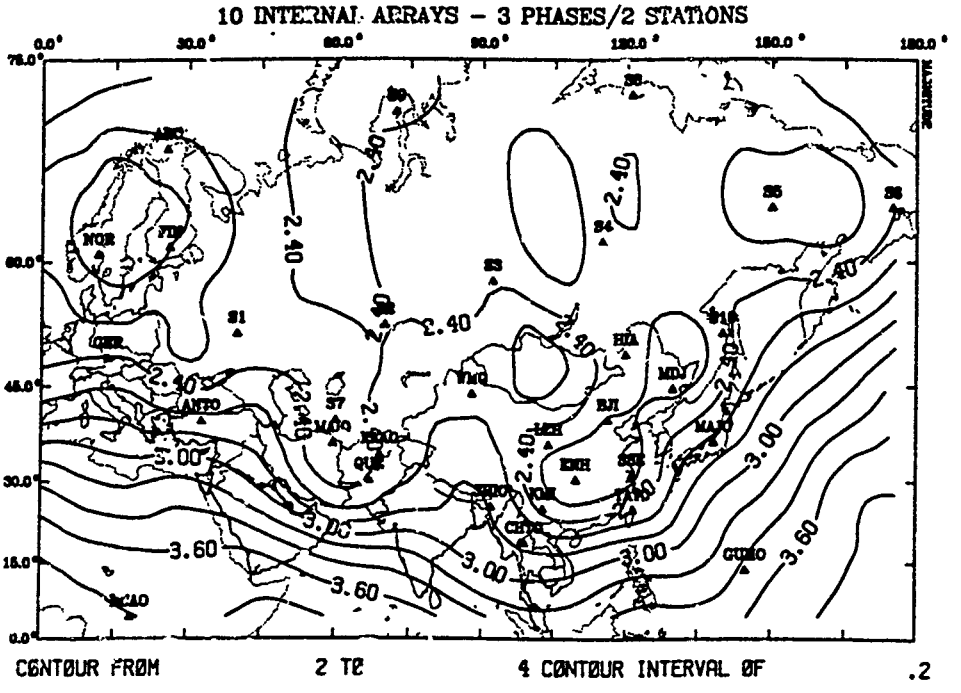

Figure 6.3. Estimates of the 90% M_L threshold for detecting 3 phases involving at least two stations are plotted for networks that include (*a*) 30 internal three-component stations, and (*b*) 10 internal NORESS-type regional arrays. The external network consists of 49 existing stations/arrays.

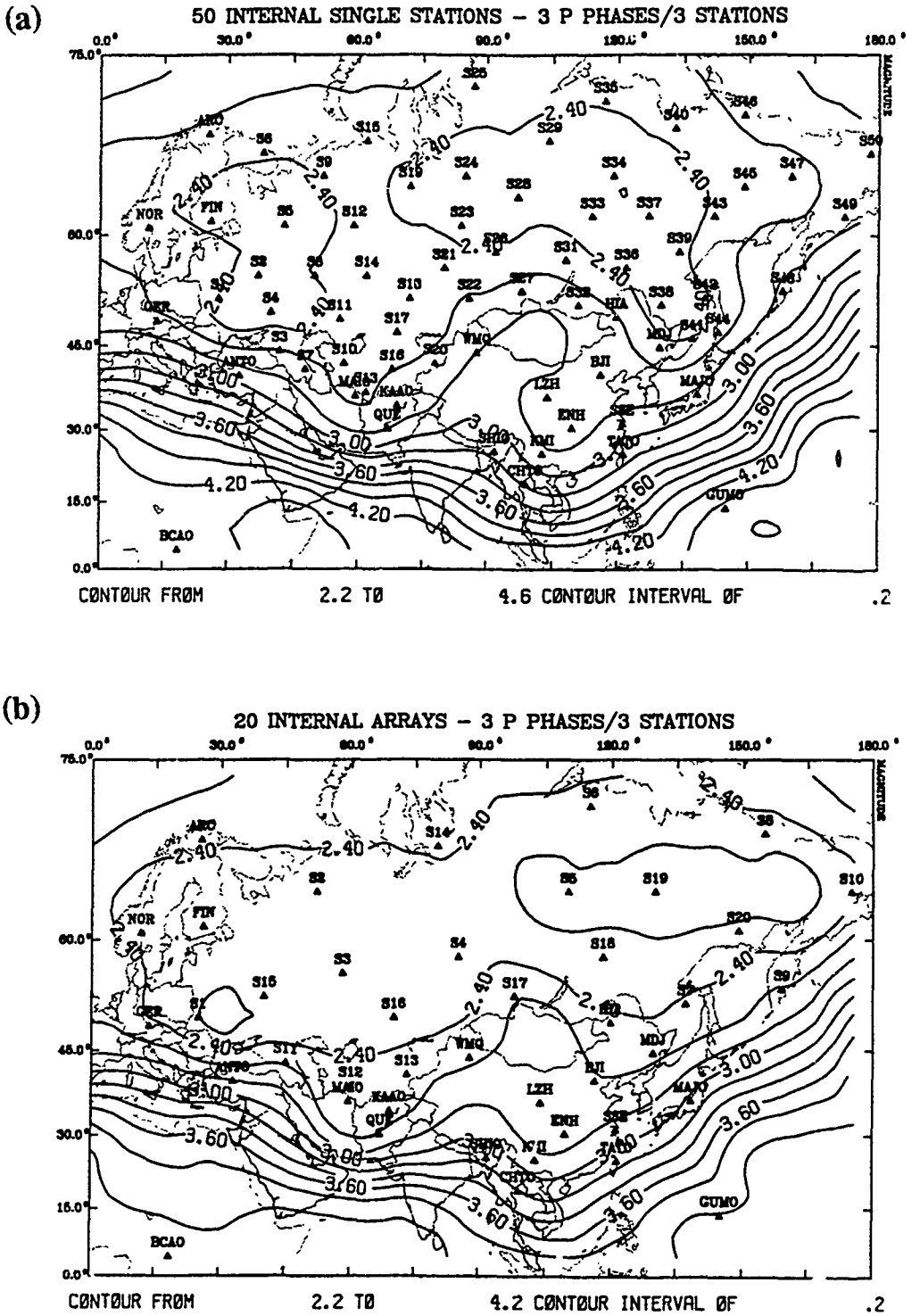

Figure 6.4. Estimates of the 90% M_L threshold for detecting 3 *P* phases involving at least three stations are plotted for networks that include (*a*) 50 internal three-component stations, and (*b*) 20 internal NORESS-type regional arrays. The external network consists of 49 existing stations/arrays.

$$\int_0^{2\pi} d\theta \int_0^{D} p(r,\theta)\, r\, dr = 0.9 \tag{6.1}$$

where $p(r,\theta)$ is the probability density function given by

$$p(r,\theta) = \frac{e^{-r^2 y(\theta)}}{2\pi ab} \tag{6.2}$$

$$y(\theta) = \frac{\cos^2\theta}{2a^2} + \frac{\sin^2\theta}{2b^2} \tag{6.3}$$

The lengths a and b are equal to the $90th$ percentile values of the semi-major and semi-minor axes divided by 2.15 (using a chi-squared distribution with 2 degrees of freedom). Substitution of (6.2) into (6.1) and performing the integration over r gives:

$$\frac{1}{4\pi ab} \int_0^{2\pi} d\theta \left[\frac{1 - e^{-D^2 y(\theta)}}{y(\theta)} \right] = 0.9 \tag{6.4}$$

which can be solved numerically for D, given estimates of the dimensions of the location error ellipse.

Figure 6.5*a* plots the location uncertainty at the 90% confidence level for the network with 10 internal NORESS-type arrays for an M_L 2.5 event. This location uncertainty (which was calculated using (6.4) and the lengths of the semi-major and semi-minor axes in Figures 6.5*b* and 6.5*c*), is less than 20 km for all epicenters in the Soviet Union. Similarly, the location uncertainty at the 90% confidence level for the network with 30 internal 3-component single stations is also less than 20 km for an M_L 2.5 event (Figure 6.6). Therefore, both of these internal networks satisfy the location capability criteria established in Section 2. If secondary phases are excluded from the detection criteria, then $\geq$ 20 internal arrays or $\geq$50 internal single stations are required to satisfy the detection capability criteria in Section 2. As shown in Figures 6.7 and 6.8, the $90th$ percentile location uncertainty for these networks is less than 15 km for an M_L 2.5 event anywhere in the Soviet Union.

An important assumption in the simulations is that each detected phase will be correctly identified and associated with other detections for event location. Of course, if the phase association is incorrect then the error in the event location will be much larger than the uncertainties predicted by the simulations. For example, if *Sn* is incorrectly identified as *Lg* for an event at 1000 km, then the single-station location error will be more than 150 km. This problem is worse for single stations than it is for arrays, since phase velocity and azimuth can be measured more accurately using array data. For either station type, the possibility of incorrect association is greatly reduced by requiring detection at a minimum of two stations (which is the minimum requirement used in our simulations).

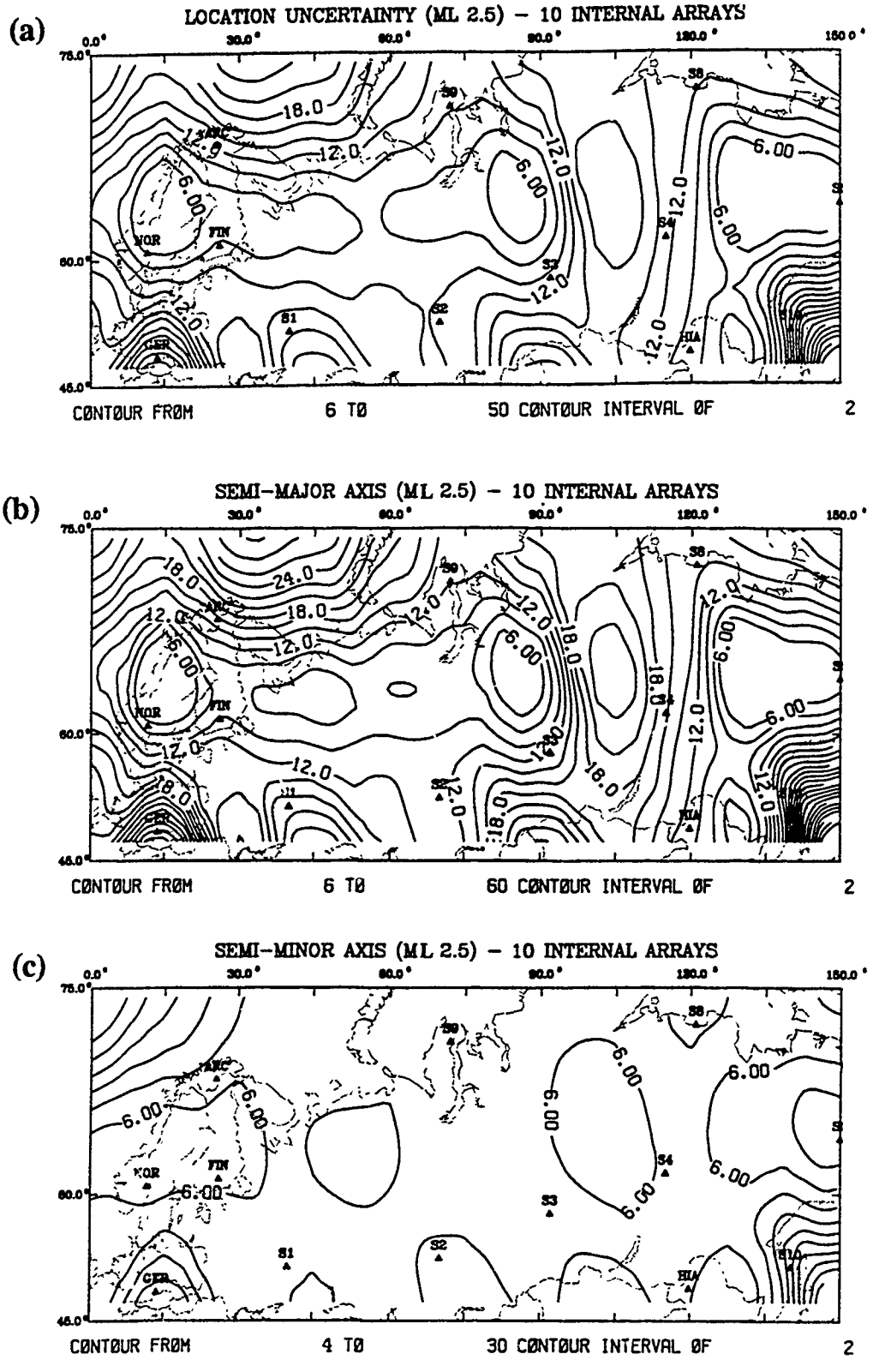

Figure 6.5. The 90th percentile (*a*) location uncertainty, (*b*) semi-major axis, and (*c*) semi-minor axis in kilometers are contoured for a fixed event size of M_L 2.5. The internal network consists of 10 NORESS-type arrays.

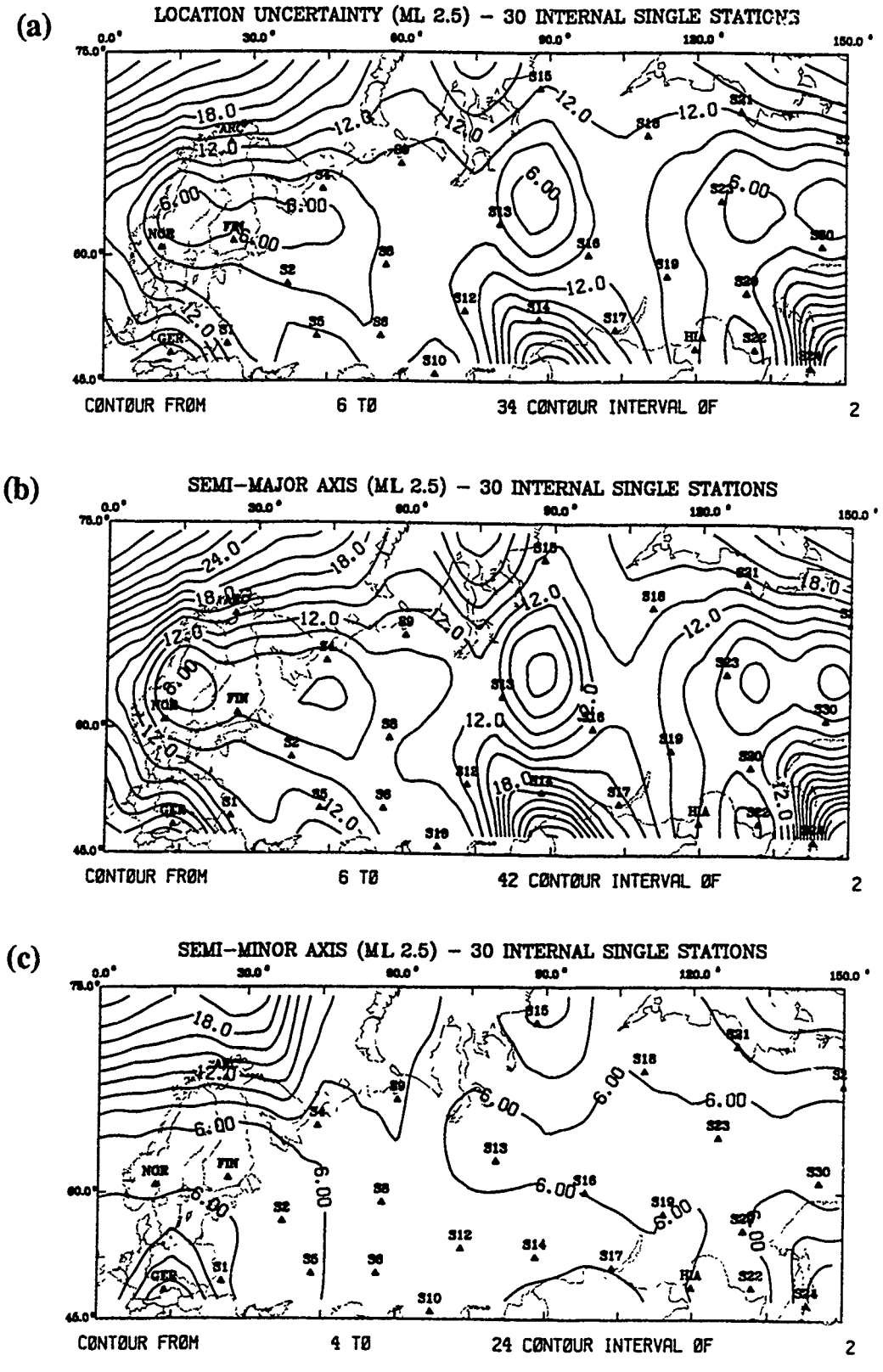

Figure 6.6. The 90th percentile (*a*) location uncertainty, (*b*) semi-major axis, and (*c*) semi-minor axis in kilometers are contoured for a fixed event size of M_L 2.5. The internal network consists of 30 IRIS-type single (3-component) stations.

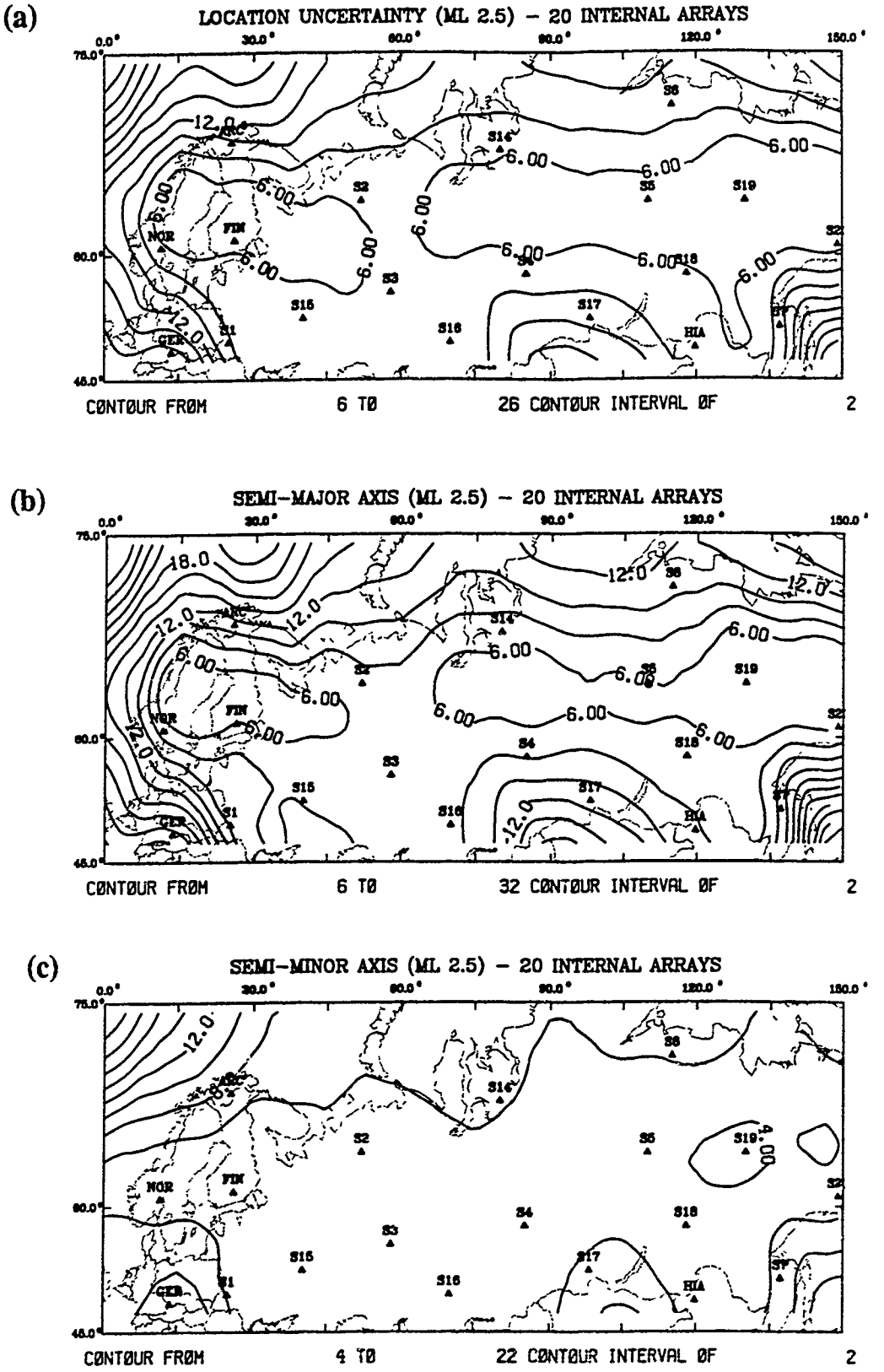

Figure 6.7. The 90th percentile (*a*) location uncertainty, (*b*) semi-major axis, and (*c*) semi-minor axis in kilometers are contoured for a fixed event size of M_L 2.5. The internal network consists of 20 NORESS-type arrays.

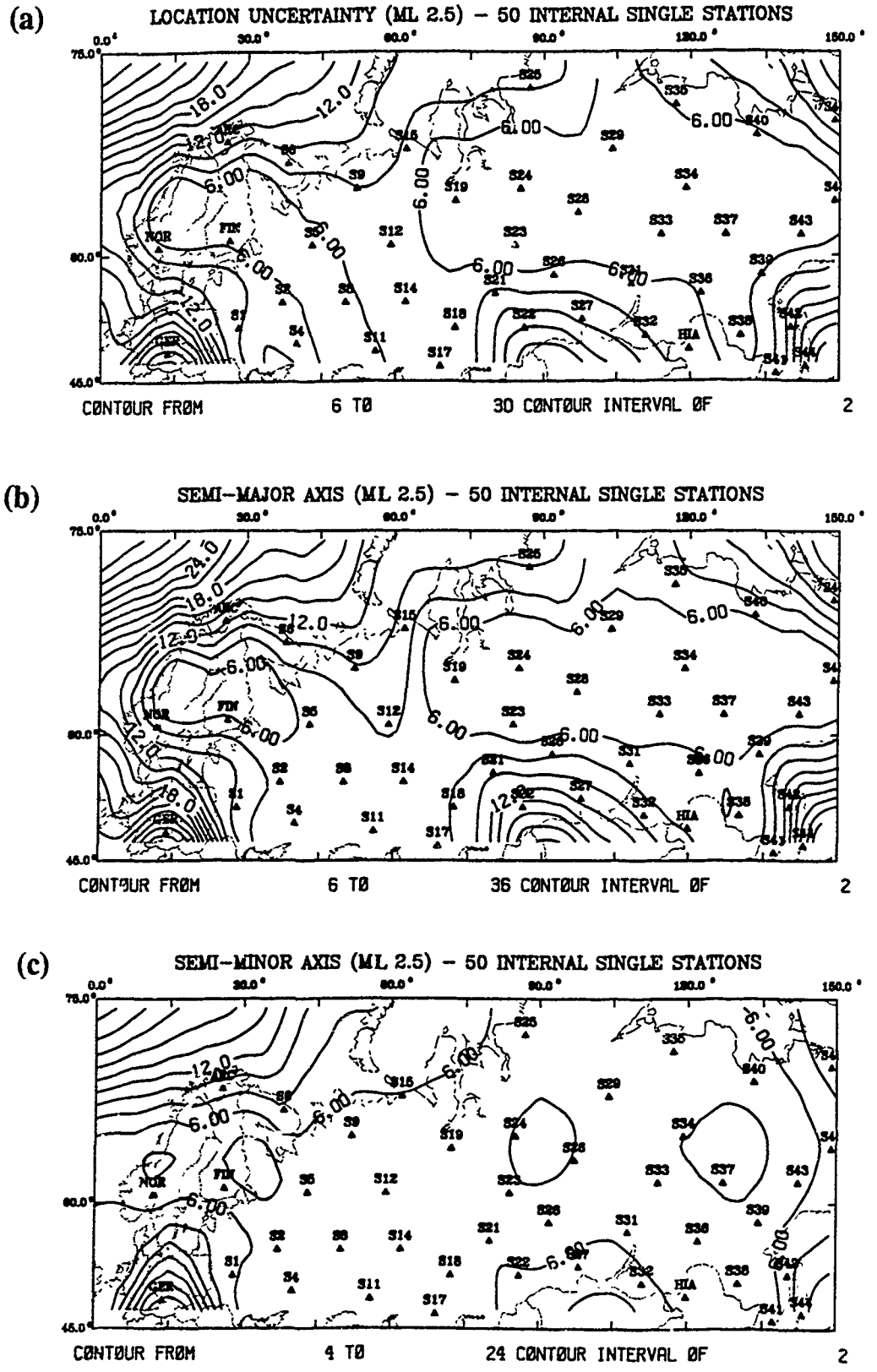

Figure 6.8. The 90th percentile (*a*) location uncertainty, (*b*) semi-major axis, and (*c*) semi-minor axis in kilometers are contoured for a fixed event size of M_L 2.5. The internal network consists of 50 IRIS-type single (3-component) stations.

6.3 Frequency Dependence

The digitization rate of the IRIS-type single stations is 20 samples/s, which is only half of the digitization rate used for the NORESS-type arrays. However, we find no reduction in the detection threshold for the network with 30 internal single stations if we increase the digitization rate to 40 samples/s. The reason is that the M_L 2.5 threshold is controlled by the capability to detect phases at distances greater than 500 km (the internal station spacing is about 800 km), and the frequency of the maximum *snr* in our parameterization for all regional phases is less than 10 Hz at these distances (as demonstrated below). Of course, there may be other advantages of higher sampling rates for nuclear explosion monitoring. For example, these higher frequencies could be useful for identifying regional events.

The frequency of the maximum *snr* for each wave type depends on epicentral distance, source corner frequency, frequency-dependent attenuation, beam gain, and noise. For example, Table 6.2 lists the frequency of the maximum *snr* for array stations predicted by our signal and noise models in Section 4 for an M_L 2.5 event (the corner frequency is 13 Hz). We do not include entries for *Pn* or *Sn* for distances less than 2° since this is close to the cross-over distance, or for *Pg* beyond 8° since it is rarely detected at distances greater than this. The frequency of the maximum *snr* generally decreases with increasing distance. The only exception is the *Sn* frequency which is 4–5 Hz for all distances in Table 6.2. The reason for this consistency is that the *Sn* signal spectrum and the pre-*Sn* noise spectrum (which includes *P* coda) have similar distance dependencies.

Table 6.2 Frequency of the maximum *snr* for regional phases.

	Frequency (Hz)			
Distance (°)	*Pn*	*Pg*	*Sn*	*Lg*
0–2	–	7–10	–	6–9
2–4	6–7	5–7	4–5	2–4
4–8	6–7	4–5	4–5	1.5–2
8–16	3–6	–	4–5	1.5–2

The frequency of the maximum *snr* predicted by our model is close to the observed frequency of the maximum *snr* for detections at NORESS and ARCESS. For example, Figure 6.9 plots histograms of the number of detections at these arrays as a function of the center frequency of the beam with the maximum *snr* for events in the *IMS* database at the Center for Seismic Studies. The *Pg* frequency is predominantly 6–12 Hz for distances less than 2°, and it decreases to 3.0–4.5 Hz between 4° and 8°. The *Lg* frequency is divided among the 3.0–4.5 Hz and 6–12 Hz bands for $\Delta < 2°$, and it decreases to 1.5–2.5 Hz for distances greater than 8°. The maximum *snr* for *Pn* occurs in the 3.0–4.5 Hz and 6–12 Hz bands for distances less than 8°, and it is predominantly 3.0–4.5 Hz at larger distances. The *Sn* frequency is nearly independent

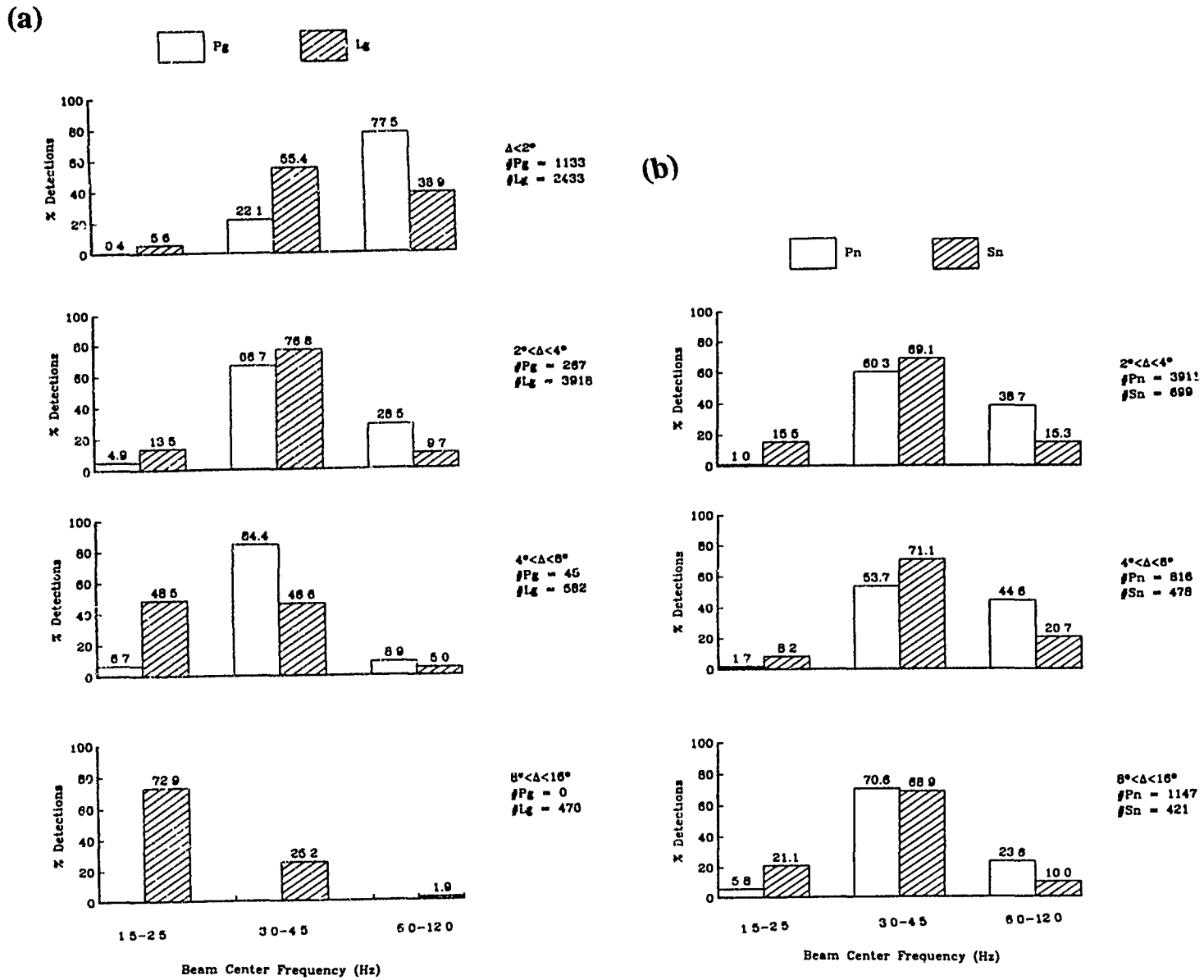

Figure 6.9. Histograms of the center frequency of the detecting beam (e.g., the beam with the maximum *snr*) in four distance ranges for (*a*) *Pg* and *Lg*, and (*b*) *Pn* and *Sn*. The distance ranges and total number of detections for each phase are listed to the

of distance (as predicted by our signal and noise models), and it occurs in the 3.0–4.5 Hz band.

6.4 Seismic Decoupling and Regions with Bedded or Domed Salt

Opportunities for cavity decoupling in the Soviet Union are primarily limited to regions with bedded or domed salt (Figure 6.10). Therefore, the number of stations needed to achieve a detection threshold of M_L 2.5 throughout the Soviet Union is a conservative estimate of the number of stations that are required to detect a 1 kt nuclear explosion. For example, Figure 6.11 plots the 90% M_L threshold for detecting 3 phases involving at least 2 stations for a network consisting of 15 internal IRIS-type single stations. The detection threshold for this network is $\leq M_L$ 2.5 for epicenters in known salt regions, and it is $\leq M_L$ 4.0 for all other epicenters in the Soviet Union. Thus, approximately half as many single stations are required to achieve a threshold of M_L 2.5 in regions of salt than are required to achieve this threshold throughout the Soviet Union.

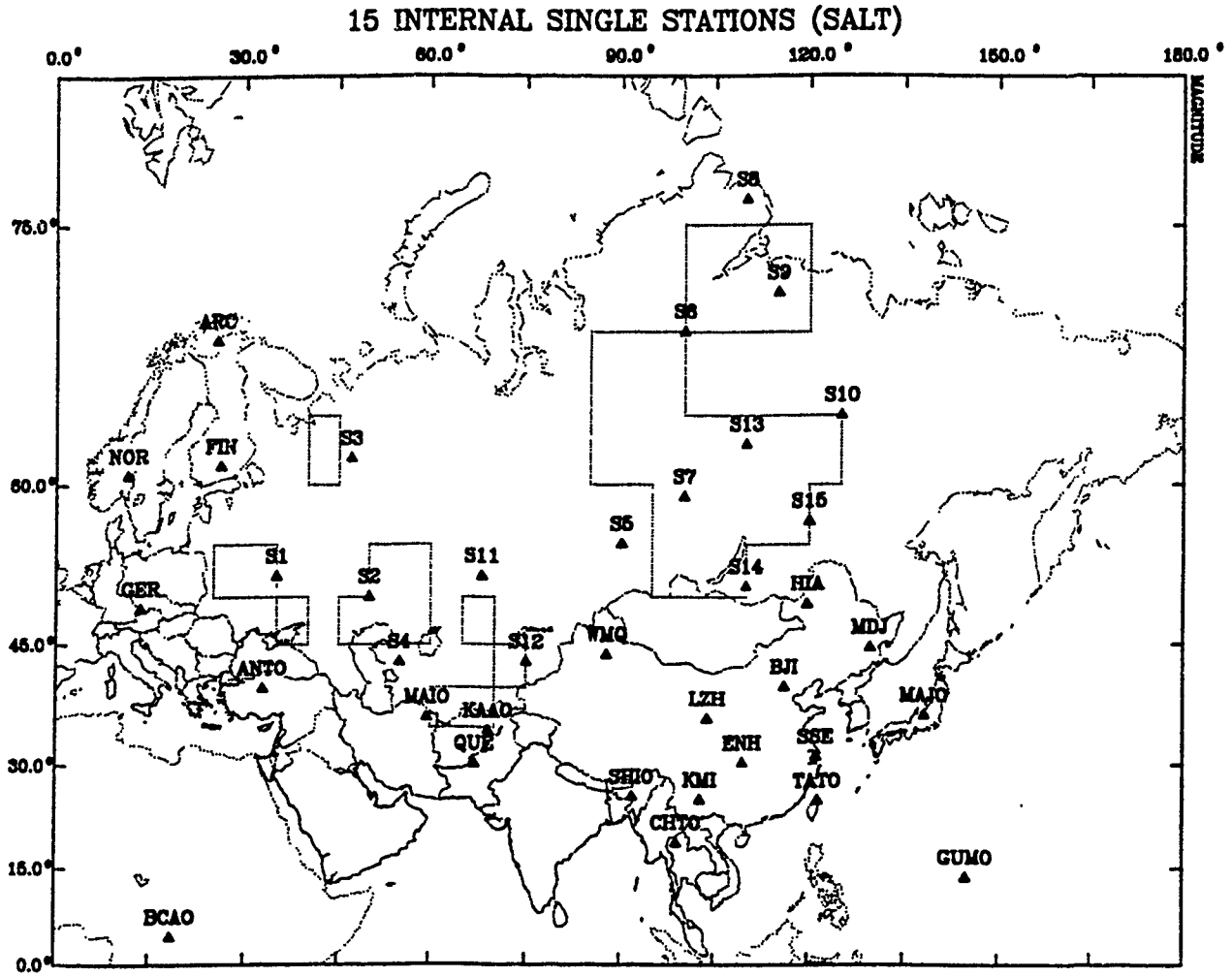

Figure 6.10. A 5°×5° grid of areas of bedded or domed salt in the Soviet Union are outlined on a map of Eurasia. This regionalization is based on a map of salt deposits in the USSR compiled by *Rachlin* [1985], and a draft version of a 1°×1° grid provided to us by Bill Leith at the USGS. Station locations for the internal and external networks are also plotted.

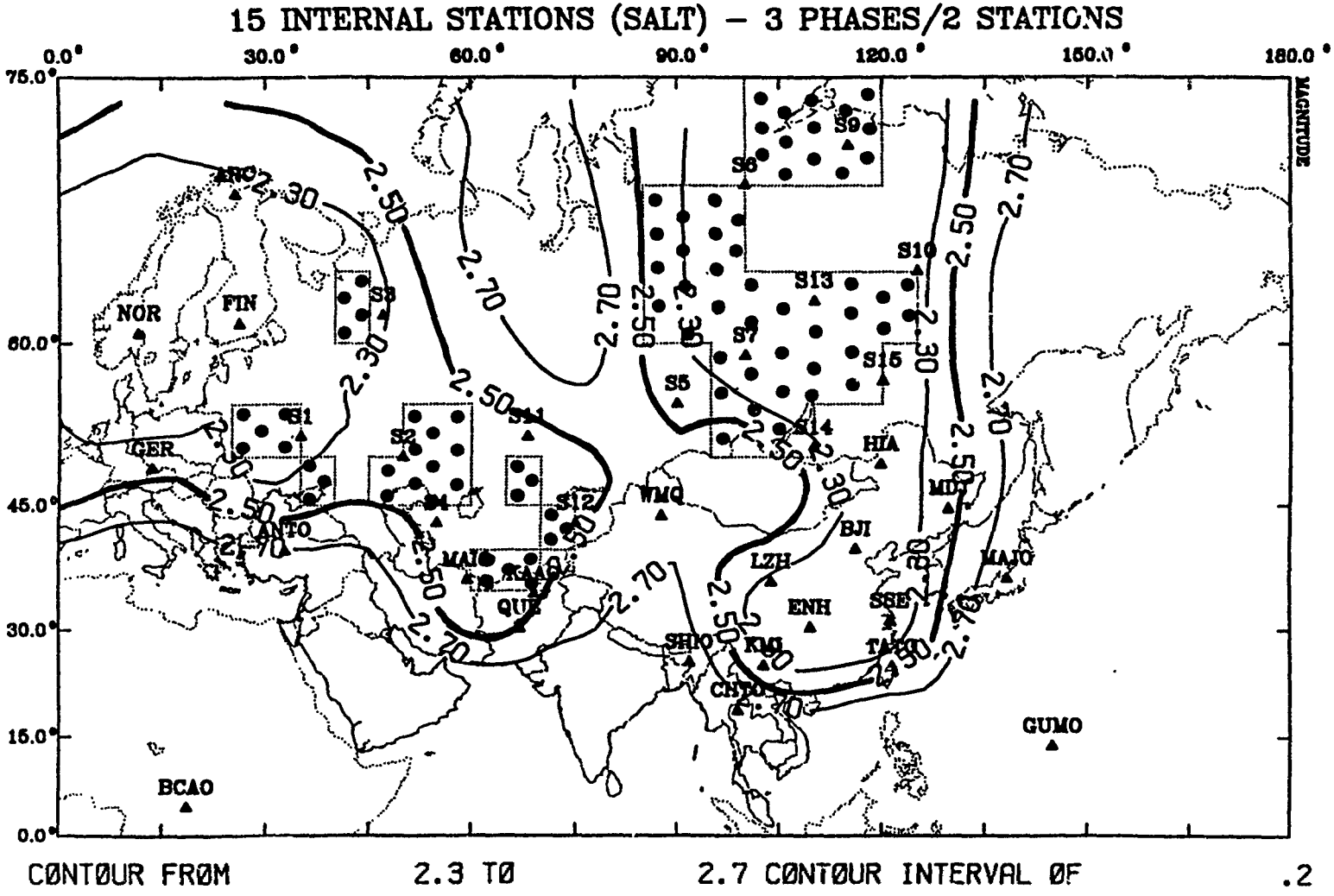

Figure 6.11. Estimate of the 90% M_L threshold for detecting 3 phases involving at least 2 stations is plotted for a network that includes 15 internal IRIS-type single stations. Only contours corresponding to M_L 2.3, 2.5, and 2.7 are shown. The dotted areas indicate regions with near-surface bedded or domed salt.

7. NOISE CONDITIONS

A key assumption used in the simulations is that the noise at each station in the network is the same as the average noise at NORESS. However, *Given* [1990] found that the ambient noise levels at the four IRIS stations in the Soviet Union (ARU, GAR, KIV, and OBN) are much higher than the ambient noise levels at NORESS. She found that the noise at Obninsk (OBN) is 10–16 dB higher than the noise at NORESS between 2 and 10 Hz. Similarly, she found that the noise at Garm (GAR) is 3-4 dB higher, and that the noise at Arti (ARU) and Kislovodsk (KIV) are 5-10 dB higher than at NORESS in this frequency band. For example, Figure 7.1 compares the average noise spectrum at NORESS used in our simulations to the average high-frequency noise spectra estimated by *Given* [1990] for the IRIS stations in Arti (ARU) and Kislovodsk (KIV). Of course, if the noise for the stations in our hypothetical network is similar to the IRIS station noise, then our estimates of the number of stations that are required to satisfy the performance criteria are too low.

Table 7.1 lists the median, minimum and maximum values of the 90% M_L threshold for detecting 3 phases involving at least two stations for several internal networks assuming that the station noise is equal to the KIV noise spectrum estimated by *Given* [1990]. Figure 7.2 shows the 90% M_L detection threshold for 30 internal single stations, and for 10 internal arrays (these networks satisfy the performance criteria if the noise is assumed to be the same as it is at NORESS). The detection threshold for the network with 30 internal single stations is M_L 2.3–3.0, and it is M_L 2.6–3.1 for 10 internal arrays. Therefore, these networks do not satisfy the performance criteria if the noise for the stations in the internal networks is the same as the noise at KIV. Figure 7.3 shows the 90% M_L detection threshold for 50 internal single stations, and for 30 internal arrays using the KIV noise. These networks achieve a threshold of M_L 2.5 for most (but not all) regions in the Soviet Union.

Table 7.1 90% M_L detection thresholds in the Soviet Union (KIV noise).

	3 Phases/2 Stations	
Internal Network	M_L^{50}	M_L^{min}–M_L^{max}
10 Arrays	2.9	2.6–3.1
30 Arrays	2.4	1.9–2.7
30 Single Stations	2.8	2.3–3.0
50 Single Stations	2.5	1.9–2.9

Approximately three times as many internal single stations are required to achieve a detection threshold of M_L 2.5 if the the KIV noise spectrum is used in the simulations instead of the NORESS noise spectrum. However, the noise at KIV may not represent the station noise for the internal network better than the noise at NORESS. For example, the NRDC station noise levels between 1 and 20 Hz in eastern Kazakhstan are within 2–3 dB of the noise levels at NORESS [*Sereno*, 1990*b*], and are

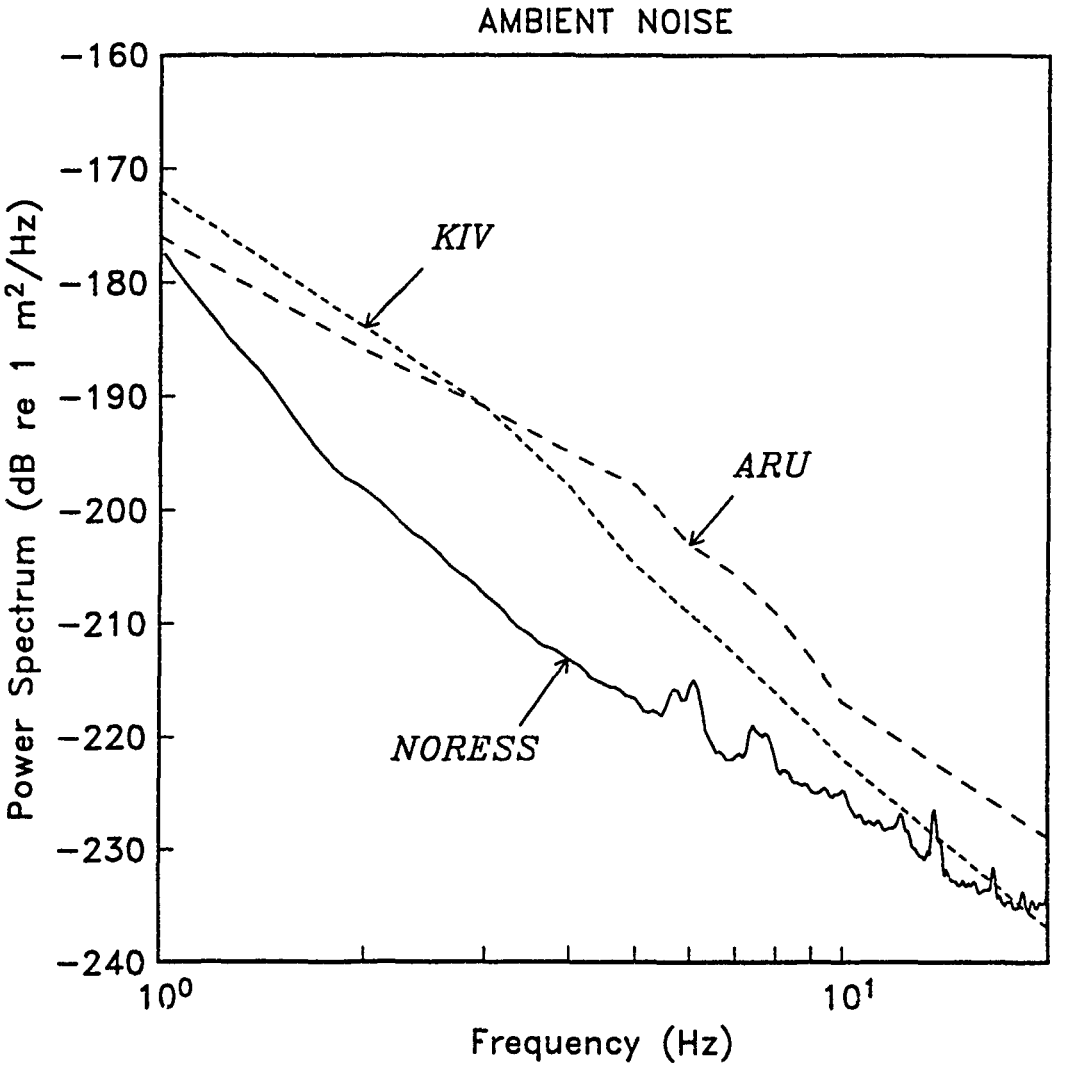

Figure 7.1. Ambient noise power spectral density is plotted for NORESS (see Figure 4.3), and for two IRIS stations in the Soviet Union (KIV and ARU). The IRIS station noise is from *Given* [1990].

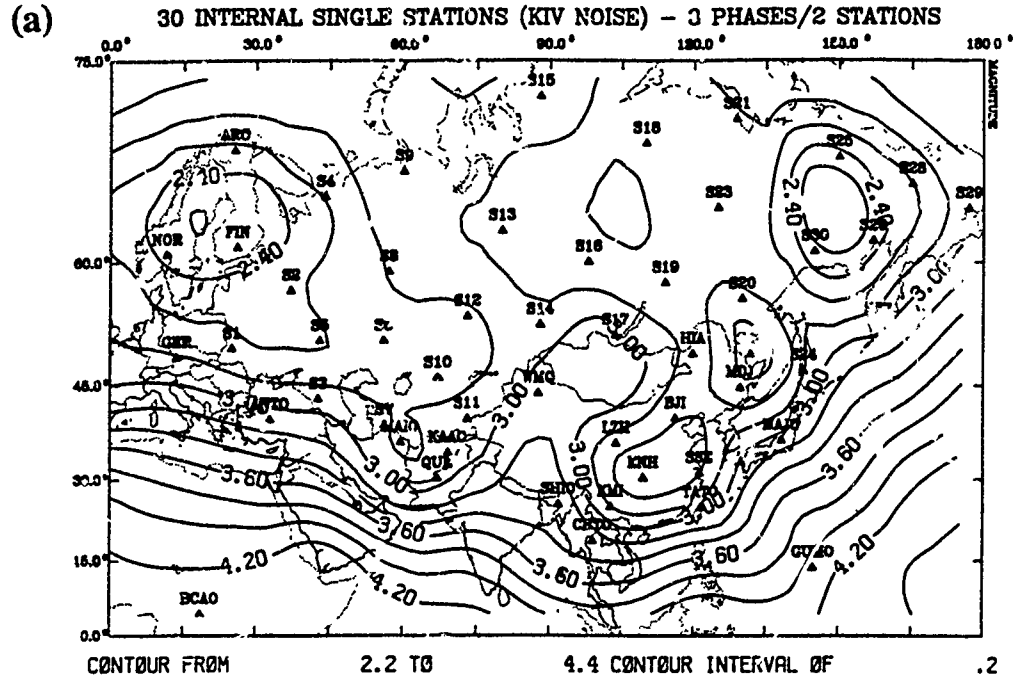

Figure 7.2. Estimates of the 90% M_L threshold for detecting 3 phases involving at least two stations are plotted for networks that include (*a*) 30 internal three-component stations, and (*b*) 10 internal NORESS-type regional arrays. The ambient noise at all stations is assumed to be the same as the average night noise estimated by *Given* [1990] for the borehole sensor at the IRIS station in Kislovodsk (KIV). The external network consists of 29 existing stations/arrays.

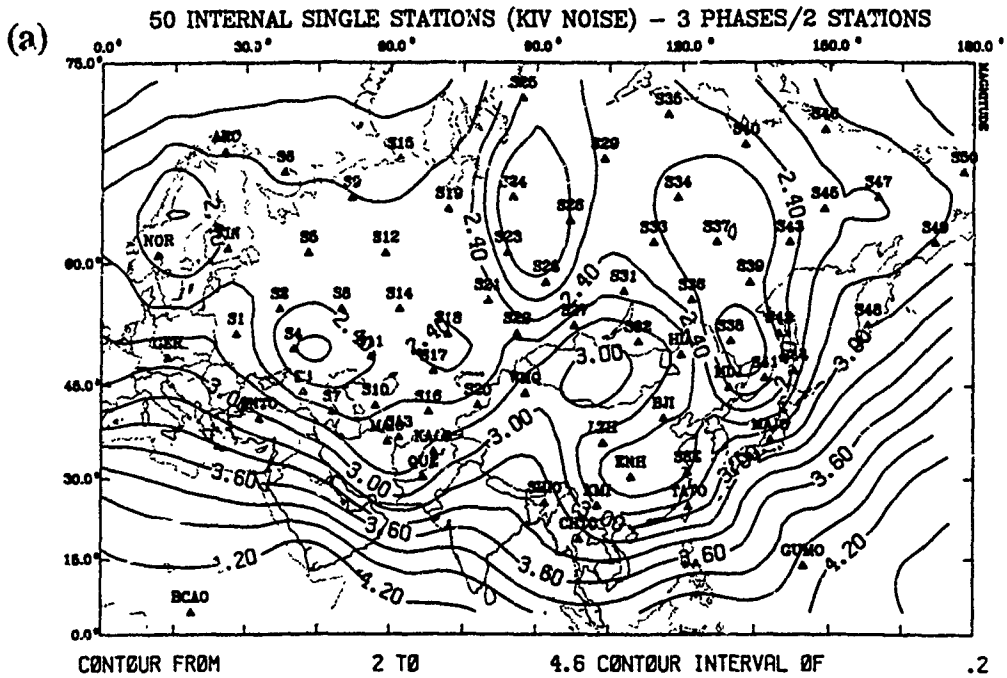

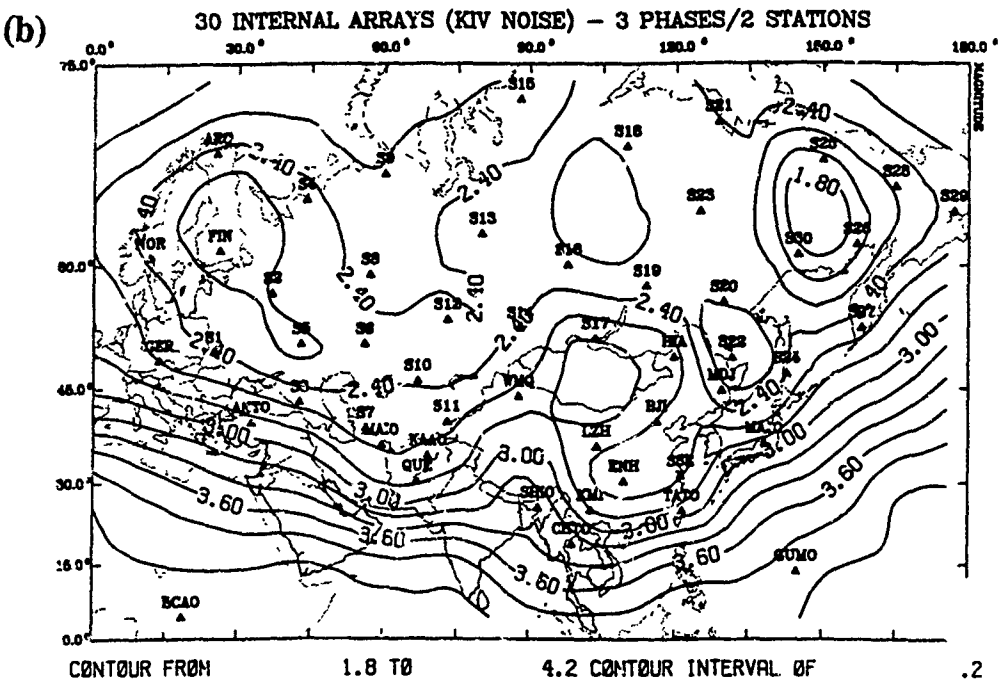

Figure 7.3. Estimates of the 90% M_L threshold for detecting 3 phases involving at least two stations are plotted for networks that include (*a*) 50 internal three-component stations, and (*b*) 30 internal NORESS-type regional arrays. The ambient noise at all stations is assumed to be the same as the average night noise estimated by *Given* [1990] for the borehole sensor at the IRIS station in Kislovodsk (KIV). The external network consists of 49 existing stations/arrays.

much lower than the noise levels at the IRIS sites. The IRIS sites are in more populated regions than the NRDC stations or NORESS because they had to be close to existing communication lines for data telemetry [*Given*, 1990]. Therefore, it is likely that sites with lower noise levels could be found in more remote areas for a seismic monitoring network.

(THIS PAGE INTENTIONALLY LEFT BLANK)

8. LATERAL VARIATIONS IN WAVE PROPAGATION

The simulations discussed so far are based on homogeneous wave propagation characteristics. However, this cannot be a good model for the propagation of regional phases in an area as large as the Soviet Union. Therefore, we developed a 5°×5° propagation grid from tectonic maps of Eurasia to approximate the effect of lateral variations (Figure 8.1). The grid includes "stable" regions (low attenuation) and "tectonic" regions (high attenuation). In this section, we use the attenuation in Fennoscandia for the "stable" regions, and we use two times this attenuation for the tectonic regions to estimate the effects of lateral variations in wave propagation characteristics on the detection thresholds. Also, since it is well-known that *Lg* propagation can be disrupted by lateral variations in crustal structure [e.g., *Kennett*, 1986; *Baumgardt*, 1990], we repeated the simulations with the assumption that *Lg* cannot propagate through tectonic regions.

Table 8.1 90% M_L detection thresholds with lateral variations in attenuation.

Internal Network	*Lg* Blockage	M_L^{50}	M_L^{min}–M_L^{max}
30 Single Stations	N	2.4	2.0–2.7
30 Single Stations	Y	2.5	2.0–2.9
40 Single Stations	N	2.2	2.1–2.7
40 Single Stations	Y	2.3	2.1–2.8

Table 8.1 summarizes our results for networks with 30 or 40 internal single stations. The 90% M_L threshold for detecting 3 phases involving 2 stations is 2.0–2.7 for the network with 30 internal single stations (Figure 8.2*a*). The median value for this network is 2.4, which is only 0.1 higher than if homogeneous stable conditions are assumed (but the variation is larger). If we assume that *Lg* is blocked by tectonic structure, then the detection threshold for this network is 2.0–2.9 (Figure 8.2*b*). Figure 8.3 plots the 90% M_L detection thresholds for the network with 40 internal single stations. The median threshold for this network is M_L 2.3 if *Lg* blockage is included, and the range is 2.1–2.8. It is likely that this large variation can be reduced by changing the locations of the internal stations.

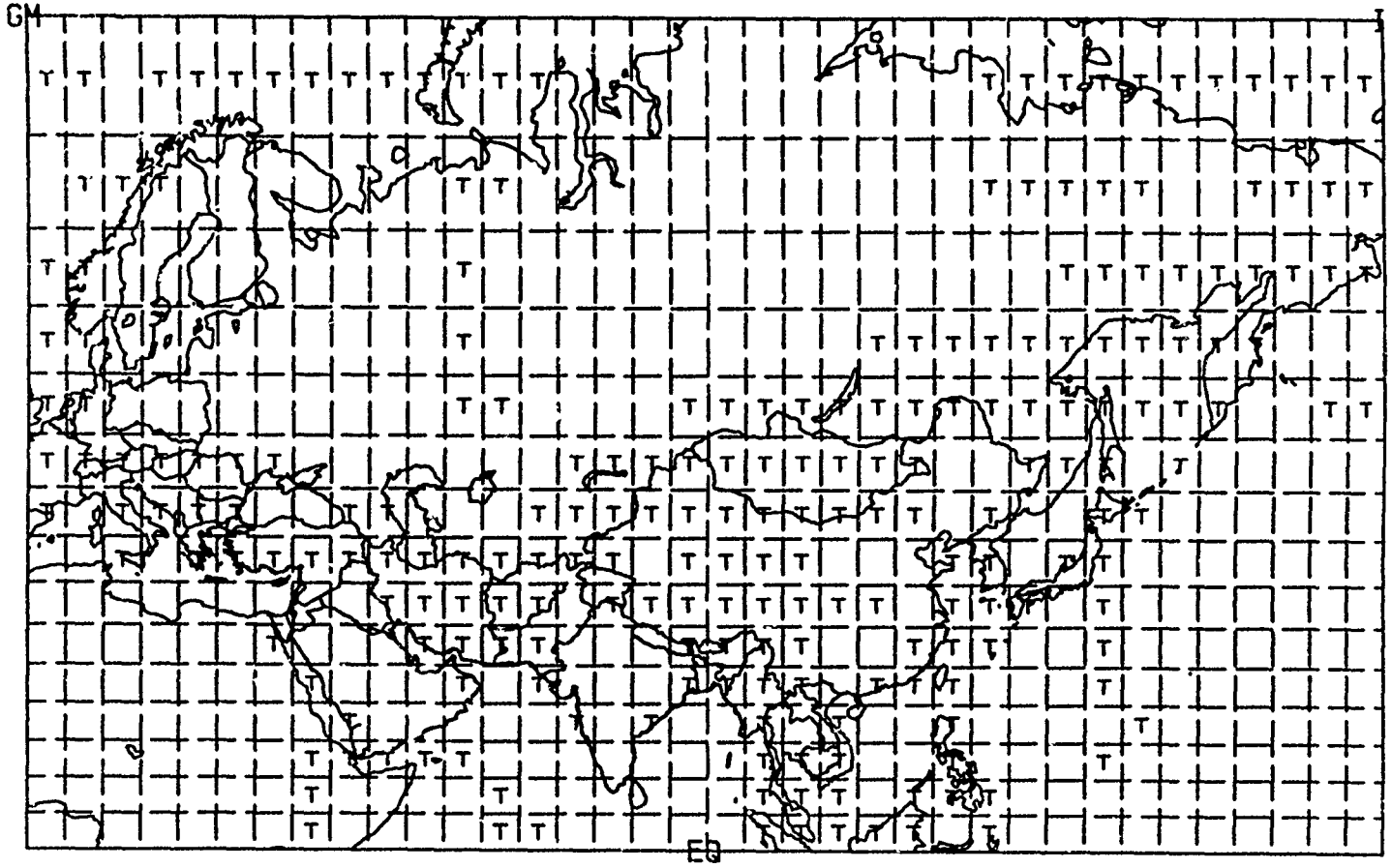

Figure 8.1. This maps shows a 5°×5° regionalization of the attenuation in Eurasia [see *Sereno*, 1990*a*]. Tectonic regions (high attenuation) are labeled "T", and stable regions (low attenuation) are not labeled.

(a)

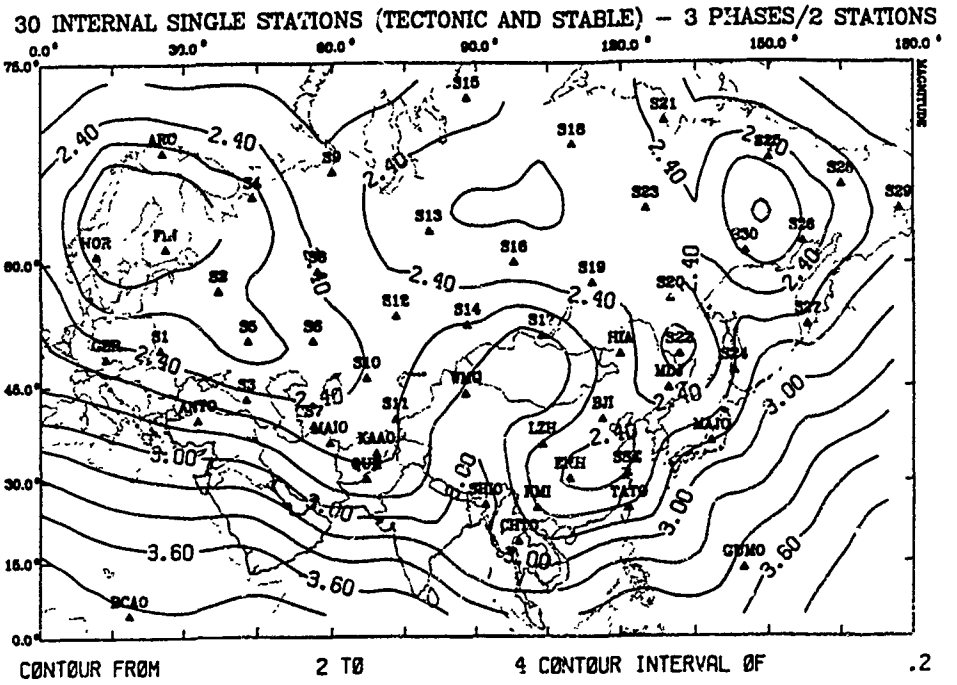

(b)

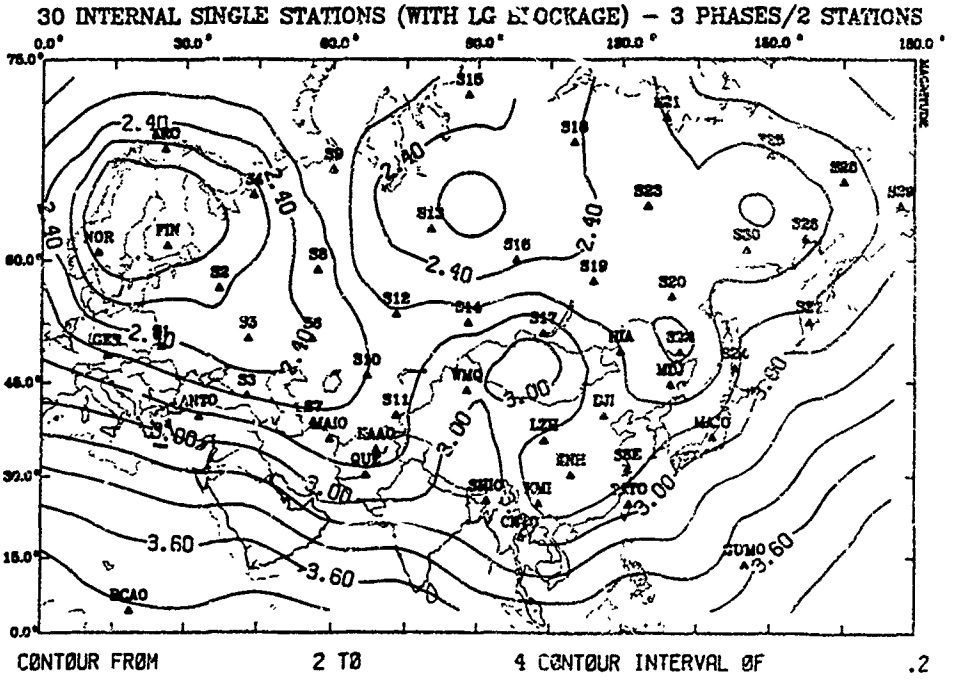

Figure 8.2. Estimates of the 90% M_L threshold for detecting 3 phases involving at least two stations are plotted for a network that includes 30 internal three-component stations. The attenuation in tectonic regions is assumed to be two times higher than it is in stable regions for *Pn*, *Pg*, and *Sn* (see the grid in Figure 8.1). (*a*) *Lg* attenuation in tectonic regions is two times higher than *Lg* attenuation in stable regions, and (*b*) *Lg* is blocked for tectonic regions.

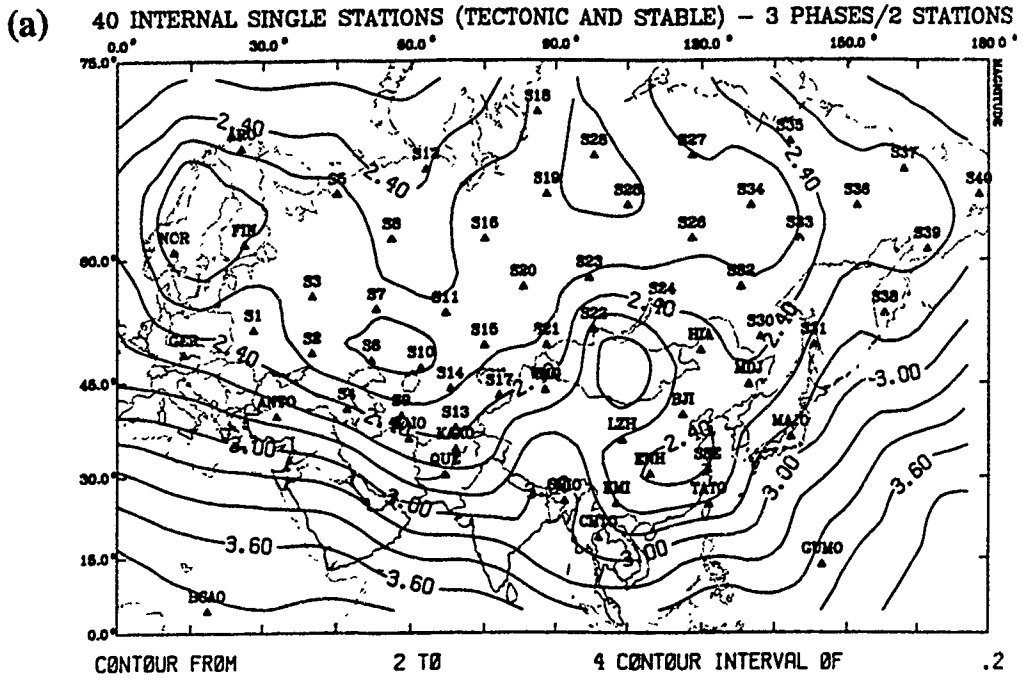

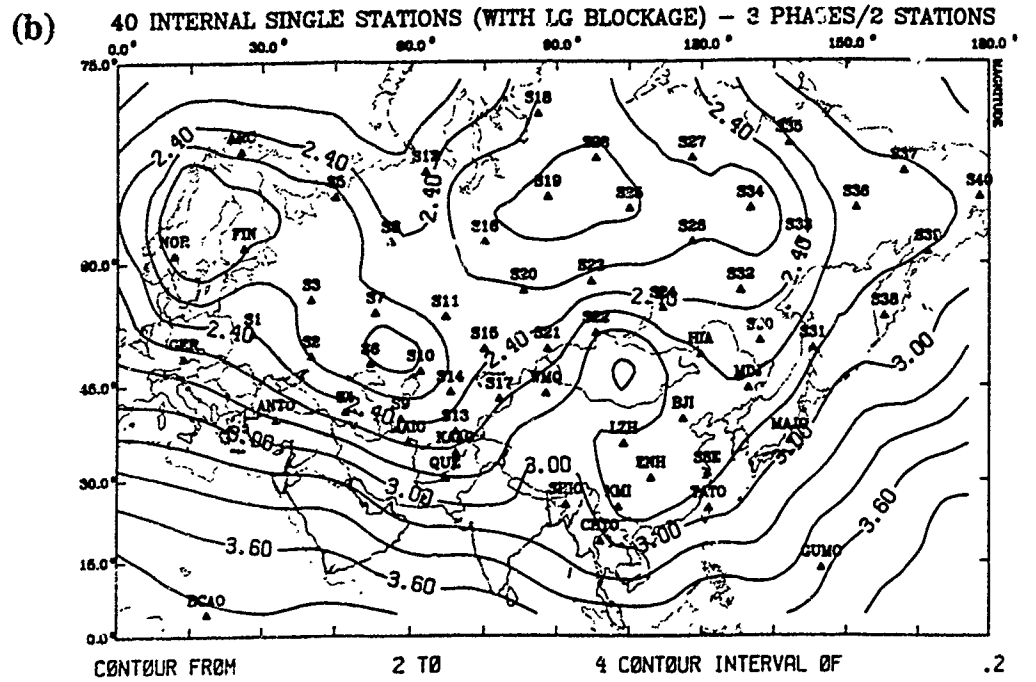

Figure 8.3. Estimates of the 90% M_L threshold for detecting 3 phases involving at least two stations are plotted for a network that includes 40 internal three-component stations. The attenuation in tectonic regions is assumed to be two times higher than it is in stable regions for *Pn*, *Pg*, and *Sn* (see the grid in Figure 8.1). (*a*) *Lg* attenuation in tectonic regions is two times higher than *Lg* attenuation in stable regions, and (*b*) *Lg* is blocked for tectonic regions.

9. CONCLUSIONS

The main objective of this two-year project is to assess the treaty monitoring capability of existing and proposed seismic networks in the Soviet Union. We define the goal of the monitoring network to be detection and accurate location of nuclear explosions in the Soviet Union with yields ≥ 1 kt. This corresponds to a detection threshold of approximately M_L 2.5 if the explosion is fully-decoupled. We concentrate on a 1-kt threshold (as opposed to lower thresholds) for the following reasons:

- This is significantly lower than the detection threshold of current monitoring systems.
- Monitoring at this level does not require many more in-country stations than have already been negotiated through IRIS.
- Data from these proposed internal stations could be used to study signal and noise characteristics of regional phases in the Soviet Union, so that requirements for achieving lower thresholds in the future can be accurately assessed.

The main results are summarized in Table 9.1. If the signal and noise conditions in the Soviet Union are the same as those in Fennoscandia, then 10 internal NORESS-type arrays or 30 internal IRIS-type single stations are required to achieve a detection threshold of ≤ M_L 2.5 throughout the Soviet Union. Here we require detection of 3 phases involving at least two stations, which gives location uncertainties ≤ 20 km at the 90% confidence level. Only half as many internal single stations are needed to reach this threshold for regions of bedded or domed salt (e.g., regions where full-decoupling is feasible). If secondary phases are not included in the detection criteria, then ≥ 20 internal NORESS-type arrays or ≥ 50 single stations are required to reach the M_L 2.5 threshold. There is no reduction in the detection threshold if the digitization rate of the internal IRIS-type stations is increased from 20 to 40 samples/s. However, there may be other advantages to higher sampling rates for monitoring nuclear explosion testing (such as event identification).

Table 9.1 Hypothetical monitoring networks.

90% Detection Threshold	Detection Criterion	Noise	Number of Arrays[1]	Number of Single Stations[2]
M_L 2.5	3 Phases/2 Stations	NORESS	10	30
M_L 2.5	3 P Phases/3 Stations	NORESS	≥ 20	≥ 50
M_L 2.5 (salt)	3 Phases/2 Stations	NORESS	–	15
M_L 2.5	3 Phases/2 Stations	KIV	≥ 30	≥ 50

1. NORESS-type arrays
2. IRIS-type 3-component stations

More stations are required to achieve the M_L 2.5 threshold if the noise at the internal stations is assumed to be like that observed at the IRIS stations. For example, $\geq$ 30 internal arrays or $\geq$ 50 internal single stations are required to achieve this threshold if the station noise for the hypothetical network is the same as the noise at the IRIS station in Kislovodsk, USSR (KIV). However, the IRIS stations are close to populated areas, and it is likely that quieter sites could be found for stations in the monitoring network. For example, the NRDC stations in eastern Kazakhstan have similar noise levels to those at NORESS, and much lower noise levels than the IRIS stations.

More stations are also required to reach the M_L 2.5 threshold if we assume that regional wave attenuation is greater for tectonic regions than it is for stable regions. For example, the 90% M_L detection threshold for the network with 30 internal single stations is 1.9–2.5 if stable propagation characteristics are assumed throughout the Soviet Union. If the attenuation for tectonic (orogenic) regions is assumed to be twice as high as the attenuation for stable regions, then the detection threshold for this network is M_L 2.0–2.7. However, the locations of the internal stations in the hypothetical network were selected on the basis of homogeneous propagation characteristics. It is likely that lower thresholds could achieved with the same number of internal stations if their locations were selected on the basis of known (or expected) lateral variations in attenuation.

The accuracy of the simulations depends on the accuracy of the normalization. We are confident that we have accurately parameterized the performance of the NORESS and ARCESS arrays in Norway, but there is still much uncertainty in extrapolating these capabilities to networks in the Soviet Union. The accuracy of the normalization can be improved as experience is gained from new stations installed in the Soviet Union. Once enough new data has been collected and analyzed, the capability of the hypothetical networks should be re-evaluated.

ACKNOWLEDGMENTS

I thank Thomas Bache and Henry Swanger for many helpful suggestions and discussions. I am also grateful to Donna Williams who did nearly all of the data processing, and analysis of geologic and tectonic maps of Eurasia. I thank Bill Leith at the United States Geological Survey for providing me with an atlas of Asia and eastern Europe, and for his regionalization of domed and folded salt in the Soviet Union. This research was funded by the Defense Advanced Research Projects Agency under Contract F08606-88-C-0033 and monitored by Air Force Technical Applications Center.

(THIS PAGE INTENTIONALLY LEFT BLANK)

REFERENCES

Aki, K., and P. Richards, *Quantitative Seismology: Theory and Methods*, W. H. Freeman, San Francisco, Calif., 1980.

Berger, J., H. Eissler, F. Vernon, I. Nersesov, M. Gokhberg, O. Stolyrov, and N. Tarasov, Studies of high-frequency seismic noise in Eastern Kazakhstan, *Bull. Seismol. Soc. Am., 78*, 1744–1758, 1988.

Baumgardt, D., Investigation of teleseismic *Lg* blockage and scattering using regional arrays, *Bull. Seismol. Soc. Am., 80*, 2261–2281, 1990.

Bratt, S. and T. Bache, Locating events with a sparse network of regional arrays, *Bull. Seismol. Soc. Am., 78*, 780–798, 1988.

Bratt, S., T. Bache, D. Williams, Seismic monitoring capability in the Soviet Union using hypothetical regional networks, *Final Tech. Rep. SAIC 87/1752*, Sci. Appl. Int. Corp., San Diego, Calif., AFGL-TR-87-0244, 1987.

Bratt, S., H. Swanger, R. Stead, F. Ryall, and T. Bache, Initial results from the intelligent monitoring system, *Bull. Seismol. Soc. Am., 80*, 1852–1873, 1990.

Bungum, H., S. Vaage, and E. Husebye, The Meloy earthquake sequence, northern Norway: Source parameters and their moment scaling relations, *Bull. Seismol. Soc. Am., 72*, 197–206, 1982.

Bungum, H., S. Mykkeltveit, and T. Kvaerna, Seismic noise in Fennoscandia, with emphasis on high frequencies, *Bull. Seismol. Soc. Am., 75*, 1489–1515, 1985.

Chun, K., Kokoski, R., and G. West, High-frequency *Pn* attenuation in the Canadian Shield, *Bull. Seismol. Soc. Am., 79*, 1039–1053, 1989.

Ciervo, A., S. Sanemitsu, D. Snead, R. Suey, and A. Watson, User's manual for *SNAP/D*: seismic network assessment program for detection, *Pacific-Sierra Research Corporation, Report 1027B*, 1985.

Fyen, J., NORESS noise spectral studies, preliminary report, *Sci. Rep. 2-85/86*, NTNF/NORSAR, Kjeller, Norway, 1986.

Fyen, J. NORESS noise spectral studies: Noise level characteristics, *Sci. Rep. 2-86/87*, NTNF/NORSAR, Kjeller, Norway, 1987.

Gibowicz, S., NORESS capability for detection and location of mining tremors in the Lubin area of Poland, *Sci. Rep. 2-86/87*, NTNF/NORSAR, Kjeller, Norway, 1987.

Given, H., Variations in broadband seismic noise at IRIS/IDA stations in the USSR with implications for event detection, *Bull. Seismol. Soc. Am., 80*, 2072–2088, 1990.

Harris, D., Comparison of the direction estimation performance of high frequency seismic arrays and three-component stations, *Bull. Seismol. Soc. Am., 80*, 1951–1968, 1990.

Hasegawa, H., *Lg* spectra of local earthquakes recorded by the Eastern Canada Telemetered Network and spectral scaling, *Bull. Seismol. Soc. Am., 73*, 1041–1061, 1983.

Jarpe, S., and F. Dowla, Performance of high-frequency three-component stations for azimuth estimation from regional seismic phases, UCRL-101181, Lawrence Livermore National Laboratory, Livermore, California, 1989.

Jurkevics, A., Polarization analysis of three-component array data, *Bull. Seismol. Soc. Am., 78*, 1725–1743, 1988.

Kennett, B., On regional S, *Bull. Seismol. Soc. Am., 75*, 1077–1086, 1985.

Kennett, B., *Lg* waves and structural boundaries, *Bull. Seismol. Soc. Am., 76*, 1133–1142, 1986.

Kvaerna, T., On exploitation of small-aperture NORESS type arrays for enhanced *P*-wave detectability, *Bull. Seismol. Soc. Am., 79*, 888–900, 1989.

Kvaerna, T., and D. Doornbos, An integrated approach to slowness analysis with arrays and three-component stations, *Sci. Rep. 2-85/86*, NTNF/NORSAR, Kjeller, Norway, 1986.

Kvaerna, T., S. Kibsgaard, and F. Ringdal, False alarm statistics and threshold determination for regional event detection, *Sci. Rep. 1-87/88*, NTNF/NORSAR, Kjeller, Norway, 1987.

Mueller, R., and J. Murphy, Seismic characteristics of underground nuclear detonations, *Bull. Seismol. Soc. Am., 61*, 1675–1692, 1971.

Mykkeltveit, S., NORESS real time processing performance for events in western Norway and the North Sea, *Sci. Rep. 2-85/86*, NTNF/NORSAR, Kjeller, Norway, 1986.

Mykkeltveit, S., and F. Ringdal, New results from processing of data recorded at the new ARCESS regional array, *Sci. Rep. 2-87/88*, NTNF/NORSAR, Kjeller, Norway, 1988.

Mykkeltveit, S., F. Ringdal, J. Fyen, and T. Kvaerna, Initial results from analysis of data recorded at the new regional array in Finnmark, Norway, *Sci. Rep. 1-87/88*, NTNF/NORSAR, Kjeller, Norway, 1987.

Office of Technology Assessment, U.S. Congress, Seismic verification of nuclear testing Treaties, *OTA-ISC-361*, Washington D.C., 1988.

Rachlin, J. Cavity construction opportunities in the Soviet Union, Proceedings of the Cavity Decoupling Workshop, Pajaro Dunes, Calif., July 29–31, Editor: Donald Larson, v53–v66, 1985.

Ringdal, F., Real time event detection using the small-aperture NORESS array, *Sci. Rep. 2-84/85*, NTNF/NORSAR, Kjeller, Norway, 1985.

Ringdal, F., Regional event detection using the NORESS array, *Sci. Rep. 2-85/86*, NTNF/NORSAR, Kjeller, Norway, 1986.

Rivers, W., A. Watson, and A. Ciervo, Data base for *SNAP/D*: Seismic network assessment program for detection, *Final Rep. PSR Report 1551*, Pacific-Sierra Research Corp., Los Angeles, Calif., 1985.

Sereno, T., Attenuation of regional phases in Fennoscandia and estimates of the arrival time and azimuth uncertainty using data recorded by regional arrays, *Semiannu. Tech. Rep. SAIC 90/1472*, Sci. Appl. Int. Corp., San Diego, Calif., 1990*a*.

Sereno, T. Frequency-dependent attenuation in eastern Kazakhstan and implications for seismic detection thresholds in the Soviet Union, *Bull. Seismol. Soc. Am.*, *80*, 2089–2105, 1990*b*.

Sereno, T., S. Bratt, and T. Bache, Simultaneous inversion of regional wave spectra for attenuation and seismic moment in Scandinavia, *J. Geophys. Res.*, *93*, 2019-2035, 1988.

Sereno, T., S. Bratt, and G. Yee, *NetSim*: A computer program for simulating detection and location capability of regional seismic networks, *Annu. Tech. Rep. SAIC 90/1163*, Sci. Appl. Int. Corp., San Diego, Calif., 1990.

Sereno, T., and J. Given, *Pn* attenuation for a spherically symmetric earth model, *Geophys. Res. Lett.*, *17*, 1141–1144, 1990.

Simarski, L., Seismic glastnost opens U.S.S.R. to U.S. researchers, *EOS*, *72*, 9–10, 1991.

Suteau-Henson, A., Estimating azimuth and slowness from three-component and array stations, *Bull. Seismol. Soc. Am.*, *80*, 1987–1998, 1990.

Suteau-Henson, A., and T. Bache, Spectral characteristics of regional phases recorded at NORESS, *Bull. Seismol. Soc. Am.*, *78*, 708–725, 1988.

The Monitor, *Quarterly Newsletter of the Nuclear Monitoring Research Office, DARPA*, *2*, 2–4, 1990.

Veith, K., and G. Clawson, Magnitude form short-period *P* wave data, *Bull. Seismol. Soc. Am.*, *62*, 435–452, 1972.

Wirth, M., Estimation of network detection and location capability, Air Force Applications Center, Washington DC, [revision of August 1970 report], 1977.

APPENDIX A: SIMULATIONS

This appendix gives plots of the 90% M_L detection thresholds for networks that include 0, 5, 10, 20, 30, 40, and 50 internal stations or arrays (Section 5). These simulations are based on signal and noise conditions in Fennoscandia. The plots are divided into two categories based on the detection criteria. The first category is for detection of 3 phases involving 2 stations. This criterion gives a location uncertainty of ≤ 20 km at the 90% confidence level for M_L 2.5 events in the Soviet Union. The second category is for detection of 3 *P*-type phases involving 3 stations. The location uncertainty in this case ≤ 15 km. Table A.1 lists the detection thresholds for each of these networks.

Table A.1 90% M_L detection thresholds in the Soviet Union.

	3 Phases/2 Stations			3 *P* Phases/3 Stations		
Internal Network	M_L^{50}	M_L^{min}–M_L^{max}	Figure	M_L^{50}	M_L^{min}–M_L^{max}	Figure
None	3.2	2.2–3.8	A.1	4.0	2.6–4.4	A.12
5 Arrays	2.6	2.2–2.9	A.2	3.1	2.5–4.0	A.13
10 Arrays	2.3	2.1–2.5	A.3	2.7	2.4–3.0	A.14
20 Arrays	2.1	1.9–2.4	A.4	2.4	2.2–2.6	A.15
30 Arrays	1.9	1.5–2.2	A.5	2.2	2.1–2.4	A.16
5 Single Stations	2.9	2.2–3.2	A.6	3.4	2.6–4.1	A.17
10 Single Stations	2.7	2.2–2.8	A.7	3.0	2.5–3.6	A.18
20 Single Stations	2.5	2.2–2.7	A.8	2.9	2.5–3.0	A.19
30 Single Stations	2.3	1.9–2.5	A.9	2.7	2.4–2.8	A.20
40 Single Stations	2.1	1.9–2.5	A.10	2.6	2.4–2.8	A.21
50 Single Stations	2.0	1.6–2.4	A.11	2.5	2.3–2.7	A.22

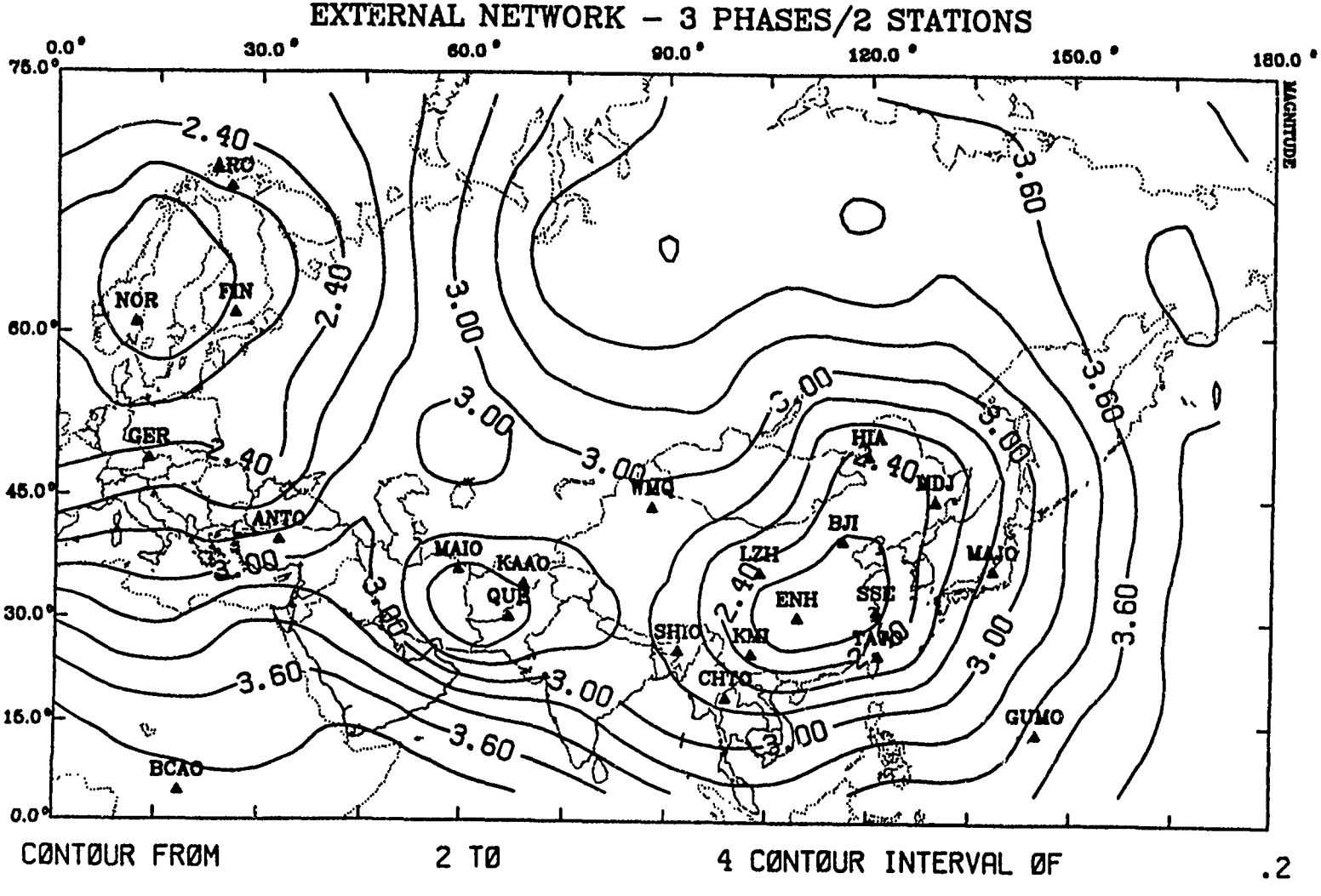

Figure A.1. Estimates of the 90% M_L threshold for detecting 3 phases involving 2 stations are plotted for a network that consists of 49 external stations/arrays.

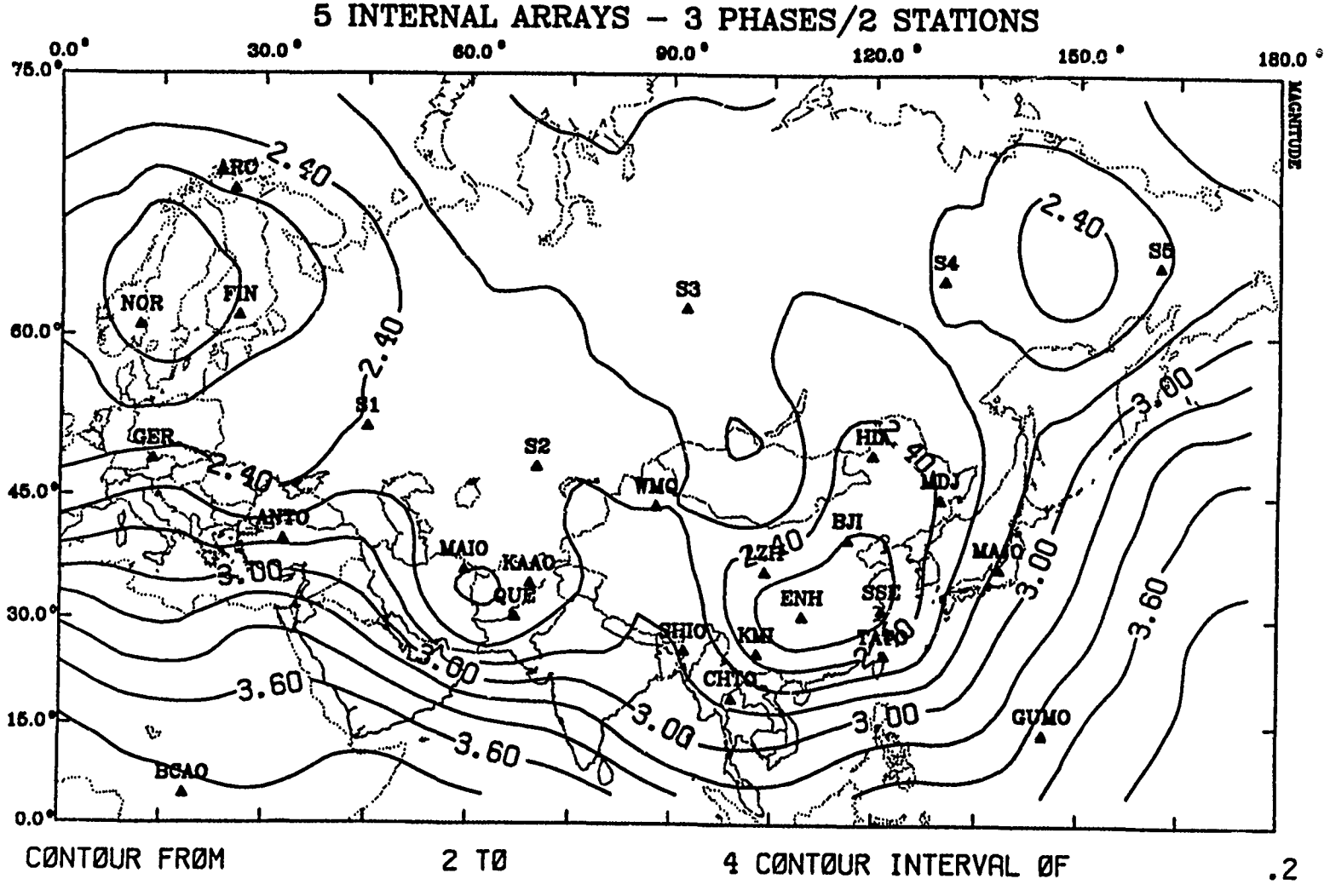

Figure A.2. Estimates of the 90% M_L threshold for detecting 3 phases involving 2 stations are plotted for a network that consists of 5 internal NORESS-type arrays and 49 external stations/arrays.

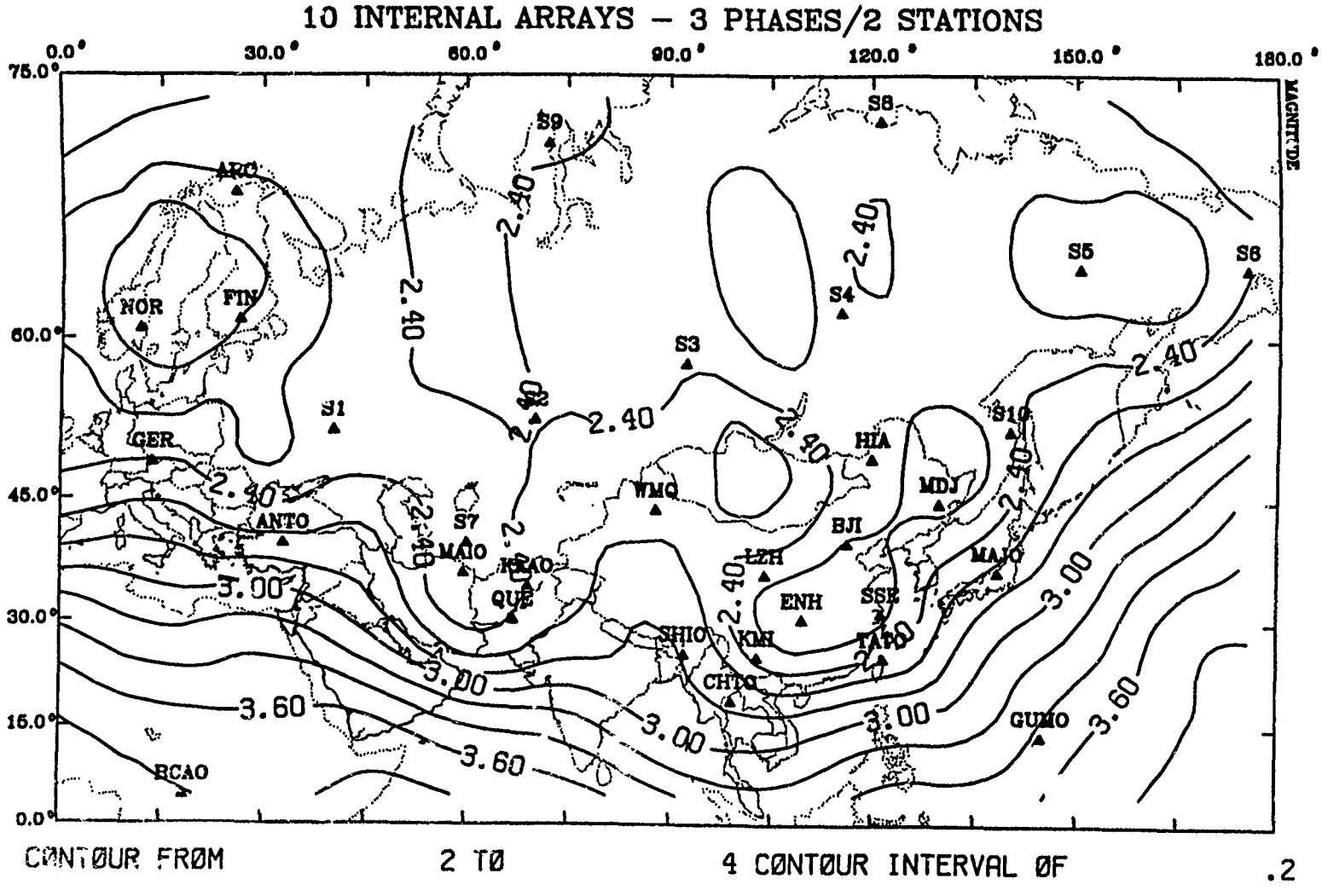

Figure A.3. Estimates of the 90% M_L threshold for detecting 3 phases involving 2 stations are plotted for a network that consists of 10 internal NORESS-type arrays and 49 external stations/arrays.

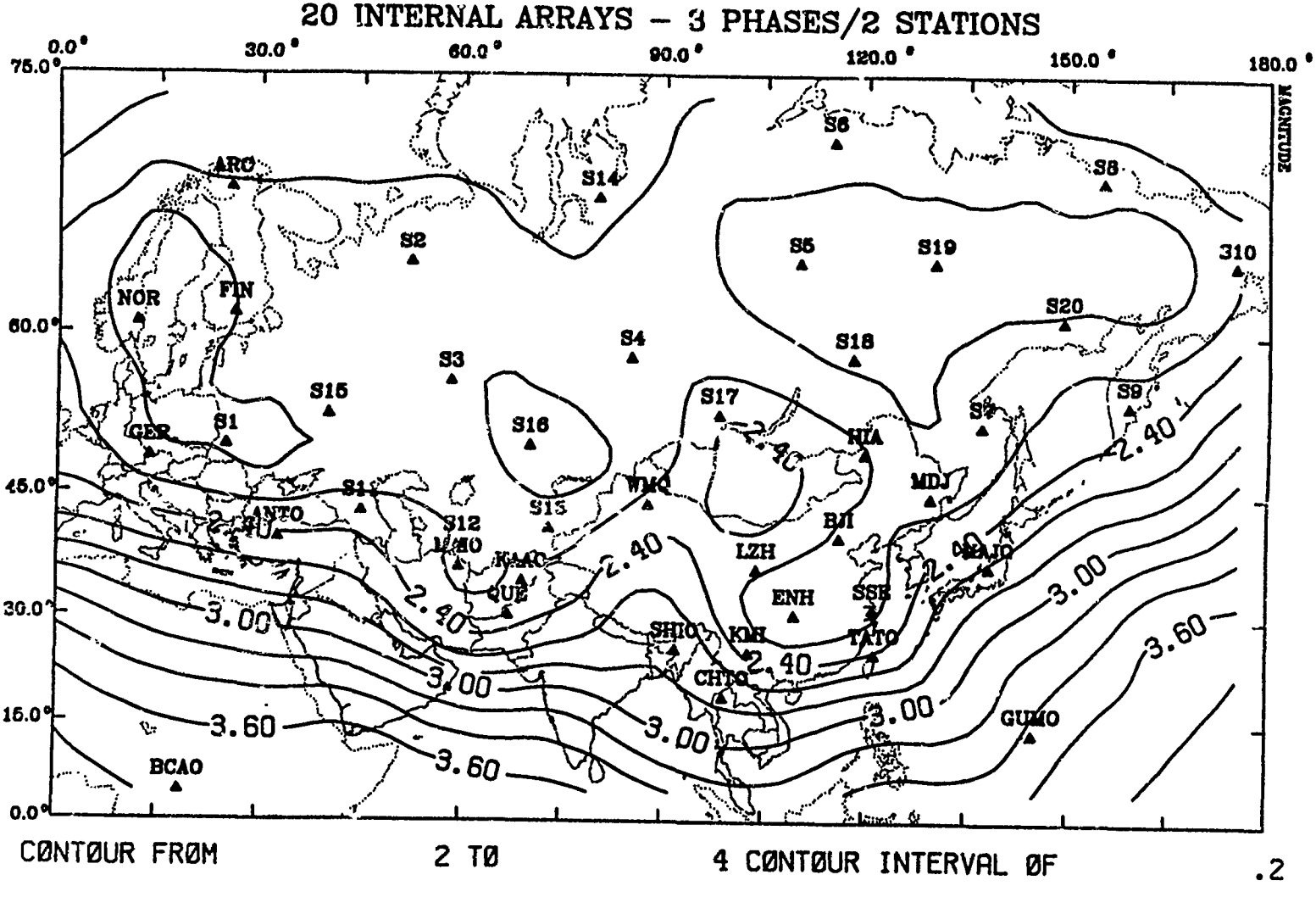

Figure A.4. Estimates of the 90% M_L threshold for detecting 3 phases involving 2 stations are plotted for a network that consists of 20 internal NORESS-type arrays and 49 external stations/arrays.

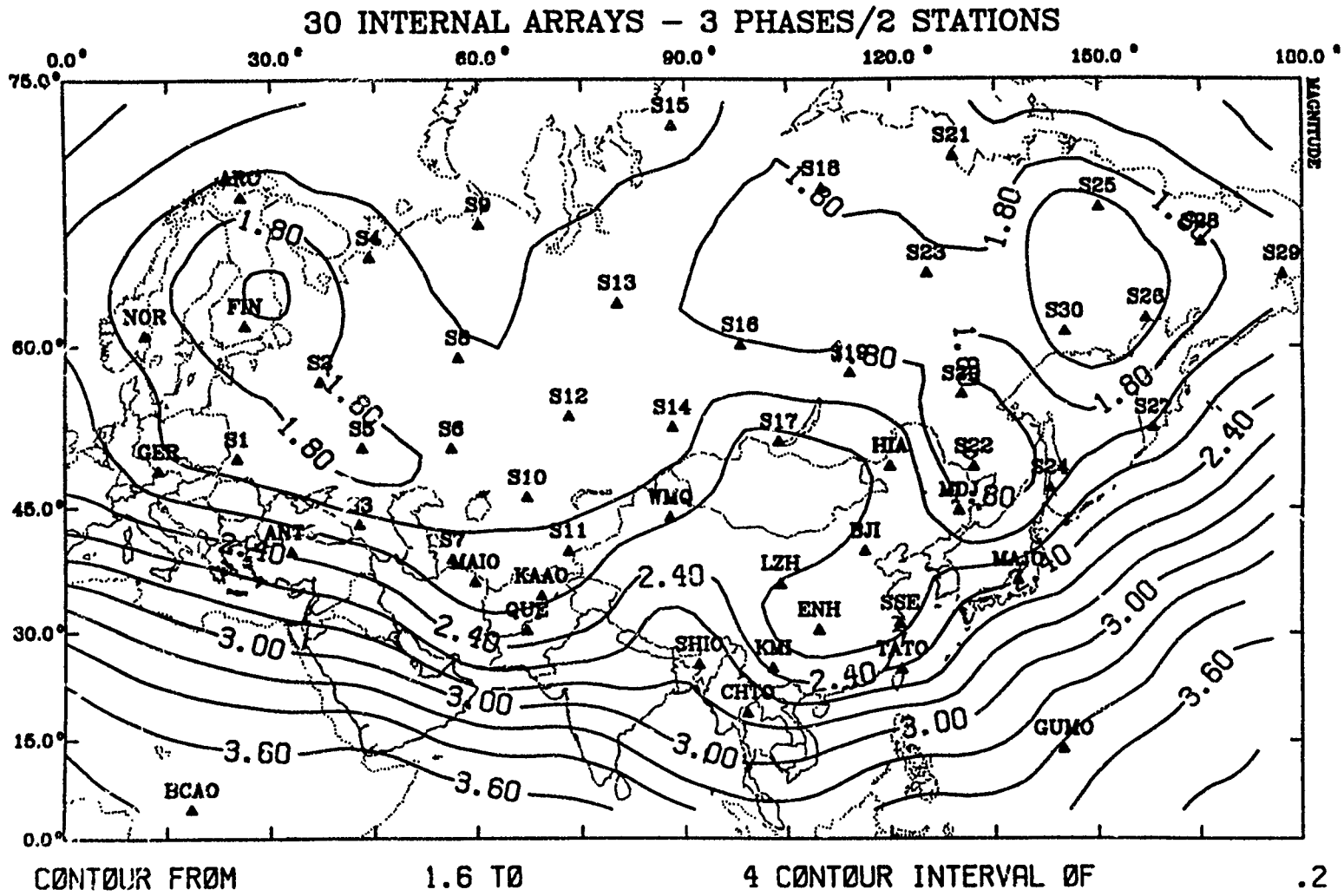

Figure A.5. Estimates of the 90% M_L threshold for detecting 3 phases involving 2 stations are plotted for a network that consists of 30 internal NORESS-type arrays and 49 external stations/arrays.

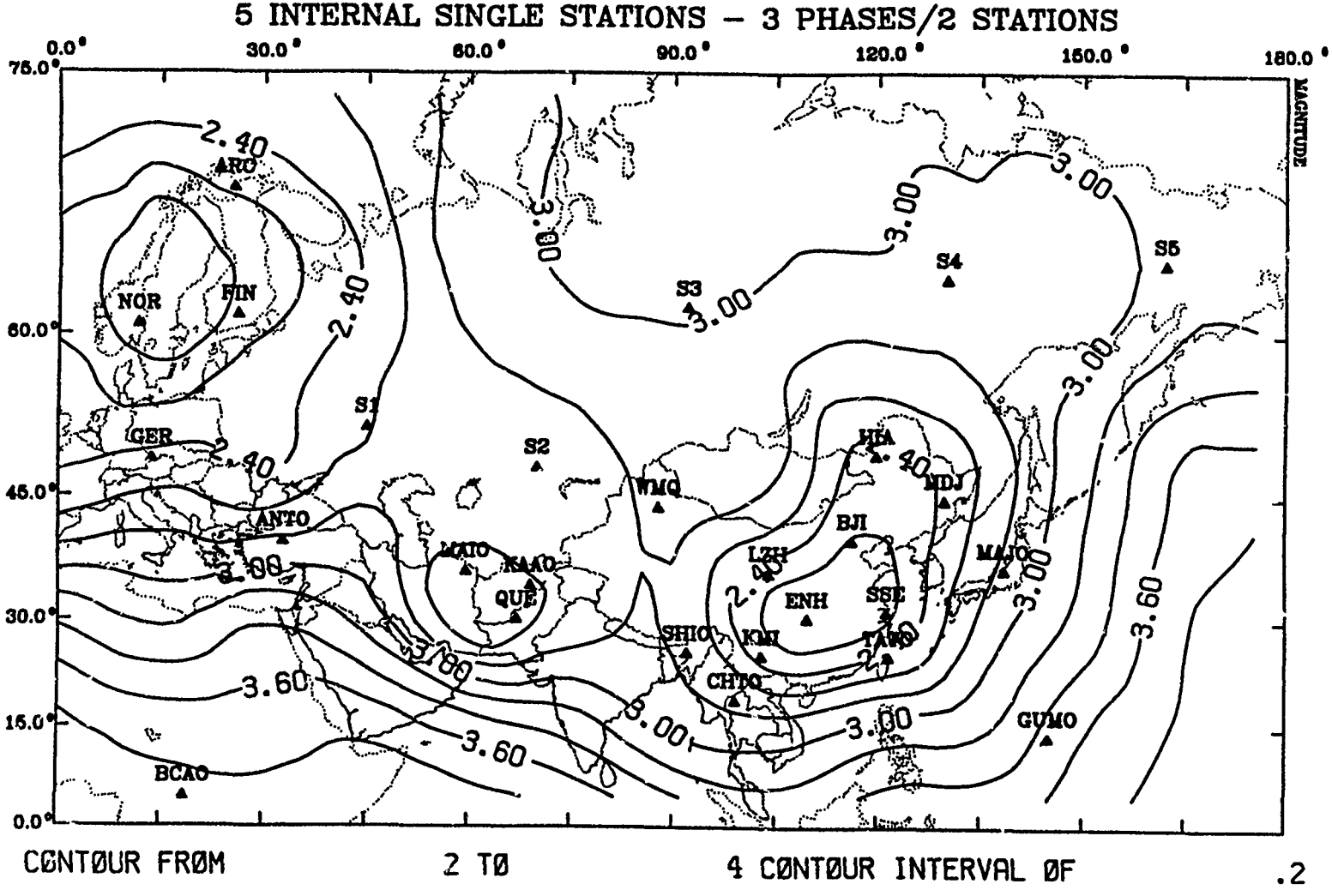

Figure A.6. Estimates of the 90% M_L threshold for detecting 3 phases involving 2 stations are plotted for a network that consists of 5 internal IRIS-type single stations and 49 external stations/arrays.

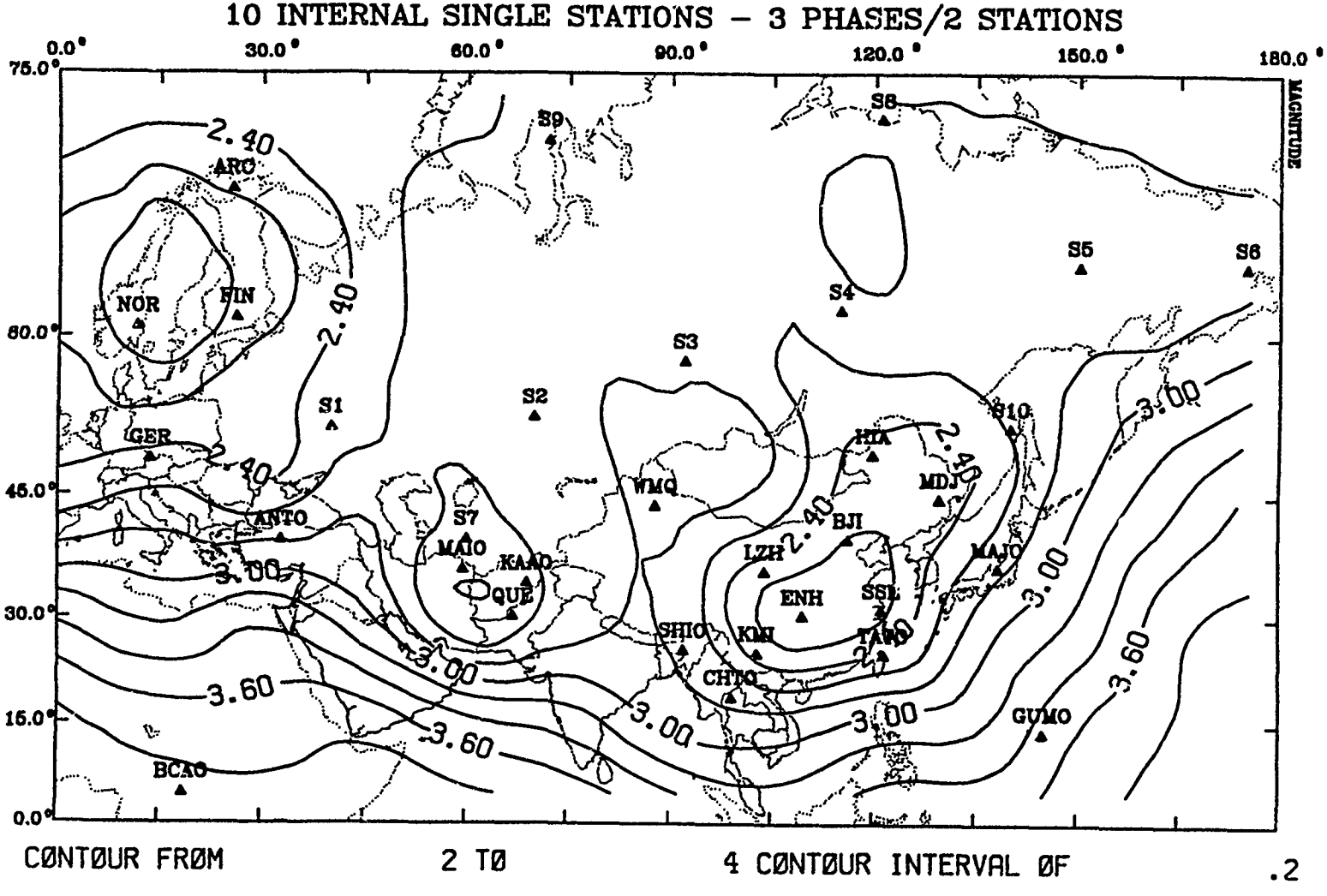

Figure A.7. Estimates of the 90% M_L threshold for detecting 3 phases involving 2 stations are plotted for a network that consists of 10 internal IRIS-type single stations and 49 external stations/arrays.

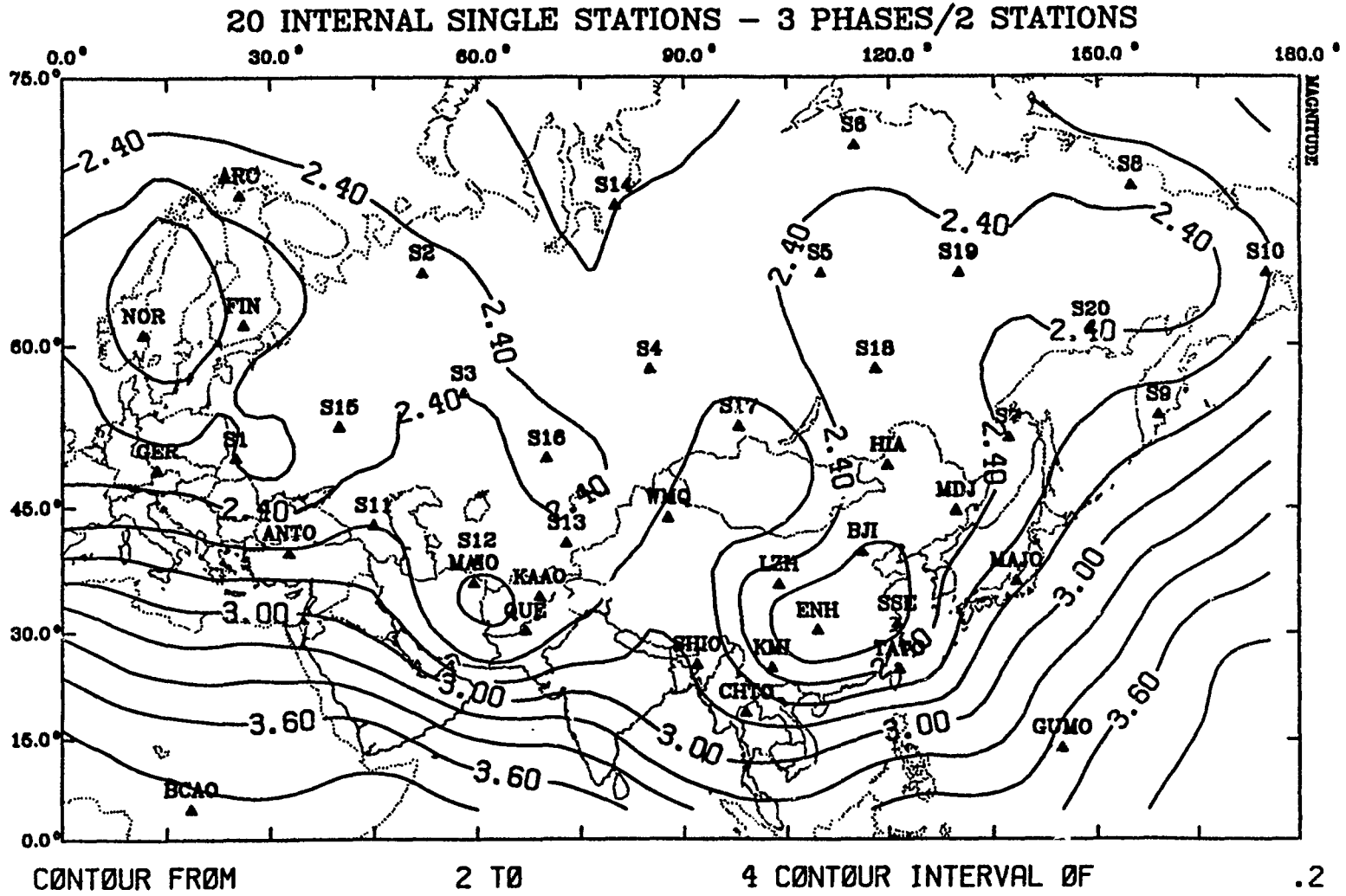

Figure A.8. Estimates of the 90% M_L threshold for detecting 3 phases involving 2 stations are plotted for a network that consists of 20 internal IRIS-type single stations and 49 external stations/arrays.

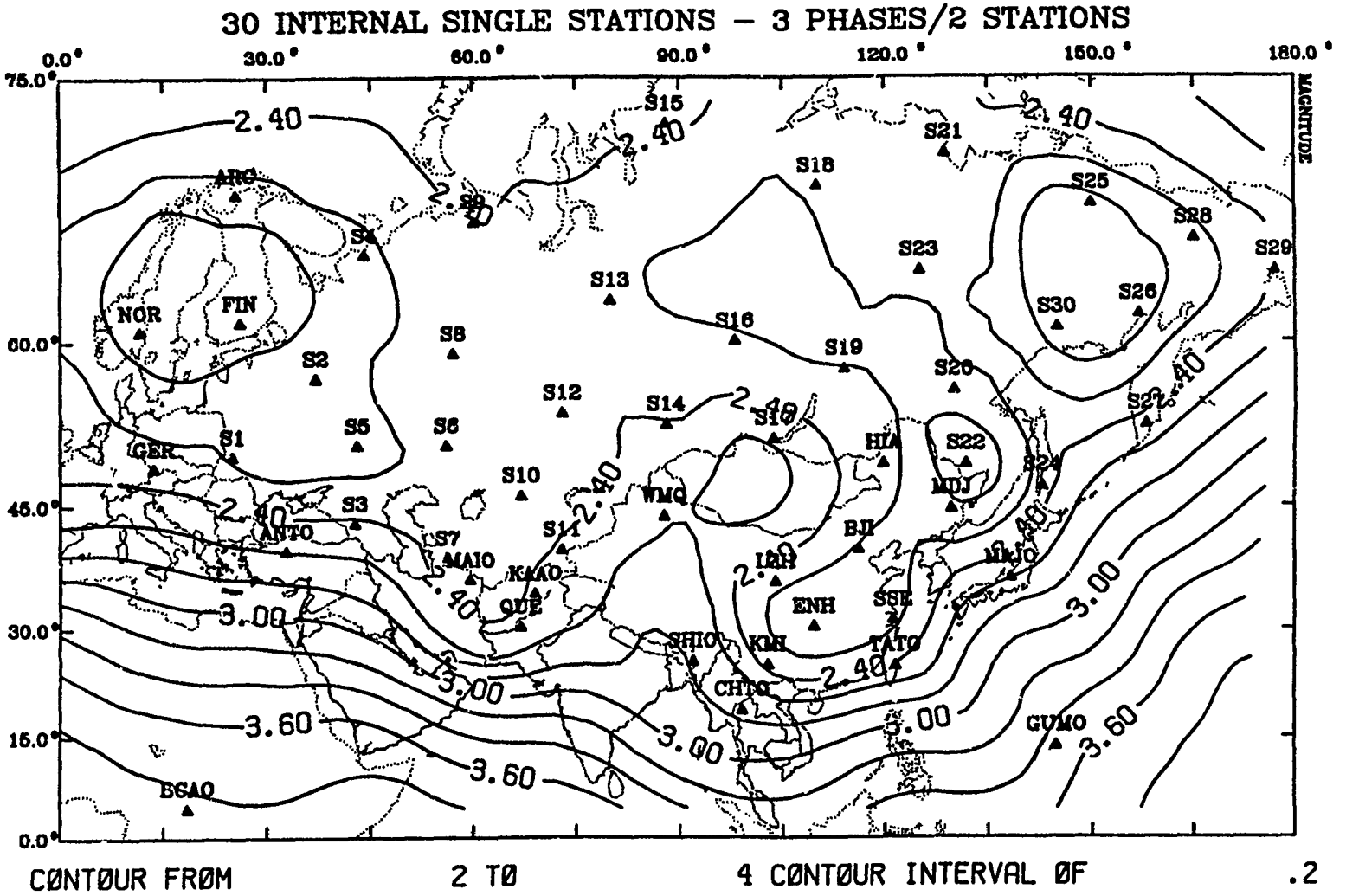

Figure A.9. Estimates of the 90% M_L threshold for detecting 3 phases involving 2 stations are plotted for a network that consists of 30 internal IRIS-type single stations and 49 external stations/arrays.

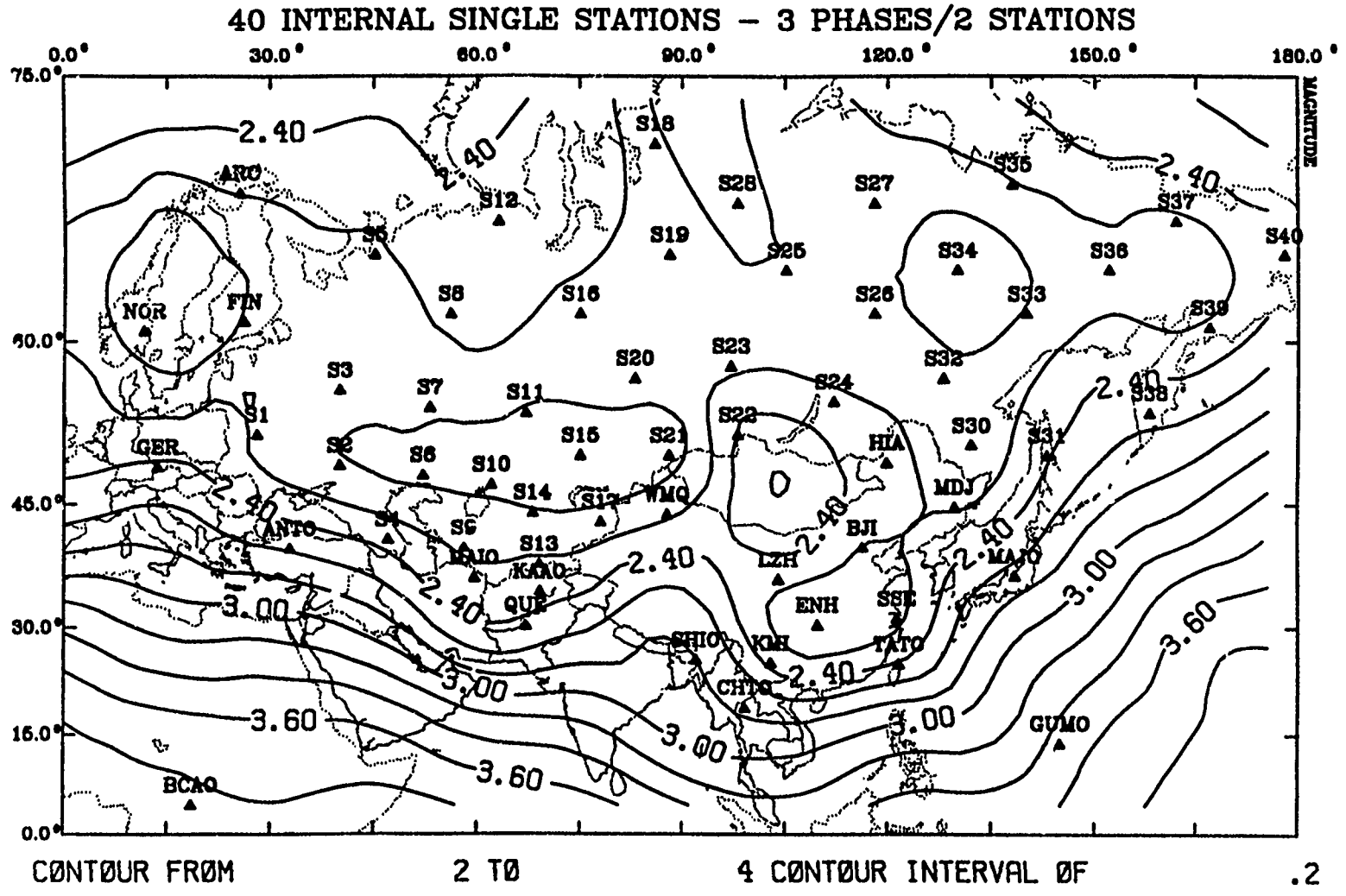

Figure A.10. Estimates of the 90% M_L threshold for detecting 3 phases involving 2 stations are plotted for a network that consists of 40 internal IRIS-type single stations and 49 external stations/arrays.

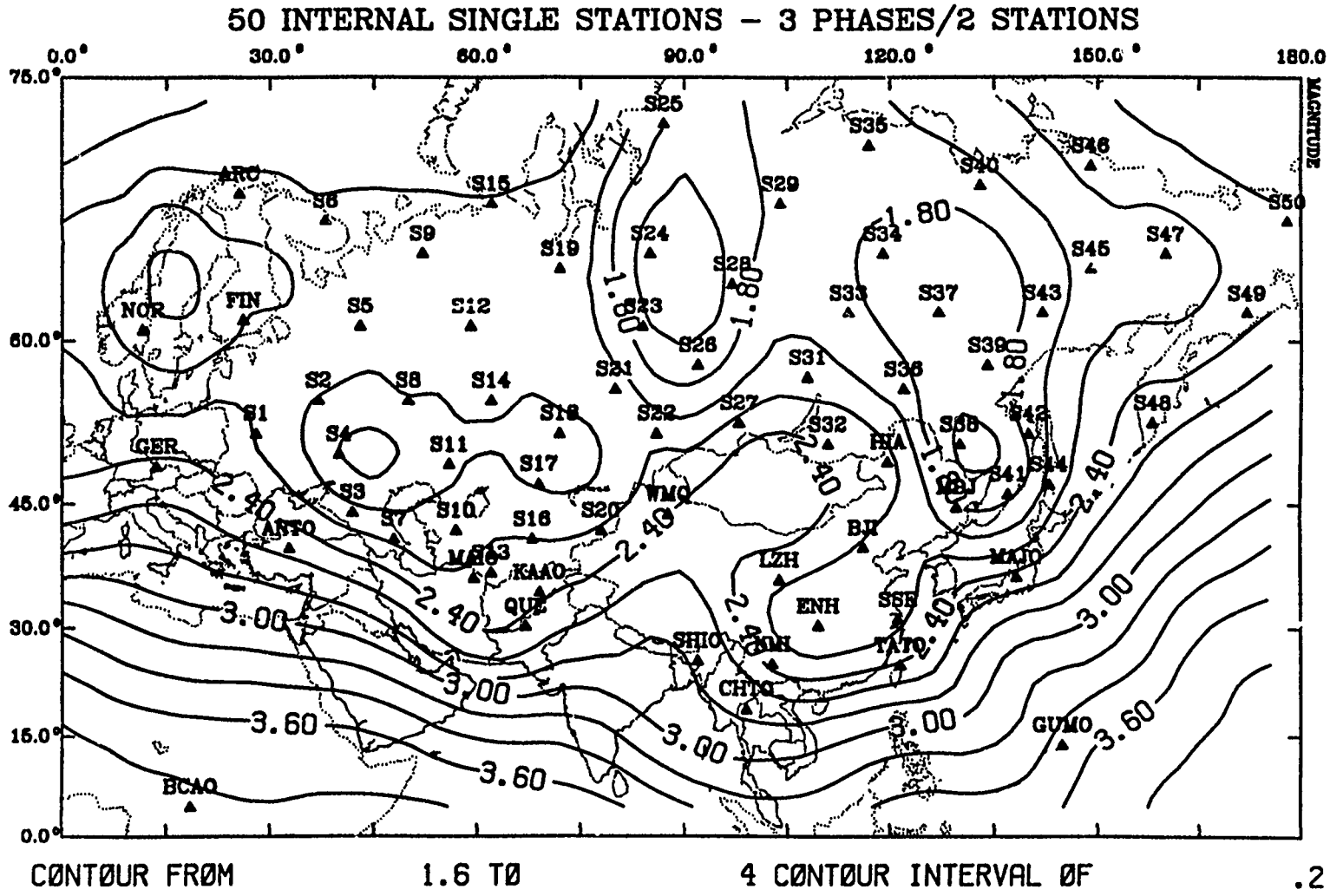

Figure A.11. Estimates of the 90% M_L threshold for detecting 3 phases involving 2 stations are plotted for a network that consists of 50 internal IRIS-type single stations and 49 external stations/arrays.

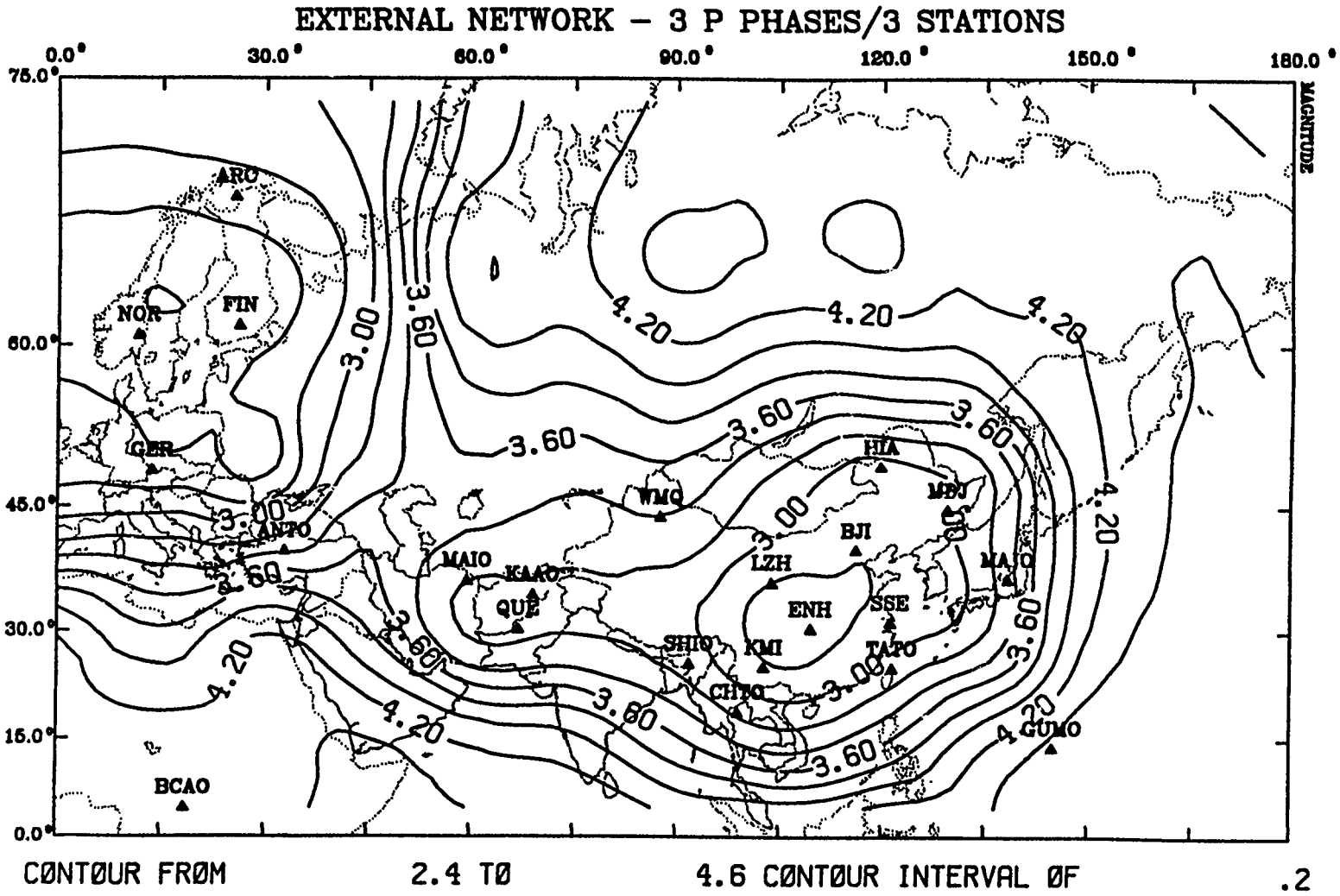

Figure A.12. Estimates of the 90% M_L threshold for detecting 3 P phases involving 2 stations are plotted for a network that consists of 49 external stations/arrays.

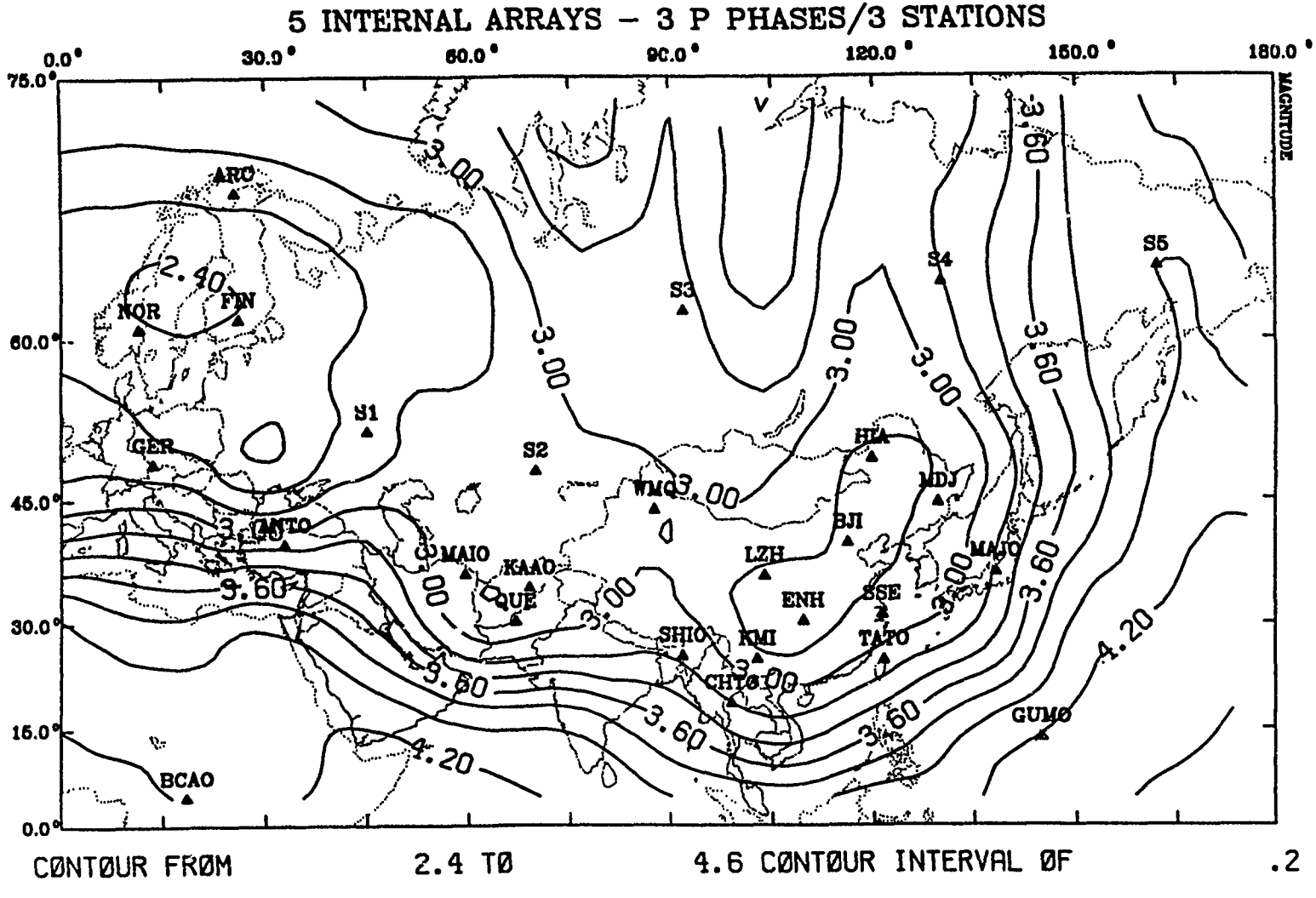

Figure A.13. Estimates of the 90% M_L threshold for detecting 3 P phases involving 3 stations are plotted for a network that consists of 5 internal NORESS-type arrays and 49 external stations/arrays.

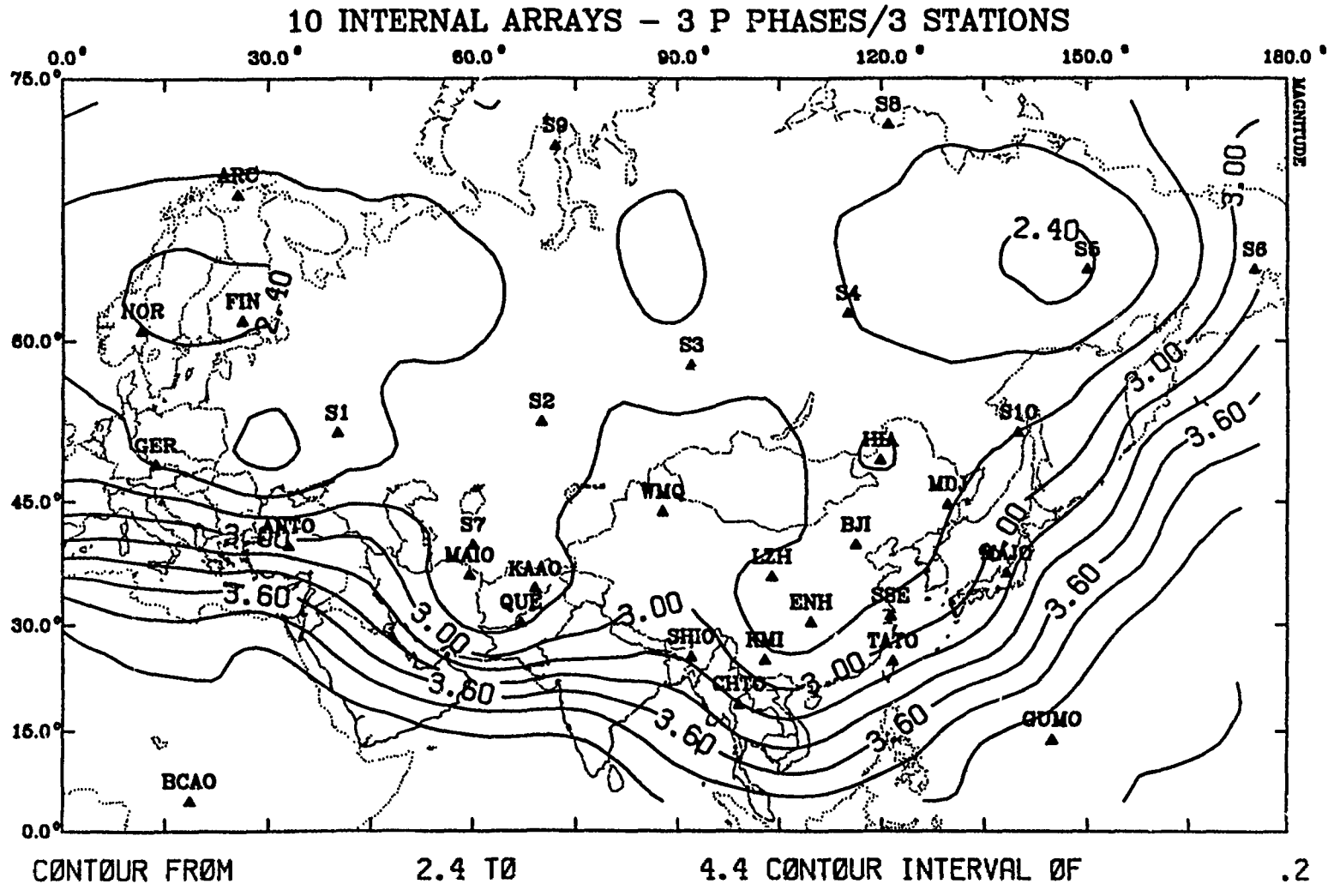

Figure A.14. Estimates of the 90% M_L threshold for detecting 3 P phases involving 3 stations are plotted for a network that consists of 10 internal NORESS-type arrays and 49 external stations/arrays.

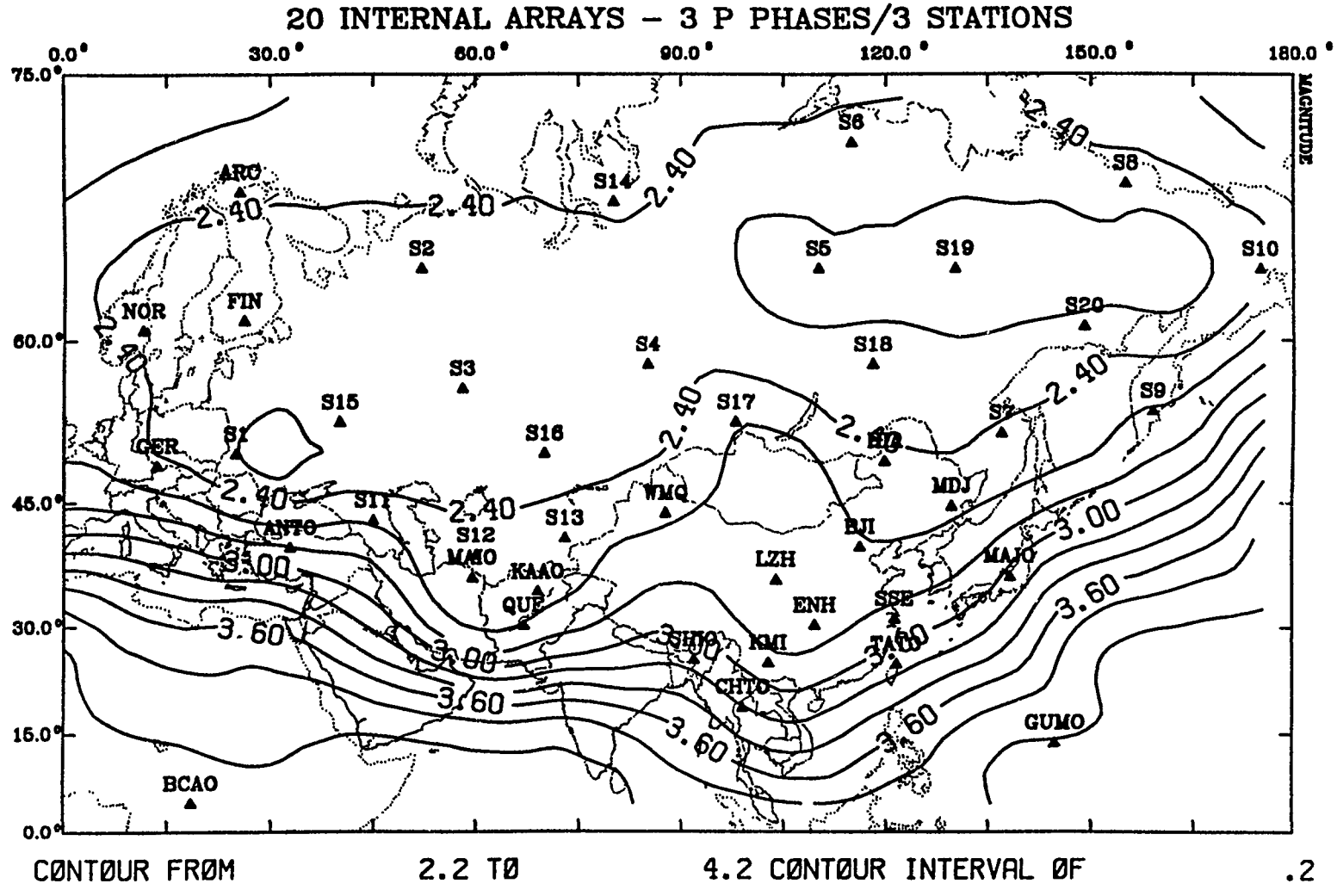

Figure A.15. Estimates of the 90% M_L threshold for detecting 3 P phases involving 3 stations are plotted for a network that consists of 20 internal NORESS-type arrays and 49 external stations/arrays.

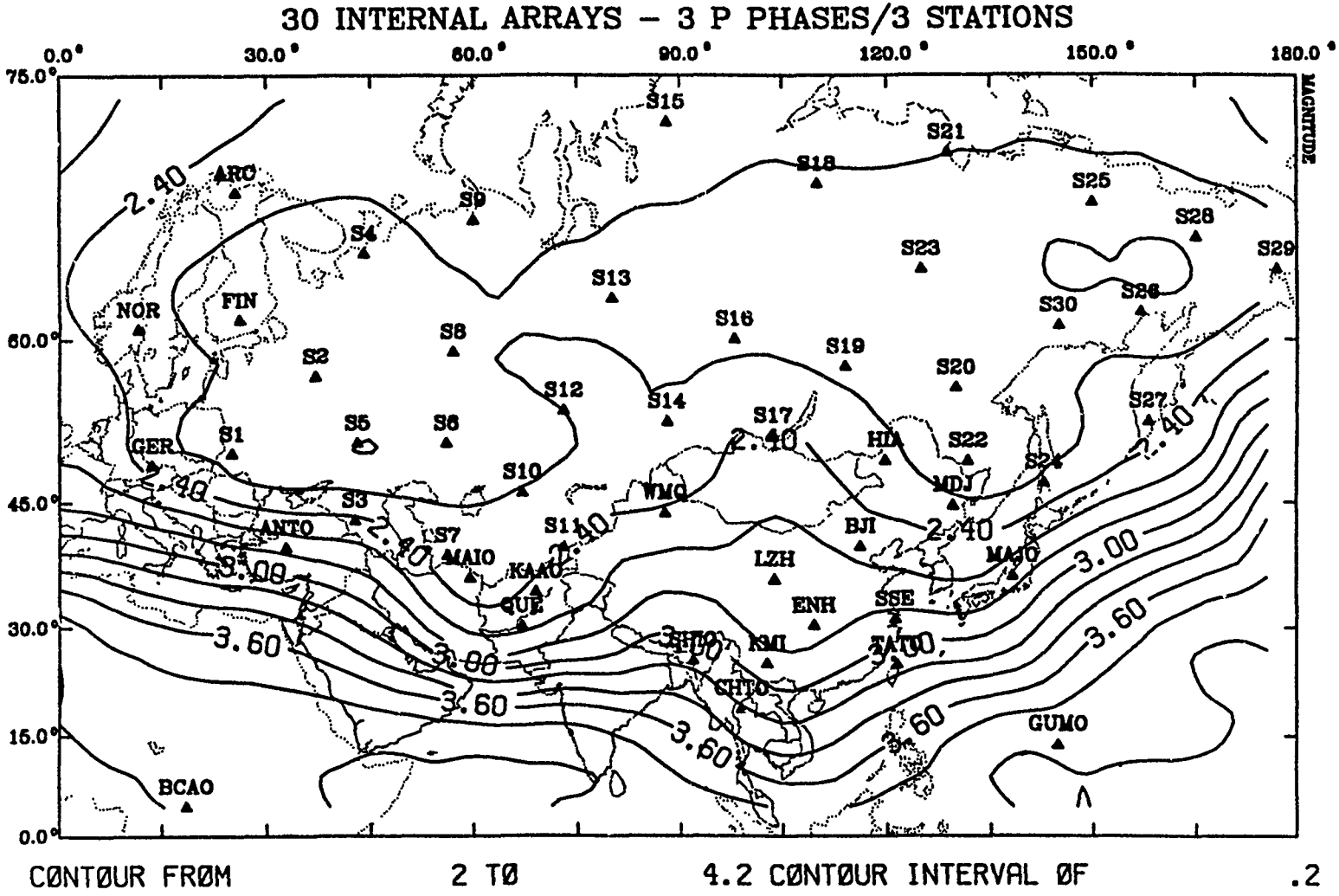

Figure A.16. Estimates of the 90% M_L threshold for detecting 3 P phases involving 3 stations are plotted for a network that consists of 30 internal NORESS-type arrays and 49 external stations/arrays.

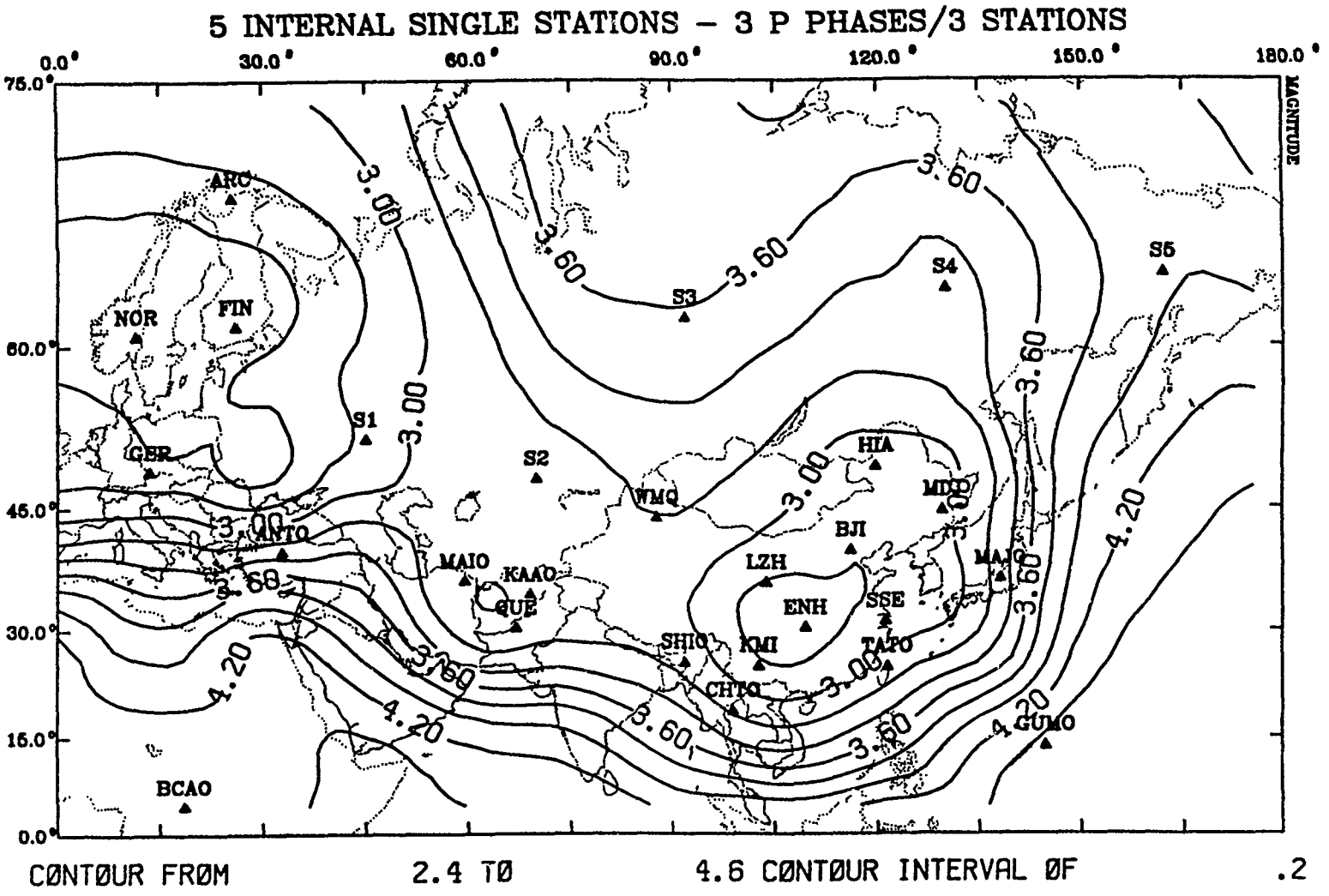

Figure A.17. Estimates of the 90% M_L threshold for detecting 3 *P* phases involving 3 stations are plotted for a network that consists of 5 internal IRIS-type single stations and 49 external stations/arrays.

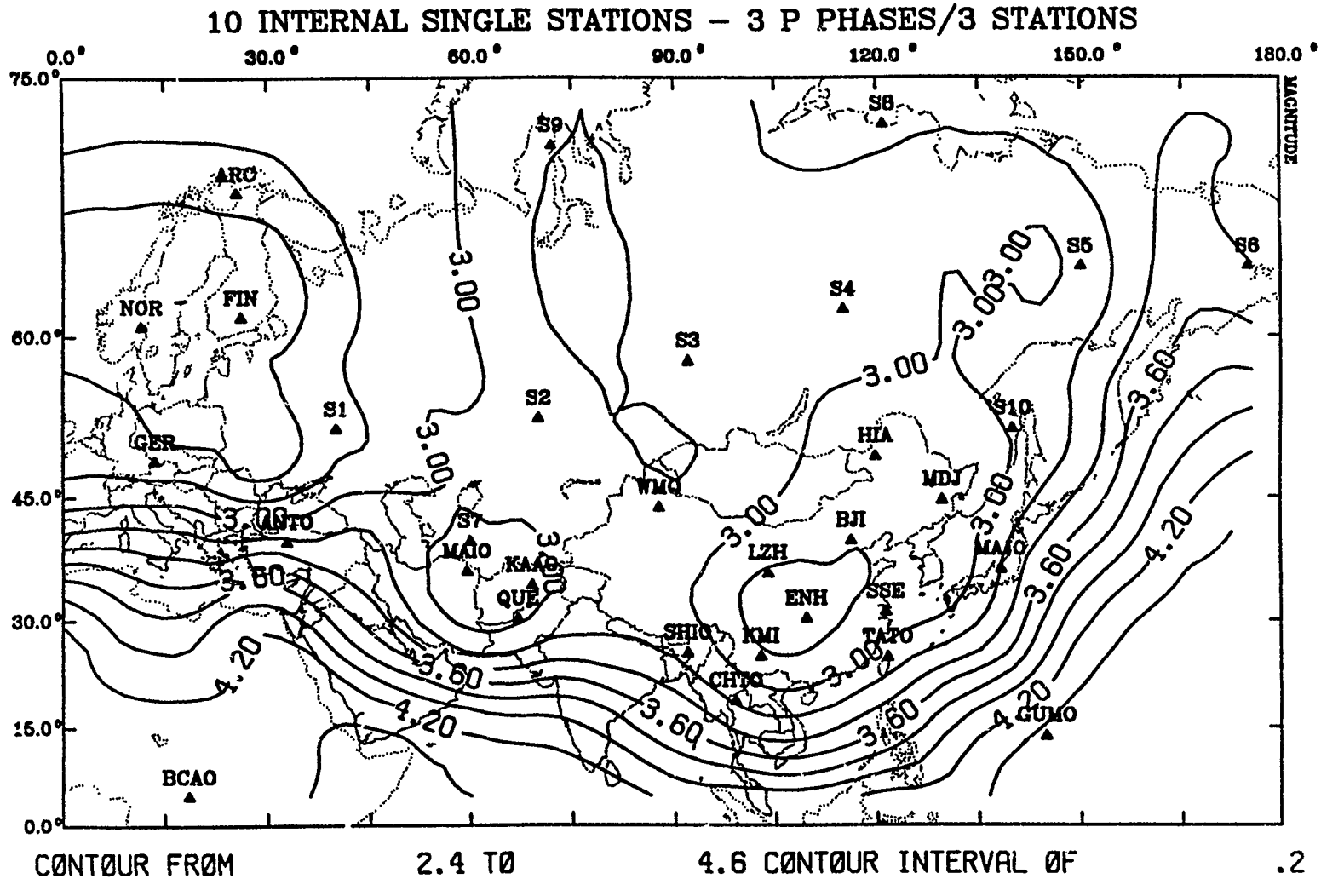

Figure A.18. Estimates of the 90% M_L threshold for detecting 3 P phases involving 3 stations are plotted for a network that consists of 10 internal IRIS-type single stations and 49 external stations/arrays.

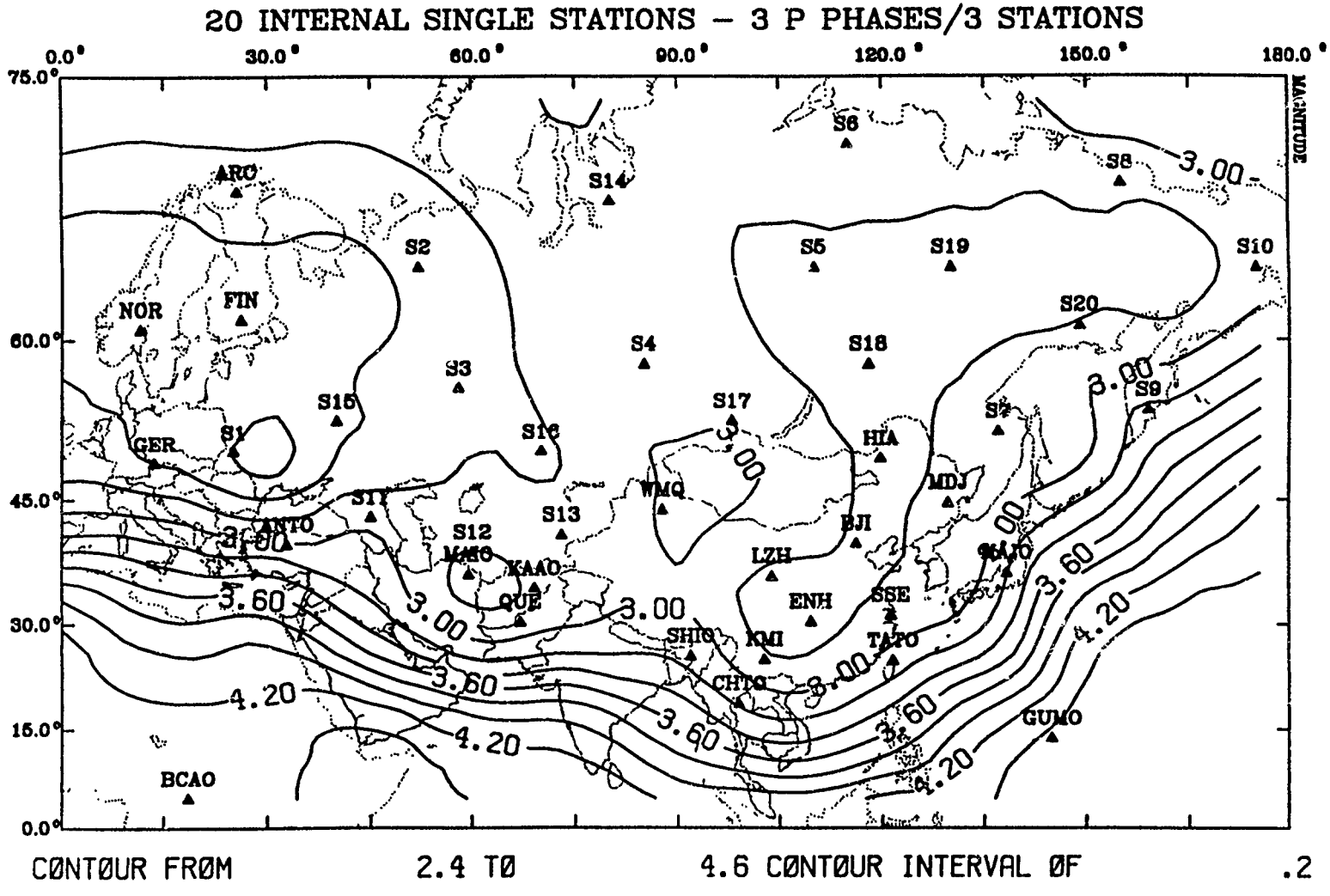

Figure A.19. Estimates of the 90% M_L threshold for detecting 3 P phases involving 3 stations are plotted for a network that consists of 20 internal IRIS-type single stations and 49 external stations/arrays.

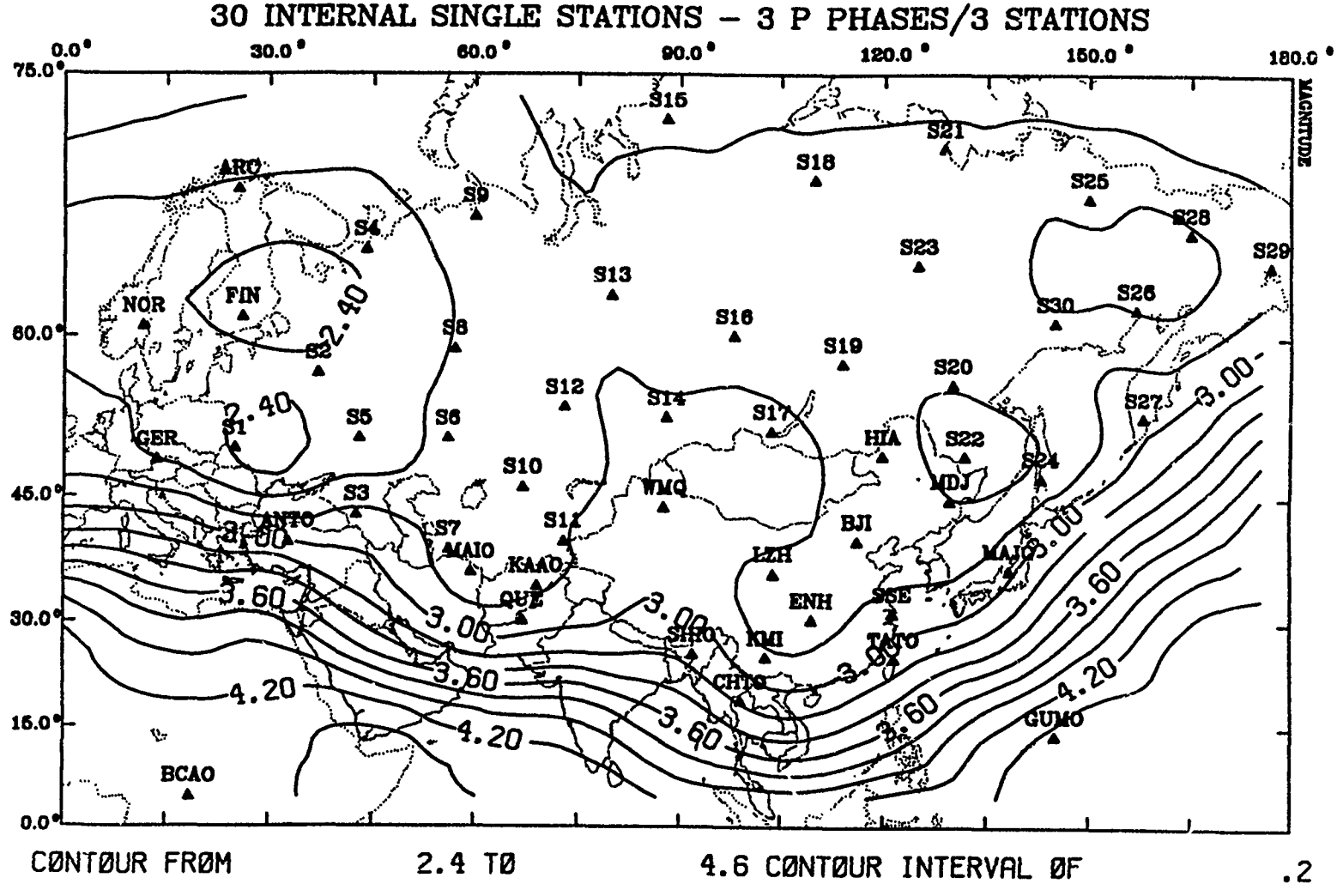

Figure A.20. Estimates of the 90% M_L threshold for detecting 3 P phases involving 3 stations are plotted for a network that consists of 30 internal IRIS-type single stations and 49 external stations/arrays.

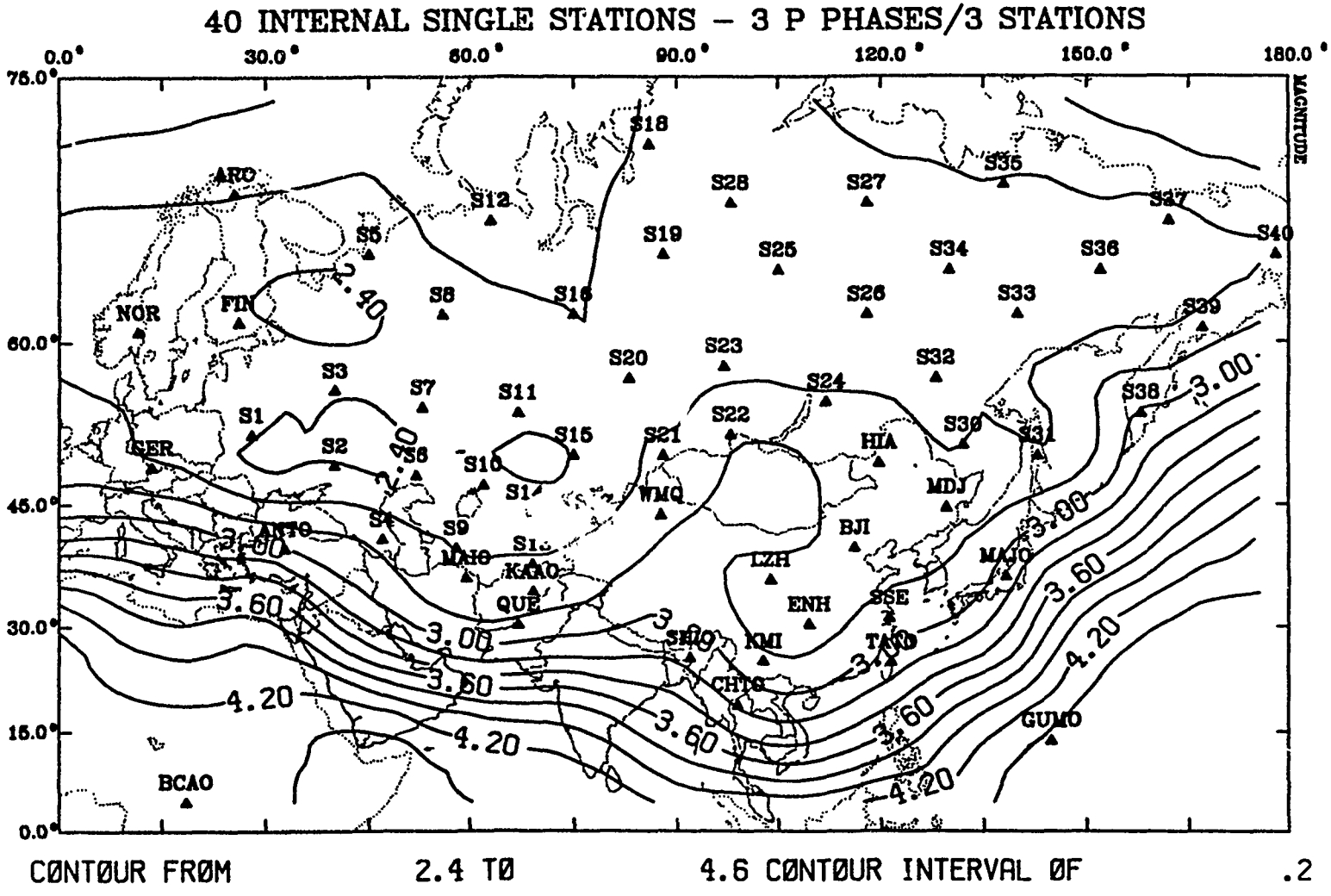

Figure A.21. Estimates of the 90% M_L threshold for detecting 3 P phases involving 3 stations are plotted for a network that consists of 40 internal IRIS-type single stations and 49 external stations/arrays.

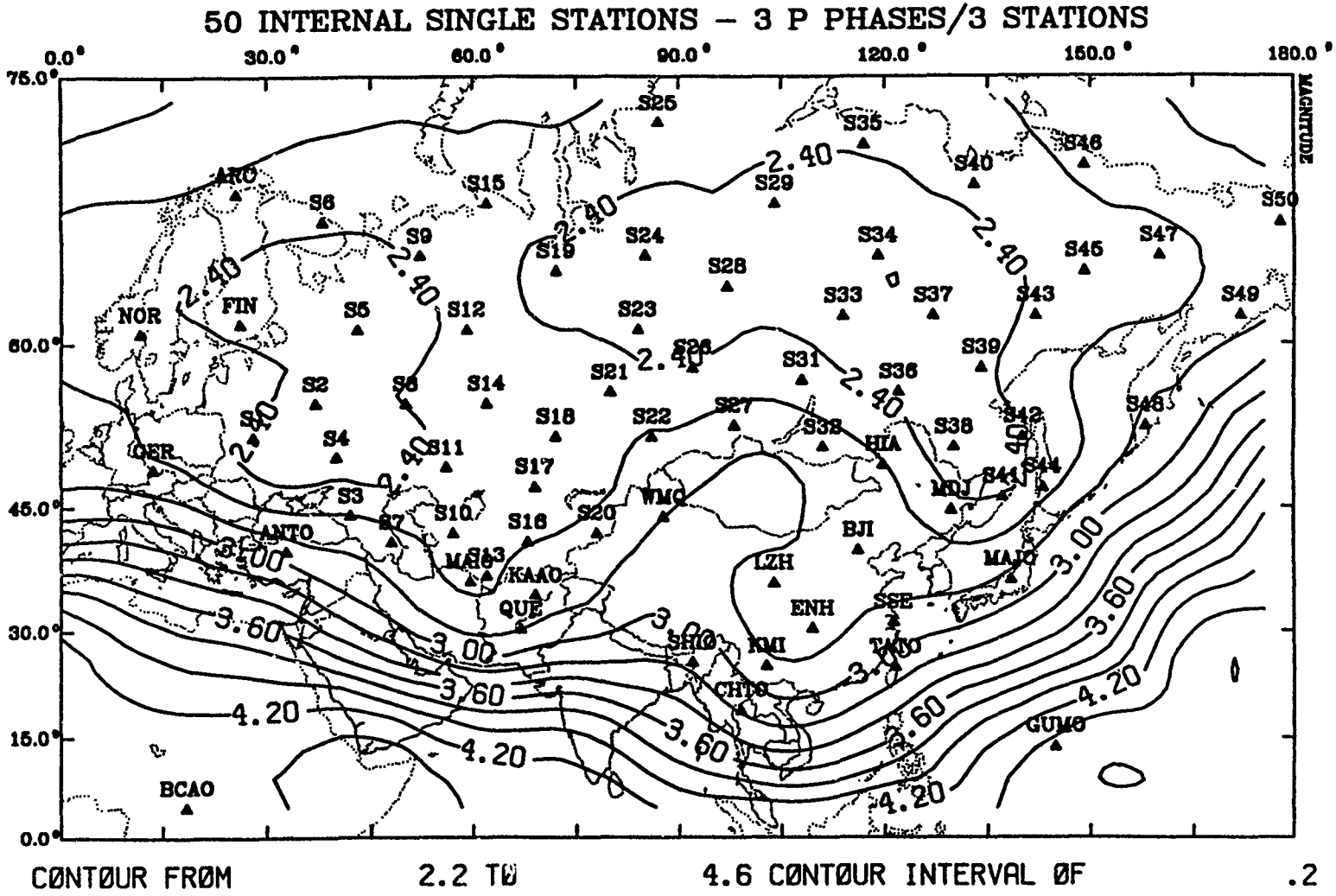

Figure A.22. Estimates of the 90% M_L threshold for detecting 3 P phases involving 3 stations are plotted for a network that consists of 50 internal IRIS-type single stations and 49 external stations/arrays.

(THIS PAGE INTENTIONALLY LEFT BLANK)

DISTRIBUTION LIST
FOR UNCLASSIFIED REPORTS
DARPA-FUNDED PROJECTS
(Last Revised: 26 Nov 90)

RECIPIENT	NUMBER OF COPIES
DEPARTMENT OF DEFENSE	
DARPA/NMRO ATTN: Dr. R. Alewine and Dr. A. Ryall, Jr 1400 Wilson Boulevard Arlington, VA 22209-2308	2
Defense Intelligence Agency Directorate for Scientific and Technical Intelligence Washington, D.C. 20340-6158	1
Defense Nuclear Agency Shock Physics Directorate/SD Washington, D.C. 20305-1000	1
Defense Technical Information Center Cameron Station Alexandria, VA 22314	2
DEPARTMENT OF THE AIR FORCE	
AFOSR/NP Bldg 410, Room C222 Bolling AFB, Washington, D.C. 20332-6448	1
AFTAC/STINFO Patrick AFB, FL 32925-6001	1
AFTAC/TT Patrick AFB, FL 32925-6001	3
AFWL/NTESG Kirkland AFB, NM 87171-6008	1

GL/LWH 1
ATTN: Mr. James Lewkowicz
Terrestrial Sciences Division
Hanscom AFB, MA 01731-5000

AFTAC/Center for Seismic Studies 1
Attn: Dr. Robert Blandford
1300 North 17th Street Suite 1450
Arlington, VA 22209-2308

DEPARTMENT OF THE NAVY

NORDA 1
ATTN: Dr. J. A. Ballard
Code 543
NSTL Station, MS 39529

DEPARTMENT OF ENERGY

Department of Energy 1
ATTN: Mr. Max A. Koontz (DP-331)
International Security Affairs
1000 Independence Avenue
Washington, D.C. 20585

Lawrence Livermore National Laboratory 3
ATTN: Dr. J. Hannon, Dr. S. Taylor, and Dr. K. Nakanishi
University of California
P.O. Box 808
Livermore, CA 94550

Los Alamos Scientific Laboratory 2
ATTN: Dr. C. Newton
P.O. Box 1663
Los Alamos, NM 87544

Sandia Laboratories 1
ATTN: Mr. P. Stokes, Dept. 9110
P.O. Box 5800
Albuquerque, NM 87185

OTHER GOVERNMENT AGENCIES

Central Intelligence Agency 1
ATTN: Dr. L. Turnbull
OSI/NED, Room 5G48
Washington, D.C. 20505

U.S. Arms Control and Disarmament Agency 1
ATTN: Dr. M. Eimer
Verification and Intelligence Bureau, Room 4953
Washington, D.C. 20451

U.S. Arms Control and Disarmament Agency 1
ATTN: Mr. R. J. Morrow
Multilateral Affairs Bureau, Rm 5499
Washington, D.C. 20451

U.S. Geological Survey 1
ATTN: Dr. T. Hanks
National Earthquake Research Center
345 Middlefield Road
Menlo Park, CA 94025

US Geological Survey 1
Attn: Dr. William S. Leith
Mail Stop 928
Reston, VA 22092

U.S. Geological Survey MS-913 1
ATTN: Dr. R. Masse
Global Seismology Branch
Box 25046, Stop 967
Denver Federal Center
Denver, CO 80225

UNIVERSITIES

Boston College 1
ATTN: Dr. A. Kafka
Western Observatory
381 Concord Road
Weston, MA 02193

California Institute of Technology 1
ATTN: Dr. D. Harkrider
Seismological Laboratory
Pasadena, CA 91125

Columbia University 1
ATTN: Dr. L. Sykes
Lamont-Doherty Geological Observatory
Palisades, NY 10964

Cornell University 1
ATTN: Dr. M. Barazangi
INSTOC
Snee Hall
Ithaca, NY 14853

Harvard University 1
ATTN: Dr. J. Woodhouse
Hoffman Laboratory
20 Oxford Street
Cambridge, MA 02138

Massachusetts Institute of Technology 3
ATTN: Dr. S. Soloman, Dr. N. Toksoz, and Dr. T. Jordon
Earth Resources Laboratory
42 Carleton Street
Cambridge, MA 02142

Southern Methodist University 2
ATTN: Dr. E. Herrin and Dr. B. Stump
Institute for the Study of Earth and Man
Geophysical Laboratory
Dallas, TX 75275

Southern Methodist University 1
ATTN: Dr. Gary McCartor
Department of Physics
Dallas, TX 75275

State University of New York at Binghamton 1
ATTN: Dr. F. Wu
Department of Geological Sciences
Vestal, NY 13901

St. Louis University 2
ATTN: Dr. B. Mitchell and Dr. R. Herrmann
Department of Earth and Atmospheric Sciences
3507 Laclede
St. Louis, MO 63156

The Pennsylvania State University 1
ATTN: Dr. S. Alexander
Geosciences Department
403 Deike Building
University Park, PA 16802

University of Arizona 1
ATTN: Dr. T. Wallace
Department of Geosciences
Tucson, AZ 85721

University of California, Berkeley 1
ATTN: Dr. T. McEvilly
Seismographic Station
Berkeley, CA 94720

University of California, Los Angeles 1
ATTN: Dr. L. Knopoff
405 Hilgard Avenue
Los Angeles, CA 90024

University of California, San Diego 1
ATTN: Dr. J. Orcutt and Ms. Ann Kerr
Scripps Institute of Oceanography
La Jolla, CA 92093

University of Colorado 1
ATTN: Dr. C. Archambeau
CIRES
Boulder, CO 80309

University of Illinois 1
ATTN: Dr. S. Grand
Department of Geology
1301 West Green Street
Urbana, IL 61801

University of California, Santa Cruz 1
ATTN: Dr. T. Lay
Institute of Tectonics
Earth Science Board
Santa Cruz, CA 95064

University of Cambridge 1
ATTN: Dr. K. Priestley
Bullard Labs, Dept of Earth Sciences
Madingley Rise, Madingley Road
Cambridge CB3, OEZ, England

University of Southern California 1
ATTN: Dr. K. Aki
Center for Earth Sciences
University Park
Los Angeles, CA 90089-0741

DEPARTMENT OF DEFENSE CONTRACTORS

Analytical Sciences Corporation, The 1
Dr. Richard Sailor
ATTN: Document Control
55 Walkers Brook Drive
Reading, MA 01867

Applied Theory, Inc. 1
ATTN: Dr. J. Trulio
930 South La Brea Avenue
Suite 2
Los Angeles, CA 90036

Center for Seismic Studies 2
ATTN: Dr. C. Romney and Mr. R. Perez
1300 N. 17th Street, Suite 1450
Arlington, VA 22209

ENSCO, Inc. 1
ATTN: Mr. John R. Stevenson
P.O. Box 1346
Springfield, VA 22151

ENSCO, Inc. 1
ATTN: Dr. R. Kemerait
445 Pineda Court
Melbourne, FL 32940-7508

Martin-Marietta 1
ATTN: Mr. R. J. Woodard
Chesapeake Instrument Division
6711 Baymeado Drive
Glen Burnie, MD 21061

Maxwell Laboratories, Inc. 1
S-CUBED Reston Geophysics Office
Reston International Center
ATTN: Mr. J. Murphy, Suite 1212
11800 Sunrise Valley Drive
Reston, VA 22091

Mission Research Corporation 1
Attn: Mark Fisk
735 State Street
PO Drawer 719
Santa Barbara, CA 93102

Pacific Sierra Research Corp. 1
ATTN: Mr. F. Thomas
12340 Santa Monica Boulevard
Los Angeles, CA 90025

Pacific-Sierra Research Corporation 1
Attn: Dr. Karl F. Veith
1401 Wilson Boulevard
Arlington, VA 22209

Rockwell International 1
ATTN: B. Tittmann
1049 Camino Dos Rios
Thousand Oaks, CA 91360

Rondout Associates, Inc. 1
ATTN: Dr. P. Pomeroy
P.O. Box 224
Stone Ridge, NY 12484

Science Applications International Corporation 1
ATTN: Document Control (Dr. T. Bache, Jr.)
10260 Campus Point Drive
San Diego, CA 92121

Science Horizons 2
ATTN: Dr. T. Cherry and Dr. J. Minster
710 Encinitas Blvd.
Suite 101
Encinitas, CA 92024

S-CUBED, A Division of Maxwell 1
Laboratories, Inc.
ATTN: Dr. Keith L. McLaughlin
P.O. Box 1620
La Jolla, CA 92038-1620

Sierra Geophysics, Inc. 2
ATTN: Dr. R. Hart and Dr. G. Mellman
11255 Kirkland Way
Kirkland, WA 98033

SRI International 1
ATTN: Dr. A. Florence
333 Ravenswood Avenue
Menlo Park, CA 94025-3493

Teledyne Industries, Inc. 1
Teledyne Geotech Alexandria Laboratories
ATTN: Mr. W. Rivers
314 Montgomery Street
Alexandria, VA 22314-1581

Woodward-Clyde Consultants 1
ATTN: Dr. L. Burdick
P.O. Box 93254
Pasadena, CA 91109-3254

NON-US RECIPIENTS

Blacknest Seismological Center 1
ATTN: Mr. Peter Marshall
Atomic Weapons Research Establishment
UK Ministry of Defense
Brimpton, Reading RG7-4RS
United Kingdom

National Defense Research Institute 1
ATTN: Dr. Ola Dahlman
Stockholm 80, Sweden

NTNF NORSAR 1
ATTN: Dr. Frode Ringdal
P.O. Box 51
N-2007 Kjeller
Norway

OTHER DISTRIBUTION

To be determined by the project office 4

TOTAL 81